

The Effects of Spatial Organization and Fluid Flow on the Social Interactions in Microbial Communities

Présentée le 1^{er} décembre 2023

Faculté des sciences de la vie

Unité du Prof. Persat

Programme doctoral en biotechnologie et génie biologique

pour l'obtention du grade de Docteur ès Sciences

par

Jeremy Pak Hei WONG

Acceptée sur proposition du jury

Prof. J. McKinney, président du jury

Prof. A. L. A. Persat, Prof. T. I. Battin, directeurs de thèse

Prof. C. Tropini, rapporteuse

Prof. M. Ackermann, rapporteur

Prof. G. D'Angelo, rapporteur

Acknowledgements

I would like to dedicate this thesis to my first supervisor, Professor Deborah Zamble, who tragically passed away on July 6, 2020. Deborah was and always will be one of the most important mentors in my scientific career. I joined Deborah's lab in May 2016, back when I was an undergraduate student with no research experience, neither stellar grades. Deborah believed in my potential, and patiently trained me as a scientist in her lab. Without the mentorship of Deborah, there will not be the Jeremy of today.

Throughout my 2 years working with Deborah, not only that I gained a lot of valuable experiences in running experiments spanning the fields of inorganic chemistry and biochemistry, but she also served as my role model of a good scientist and mentor.

Throughout my 8-year scientific career, Deborah also encouraged me to travel abroad and learn from how scientists from other countries perform research, which led to my decisions to work in Germany and Switzerland. She also was the most influential person in my decision to pursue a PhD. When I heard about the sad news from my colleagues 3 years ago, nothing can describe my grief. It had been three years now since her death and it stings me. Deborah, with this PhD, I hope I have made you proud. You have always been my influence and a role model I look up to as a scientist. It is very sad that you will not be able to witness this moment of happiness with me, but I thank you from the bottom of my heart for your years of mentorship, kindness. I really learned a lot from you and hope I can continue your legacy and spirit in scientific research. Without you, there will not be the Jeremy of today, here defending his thesis.

I would like to thank by two supervisors Alex Persat and Tom Battin for their mentorship throughout the past 5 years. Thank you both for putting so much trust in me and allowing me so much autonomy in the lab to explore. Throughout my ups and downs of the past 5 years, I really transformed from a little chemist who knows nothing much about microbiology, to a well-rounded scientist who can run experiments spanning many fields: chemistry, microbiology, physics and ecology who can think critically.

I would like to thank my previous supervisor Rebecca Jockusch, whom I have performed my bachelor thesis with. Thank you for always making time for me when I wanted to speak to you, even when you are enjoying your coffee at your favourite café! Thank you for putting so much trust in me during my bachelor thesis time, allowing me to operate the 1 million dollars ion cyclotron resonance mass spectrometer as an undergraduate student, and nurturing me into an independent scientist. Thank you for teaching me through your lectures the importance of passion in both teaching and work. You serve as my role model to an ideal professor/ teacher. Whenever I am teaching a lecture, I always remember what you tell me: be passionate about the topic, then you will make all the student's life much better in the classroom.

I would like to thank my previous supervisor Martin Müller who supervised me during my short 5 months in Dresden. Although my time was short and I clearly did not have the expertise to perform experiments when I first joined Martin's lab, Martin was always happy to spend time supervising me in the lab. I also enjoyed a lot all the conversations we had regarding the Bundesliga. Thank you, Martin, for giving me the opportunity to learn from you, and constantly supporting me whenever I needed it.

I would like to thank Prof. Giovanni D'Angelo and Loïc Dayon for giving me the countless opportunities to teach your courses involving subjects I am very passionate about. I truly enjoyed the experience of teaching various exercises and even lectures throughout the 5 years of my PhD journey. It not only gave me the opportunity to review basic concepts in metabolism and mass spectrometry, two fields which I love, but also the opportunity to improve my scientific communication skills through the form of teaching. I would also like to thank Giovanni for all your constant emotional support while I was going through some tough times. Your support motivated me to keep fighting during that period, which led me to achieving many great things in the later years of my PhD.

I would like to thank all the colleagues whom I encountered in Alex and Tom's labs over the past 5 years. First, from Tom's lab, I would like to thank Amin, Åsa, Marta, David

Schildweiler, Pier Luigi, Leïla, Stelios, Massimo, Lluís, Kevin, Matteo, Martina, Geraldine and Andrew for your efforts in helping me integrate into the lab. Although I have not spent too much time in Tom's lab in the beginning of my PhD, it was always a pleasure talking to you all, and of course also spending time with you guys. I would like to thank Hannes and Paraskevi, who was always supportive throughout my PhD and being someone who I can always talk to about anything from my project to life. Although the scope of my project is quite far from the core research of Tom's lab, you two were always happy to help with instrumentations and provide me with feedback whenever I needed them. I would then like to thank the three members whom I have had most contacts with: David Touchette, Anna and Jade. Although our overlap had been relatively short, I thank you David, for always helping me whenever I have questions regarding the EPFL in Valais. It was always nice having conversations with you, not only concerning our research, but of course, also about Canada and the mountains! Then I would like to thank Jade, whom I am very thankful to have met during my PhD. Thank you for always being the supportive character you are! I learned a lot from you over the past 5 years, and I enjoyed very much the time we spent together at the fields in Valais. Finally, I would like to thank Anna, who helped me a lot with experimental setup and designs. It was always great discussing science with you Anna, and talking to you helped me a lot, particularly during the early phase of my PhD.

I would like to thank everyone in Alex's lab that I have encountered over the past 5 years. In particular, the original core members of the lab: Zaïnebe, Lorenzo, Xavier, Tamara, and Alice. To Zaïnebe, thank you very much for your help when I first arrived in Switzerland: helping me with anything from administrative documents to helping me find a place to stay, it really helped relieve a lot of stress! To Xavier, thank you for always being the entertaining character of the lab, you bring me a lot of joy with your serious yet humorous character. To Lorenzo, thank you very much for everything you have done for me. You are really everything I can ask for from a friend: always happy and patient to explain to me things I don't understand, taking care of me when I arrived all alone in Switzerland, and constantly showing your love and care. You are someone I really look up to and I hope I can replicate your positive energy to others whom I will encounter in

the future. I will come back to Tamara and Alice later because I have a lot to say about them, but I would like to first thank the other members of the Persat Lab: Marco, Alessandra, Sourabh, Pascal, Sonia, Tania, Lucas, Hanyi, Gani, Eric and Polong. To Marco and Eric, thank you both for the great moments we had together in the mountains! I truly enjoyed spending time with the two of you in the nature, plus the great conversations we have about life and work. To Sourabh and Tania, thank you both for always being caring and supportive during my difficult times. I am very thankful to have friends like the two of you. Hopefully, we can continue our tradition of going for drinks and food in the evenings after I graduate! To Alessandra and Sonia, it had been my pleasure to work with the two of you. I will never forget the moments in the lab where I managed to purify 12 proteins concurrently with Alessandra and trying to figure out how to form an aerobic-anaerobic interface with Sonia. You are both amazing people and scientists and I really enjoyed my time with the two of you both in and out of the lab. To Lucas and Pascal, thank you very much for always looking out for me and providing me with useful feedback and help when I needed them. I also valued a lot our common interests in football and our random football talks in the lab. I will for sure miss that when I leave the lab. To Hanyi, Gani and Polong, thank you very much for being great colleagues, it was a very enjoyable atmosphere working with the three of you. For Hanyi, I also would like to thank you for constantly supporting me and travelling with me to things like operas and concerts. It is very nice to have someone who shared common interests with me and I enjoyed all the trips we made together.

I would now like to thank Alice and Tamara, who are the two best friends I have made during my time in Switzerland. Honestly, we have been through a lot together. From me joining the lab as Tamara's student back in 2018 to me starting my PhD officially to the three of us moving in together as flatmates. Nothing can describe how thankful I am to have met the two of you. There are just too many beautiful memories between the three of us that I cannot even list them all here! I deeply thank the two of you for constantly being patient and supportive, throughout all my ups and downs. You two really played an integral role in helping me stand back up during the extraordinarily bad times I was going through back in early 2021. I truly enjoyed every moment of time I spent with the

two of you, from having our daily coffees in the lab to cooking together in the evenings when we were living together. As I am the youngest one out of the three of us, it really does feel like the two of you are like my moms in Switzerland. Thank you for always willing to listen to all my crazy stories and giving me love when I needed it. I already miss you both dearly since your respective graduations from the lab. Thank you very much Mamalice and Mamara for everything over the past 5 years! I hope our friendship can stay strong for many years to come!

I would like to thank my 4 students whom I supervised: Audrey, Noemie, Alix and Ivona. As my first student, I have to say that Audrey was simply amazing. She was super independent, and always have her own opinion regarding experimental setups. Thank you for all the great work you have contributed to my projects. I also thank you for being the caring person you are! Noemie, you are also an amazing student and deserve a lot of credits! Even though I was mostly on vacation during your time in the lab, you managed to learn super quick, become independent and perform good research! You should be very proud of your achievements in the lab and hopefully I will be able to gather all your data and put it into a story before I graduate! I would also like to thank Alix and Ivona for their efforts and contributions towards my projects.

I would like to then thank my friends from Canada. First, my group of elementary school friends: Jeffrey, Samantha, Calvin and Adrienne. Really, we have known each other for more than 15 years now! Thank you for always walking by my side throughout the different journeys of my life, of course, also including the PhD. You guys are really my best friends and people I am always comfortable around. Much love for you all! Second, my group of friends from high school: Joshua, Matthew, Steven and Eric. Just like the elementary school crew, you guys have also been with me for the past 10 years. Thank you all for always being super supportive to me and bringing me numerous moments of joy during my PhD time! You guys are great! Finally, I would like to thank my friends from university: Sarah, Deeba, William, Jessica and Gloria. You all were also always there for me whenever I am going through trouble during my PhD. I am very glad to

have met wonderful, caring friends like you guys throughout my time in Canada. You all mean a lot to me and played a huge role in my successes throughout my PhD.

I would then like to thank all my other important friends scattered around the globe: Alexandra, Johannes, Lia, Chris, Shahriah, Mirjam, Ingo, and Diana. To Alexandra, thank you very much for your love and support throughout my PhD. I really enjoyed every moment we spend together from zoom calls providing each other with presentation feedbacks, to travelling to interesting places together. I am very glad to have you around me during the past 5 years! To Johannes, thank you for also being the direct, and supportive person you are. I remember every moment of joy we had, travelling together numerous times throughout our PhD journeys. I must say, you are a great travel buddy, of course, someone who can keep up with my crazy intensity! I hope you will be able to make it down to Lausanne to see my presentation in person! To Lia and Shahriah, thank you both for always having me in mind and checking in on me occasionally. I would love to see you both again soon and conversations with you guys are always great. To Chris, although we only text occasionally, whenever we meet, it is always the same! Thank you for always being supportive to me throughout my PhD. I will never forget the moments we spent together in Baltimore. Now it is time for you to come to Sion! To Mirjam and Ingo, thank you very much to you both for always willing to host and catch up with me whenever I am back in Dresden over the past 5 years! It is always very nice talking to the two of you about both my life and my PhD work! To Diana, I am very thankful to have met an amazing person like you during my travels! You were always there for me when things are not going well, which means a lot to me. I also enjoyed our travels together: in Switzerland and in Romania and I hope we will be able to travel more together soon.

I would then like to thank my friends in Switzerland which are not part of either labs: Mario, Patrycja, Simona, Andrina, Lena, and Christine. To Mario and Patrycja, thank you very much to you both for your hospitality and love. Mario basically became one of my most important friend here in Switzerland since we met at the mass spectrometry course back in 2019. Thank you to you two for always having me in mind, always

allowing me to stay at your flat whenever I couldn't go home from Zurich, and all the wonderful moments we spent together. You both are truly amazing people! To Simona and Andrina, I would never forget the day we met in Slovenia, then managed to meet again in Croatia during our respective travels. Since Covid, we have not been seeing each other as often, but things never change. Thank you for always being supportive throughout my PhD. It is always very pleasant to have conversations with the two of you and hope we will be able to meet more often again in the near future! To Lena and Christine, thank you very much for being my "Valais people". When I first moved to Sion, I really had no friends around. Having the two of you, Christine as my coffee buddy and Lena as my bar buddy, really brought me a lot of joy throughout the mid-late stage of my PhD! Thank you both for always being there for me!

Finally, I would like to thank my girlfriend, Chanel. Meeting you is probably my greatest gift of the year. You really played a huge role in bringing pure happiness to the final stretch of my PhD life! I truly treasure every moment we spend together. Speaking with you always inspires me with new, crazy ideas in the lab! You also bring me the motivation to the thesis writing, which I never believed could be so fun! I would also really like to thank you for helping me rediscover all my forgotten interests and hidden talents such as cooking, writing beautiful poems and perhaps also music. I am extremely happy to have met someone who happened to share so many common interests with me. I will always remember all the wonderful times we spent together, from going to ballets in Zurich to our gastronomy experiences in Budapest. You really mean a lot to me, and I really look forward to more journeys with you in the future. Love you!

Contents

Acknowledgements.....	2
List of Figures.....	13
List of Supplementary Figures	14
List of Tables	14
List of Abbreviations	15
Abstract	17
Keywords	17
Chapter 1. Introduction.....	18
1.1 Biofilms.....	18
1.2 Social interactions and spatial organization in biofilm communities	20
1.3 Fluid flow and social interactions	22
1.4 Human gut microbiota	24
1.5 Motivation and aim of the thesis.....	26
Chapter 2. Biofilm formation by the gut microbiota <i>Bacteroides</i>.....	29
2.1 Abstract	30
2.2 Additional Background.....	30
2.3 Results	32
2.3.1 <i>Bacteroides</i> form unique biofilms in TYG medium	32
2.3.2 Proteins upregulated in biofilm formation by <i>Bt</i>	35
2.3.3 Mechanisms of biofilm filamentation by <i>Bf</i>	36
2.3.4 Duo-species <i>Bacteroides</i> biofilms in TYG Medium	38
2.3.5 Nutrient source impacts biofilm morphology	41
2.4 Discussion	44
2.5 Methods	47
2.5.1 Strains and culture media.....	47
2.5.2 Microchannels fabrication	48
2.5.3 Biofilm growth and microscopy.....	49

2.5.4 Sample preparations for proteomics	49
2.5.5 Sample preparation, RNAseq and data analysis	50
2.6 Supplementary information	51
2.6.1 Supplementary figures.....	51
Chapter 3. Fluid flow structures gut microbiota biofilm communities by distributing public goods	53
3.1 Abstract	54
3.2 Additional Background.....	54
3.3 Results	56
3.3.1 <i>B. theta</i> and <i>B. fragilis</i> form biofilms in flow	56
3.3.2 Cross-feeding between <i>B. theta</i> and <i>B. fragilis</i>	59
3.3.3 Nutrient sharing structures <i>Bacteroides</i> biofilms.....	63
3.3.4 Flow impacts biofilm community organizations by transporting public goods.....	66
3.3.5 Small geometrical features have a local impact on community organization	68
3.3.6 Simulating glucose transport predicts <i>Bf</i> biofilm growth.....	70
3.3.7 Flow impacts community composition	73
3.4 Discussion	74
3.5 Methods	78
3.5.1 Strains and culture media.....	78
3.5.2 Microchannels fabrication	78
3.5.3 Biofilm growth	79
3.5.4 Calculation of Péclet numbers (Pe).....	80
3.5.5 Microscopy	80
3.5.6 Image analysis	80
3.5.7 Simulations of concentration gradients in flow	81
3.5.8 Competition experiments in test tubes.....	82
3.5.9 Sample preparation, mass spectrometry and data analysis for proteomics.....	83
3.5.10 Glycan analysis using HPAEC-PAD	84
3.6 Supplementary information	85
3.6.1 Supplementary figures.....	85

Chapter 4. <i>Bacteroides thetaiotaomicron</i> metabolic activity decreases with polysaccharide size	91
4.1 Abstract	92
4.2 Additional Background.....	92
4.3 Results	95
4.3.1 <i>Bt</i> uses PUL48 to degrade dextran	95
4.3.2 <i>Bt</i> growth dynamics in dextran is dependent on dextran size	98
4.3.3 Tracking dextran binding using fluorescent polymers.....	101
4.3.4 PUL48 proteins and dextran size defines the extent of nutrient sharing by <i>Bt</i>	104
4.4 Discussion	107
4.5 Methods	109
4.5.1 Strains and culture media.....	109
4.5.2 Recombinant expression and purification of <i>Bt</i> GHs	111
4.5.3 GHs activity analysis by HPAEC-PAD	111
4.5.4 In-frame deletion knockouts in <i>Bt</i>	112
4.5.5 Insertion of <i>sfGFP</i> and <i>mCherry</i> into <i>Bt</i> and <i>Bf</i>	113
4.5.6 Test tube mutant growths and competitions.....	113
4.5.7 Growth curves analysis of <i>Bt</i>	114
4.5.8 <i>Bt</i> binding to fluorescently labelled dextran	114
4.5.9 Microscopy	115
4.5.10 Sample preparation for proteomics	115
4.6 Supplementary information	116
4.6.1 Supplementary figures.....	116
4.6.2 Appendix	122
 Chapter 5. Conclusion	 130
5.1 Achieved results and discussion	130
5.1.1 Biofilm formation by the gut commensals <i>Bacteroides</i>	130
5.1.2 Nutrient sharing biofilms in flow	131
5.1.3 Mechanisms of dextran utilization and nutrient sharing	131
5.2 Future directions	132
5.2.1 Roles of fimbriae and pili in <i>Bacteroides</i> biofilm formation	132

5.2.2 Fluid flow and nutrient source in <i>Bf</i> filamentation	133
5.2.3 Dynamics of gur microbiota biofilms.....	133
5.2.4 Biofilm growth pf other anaerobes such as <i>C. difficile</i>	134
5.2.5 A carbohydrate screen for the metabolic steering of microbiota communities.....	135
5.2.6 Microbiota-host interactions in the colon.....	137
5.2.7 Nutrient sharing and T6SS	138
 References	 142
Curriculum Vitae	161

List of Figures

Figure 1.1: The biofilm formation cycle of the human pathogen <i>P. aeruginosa</i>	19
Figure 1.2: The function and importance of the biofilm matrix	19
Figure 1.3: Type VI secretion system (T6SS) of <i>Bacteroidetes</i>	20
Figure 1.4: Biofilms promote interspecies interactions.....	21
Figure 1.5: The importance of spatial organizations in the maintenance of biodiversity....	22
Figure 1.6: Fluid flow and the concentration of common goods.....	24
Figure 1.7: Gut microbiota and diseases associated with dysbiosis	26
Figure 2.1: <i>Bacteroides</i> biofilms in nutrient rich conditions	34
Figure 2.2: Proteomic analysis of <i>Bt</i> biofilms	36
Figure 2.3: Transcriptomic analysis of <i>Bt</i> biofilms	38
Figure 2.4: Duo species biofilms in nutrient rich conditions.	40
Figure 2.5: <i>Bacteroides</i> biofilms under flow in minimal medium.	43
Figure 3.1: <i>Bt</i> and <i>Bf</i> form biofilms in flow.....	58
Figure 3.2: <i>Bt</i> shares a dextran degradation by-product to <i>Bf</i>	62
Figure 3.3: Flow structures syntrophic <i>Bt-Bf</i> biofilm communities at the microscale.....	65
Figure 3.4: Flow impacts biofilm community organization by transporting public goods ...	67
Figure 3.5: Spatial organization of <i>Bt-Bf</i> biofilms in crypt-like features.	69
Figure 3.6: Flow impacts community organization by distributing metabolic by-products..	72
Figure 3.7: Flow impacts community composition during nutrient sharing.....	74
Figure 3.8: How fluid flow structures nutrient sharing microbial communities.....	77
Figure 4.1: The roles of PUL48 proteins in <i>Bt</i> dextran metabolism.....	97
Figure 4.2: Growth curves of various <i>Bt</i> mutants in 3 different sizes of dextran ..	100
Figure 4.3: Fluorescent dextran localization to <i>Bt</i> cells.....	103
Figure 4.4: PUL48 proteins contributes to the extent of nutrient sharing	106
Figure 5.1: Biofilm formation by <i>C. difficile</i>	135
Figure 5.2: Experimental set-up for identifying polysaccharide targets which steers the metabolism of infant microbiota communities	137
Figure 5.3: <i>Bf</i> downregulates T6SS in the presence of <i>Bt</i> nutrient sharing	139
Figure 5.4: Contact dependent killing by <i>Bf</i> on <i>Bt</i>	141

List of Supplementary Figures

Figure S2.1: Genes significantly upregulated or downregulated in <i>Bf</i> biofilms from RNAseq differential expression analysis.....	52
Figure S3.1: <i>Bt</i> spent dextran medium supports the growth of <i>Bf</i>	86
Figure S3.2: HPAEC-PAD standards for sugar identification.....	86
Figure S3.3: <i>Bt</i> biofilm growth in dextran is insensitive to the presence of <i>Bf</i>	87
Figure S3.4: <i>Bf</i> growth in co-culture biofilms are delayed compared to <i>Bt</i>	87
Figure S3.5: Abundance of <i>Bf</i> in glucose co-culture biofilms in lumen and crypts.	88
Figure S3.6: Simulation of glucose concentration gradient along channels in the presence of flow	88
Figure S3.7: <i>Bf</i> growth was observed in downstream regions of the long channels under high flow	89
Figure S3.8: Less <i>Bt</i> cells were observed in biofilms grown under higher flow conditions	90
Figure S3.9: Flow produces a comet-like shape <i>Bt</i> biofilms at upstream positions	90
Figure S4.1: Recombinant expression of GHs BT3086, BT3087 and BT4581....	116
Figure S4.2: Growth curves of <i>Bt</i> WT and various PUL48 mutants in 3 different sizes of dextran over the course of 3 days.....	117
Figure S4.3: Growth of <i>Bt</i> double and triple GH mutants in 3 different sizes of dextran	119
Figure S4.4: Dextran uptake capacity of 10 kDa dextran by <i>Bt</i> WT and 3 PUL48 mutants	121
Figure S4.5: Visualization of dextran localization to <i>Bt</i> cells	122

List of Tables

Table S4.1: Dextran utilization knockout strains generated	96
Table S4.2: List of strains and plasmids generated for study	122
Table S4.3: List of primers used for study.....	126

List of abbreviations

PDMS	polydimethylsiloxane
BMM	Bacteroides Minimal Medium
TYG	Tryptone Yeast Extract Glucose Medium
BHI	Brain Heart Infusion
BHI-SB	Brain Heart Infusion supplemented with 10% sheep blood
<i>Bt</i>	<i>Bacteroides thetaiotaomicron</i>
<i>Bf</i>	<i>Bacteroides fragilis</i>
<i>Bo</i>	<i>Bacteroides ovatus</i>
<i>Bu</i>	<i>Bacteroides uniformis</i>
<i>Bv</i>	<i>Bacteroides vulgatus</i>
LC-MS	Liquid Chromatography Coupled to Mass Spectrometry
HPAEC	High Performance Anion Exchange Chromatography
PAD	Pulsed Amperometric Detection
RNA-Seq	RNA sequencing
GI tract	gastrointestinal tract
PULs	polysaccharide utilization loci
GH	glycosylhydrolase
sus	Starch utilization system
OD	optical density
FDR	false discovery rate
PBS	Phosphate buffered saline

Abstract

Bacteria often engage in social interactions with neighbouring bacteria. Ecosystems which are subjected to social interactions have been widely studied in well mixed settings such as test tubes, allowing us to identify the cellular components contributing to fitness. However, such growth condition does not resemble conditions in nature as bacteria often co-exist with defined spatial organizations. Furthermore, influences from common environmental forces such as fluid flow on bacteria growth is also neglected. For example, fluid flow may modulate the concentration landscape of public goods, limiting its dispersal to surrounding bacterial communities. Our aim is to systematically examine the impacts of fluid flow, relative spatial arrangement and biofilm morphologies on the fitness, metabolic activity, and organization of surface-associated bacterial communities. We chose to focus our work on the microbial communities found in human gut microbiota as the organization and abundance of member species can have a major impact on host health. To achieve this, we first developed a novel technique combining anaerobic microfluidics and fluorescence confocal microscopy which allowed us to identify that the *Bacteroides*, a common class of bacteria found within the gut microbiota, forms robust biofilms in flow. We then characterized the nutrient sharing capabilities of gut microbes by utilizing a model gut microbiota consisting of two species: *Bacteroides thetaiotaomicron* (*Bt*) and *Bacteroides fragilis* (*Bf*), where *Bt* metabolizes the polysaccharide dextran and cross-feeds its metabolic by-product glucose to *Bf*, which promotes *Bf* biofilm formation. By transporting this public good, flow structures the spatial organization of the community, positioning the *Bf* population downstream from *Bt*. We show that sufficiently strong flows abolish *Bf* biofilm formation by limiting the effective public good concentration at the surface. Physical factors such as flow may therefore contribute to the composition of intestinal microbial communities, potentially impacting host health. Finally, we also demonstrated that intrinsic properties of polysaccharides such as molecular weight impacts the rate of sugar metabolism by microbes and the extent of nutrient sharing within the community, which may lead to overall changes in community composition.

Keywords

Biofilms; microbial communities; metabolism; cross-feeding; polysaccharide utilization; gut microbiota; commensals; fluid flow; social interactions; nutrition

Chapter 1. Introduction

1.1 Biofilms

Bacteria have evolved to colonize almost every single surface possible on earth. Upon surface attachment, these bacteria often assemble into communities embedded in a self-produced matrix known as biofilms¹. In nature, biofilms play crucial roles from global biogeochemical cycling^{2,3} to the healthy functioning of the microbiota of multicellular organisms⁴. However, biofilms are great concern in the medical and industrial fields as they are also the main contribution to antibiotic-tolerant infections⁵ and the destruction of surfaces^{6,7}. A representative biofilm forming organism is the opportunistic pathogen *Pseudomonas aeruginosa* (*P. aeruginosa*), which is responsible for various infections, particularly in immunocompromised individuals⁸. *P. aeruginosa* infections became notorious in the field of medical sciences due to its biofilm forming capabilities, which often lead to antibiotic resistant infections. Due to this reason, *P. aeruginosa* serve as an important organism for studying the mechanisms and cycles of biofilm formation. The biofilm formation cycle of *P. aeruginosa* is highly complex and involves the initial attachment of cells to a surface, followed by the secretion of many matrix compounds including extracellular DNAs (eDNA), and three polysaccharide sugars: alginate, pel and psl⁹ (Fig. 1.1). The secreted matrix components serve critical functions in surface attachment, cell to cell adhesion, biofilm structure integrity, nutrient sequestering, and many other functions including protection against antibiotics¹ (Fig. 1.2). Although a lot is known regarding the biofilm formation of pathogens such as *P. aeruginosa*, little is known regarding the surface attachment and biofilm formation capabilities of commensal bacteria such as the *Bacteroides*, which are prominent members of the human gut microbiota. Having an understanding in the attachment and biofilm formation capabilities of individual species in the gut microbiota may provide a potential explanation to the varying abundances of individual species within the community, which has a major impact on host health.

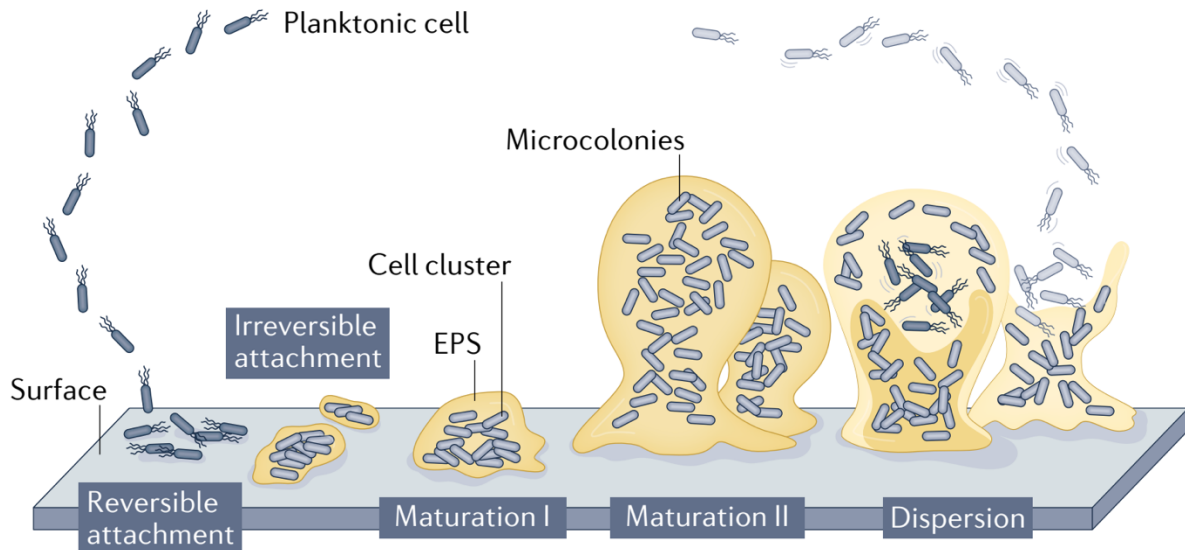


Figure 1.1¹⁰: The biofilm formation cycle of the human pathogen *P. aeruginosa*. Initially, planktonic cells attach to a surface, which triggers matrix production and the promotion of cell-cell adhesion, forming microcolonies. These microcolonies then develop over time to mature biofilms, where cells would eventually disperse from the biofilm and this process repeats.

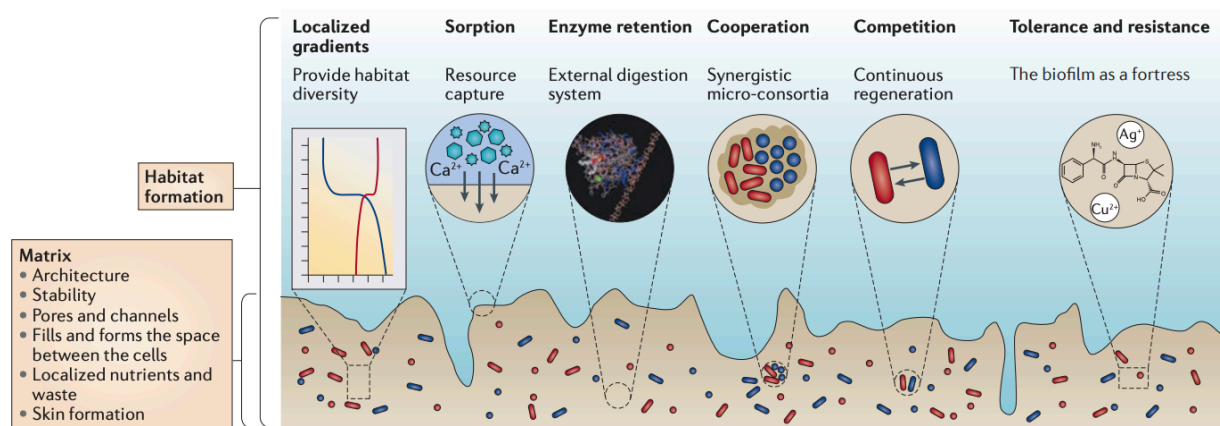


Figure. 1.2¹: The function and importance of the biofilm matrix. The matrix plays an integral role in maintaining biofilm architecture, nutrient capturing, promoting cellular-interactions and population diversity, and act as a fortress which protects cells from external threats such as antibiotics.

1.2 Social interactions and spatial organization in biofilm communities

Biofilm communities are often biologically diverse and complex in terms of composition¹¹. Cells within the biofilm community often interact and influence each other's fitness through social phenotypes¹². Under conditions of limited nutrients and space for expansion, competition dominates^{13,14}, where bacteria have evolved various strategies for the targeting and killing of direct competitors¹⁵. An example to such strategy includes the type VI secretion system (T6SS) in *Bacteroides fragilis*, a prominent member of the human gut microbiota, which kills antagonistic bacteria through toxin secretion (Fig. 1.3)^{16,17}.

T6SSⁱⁱⁱ mediates interbacterial antagonism

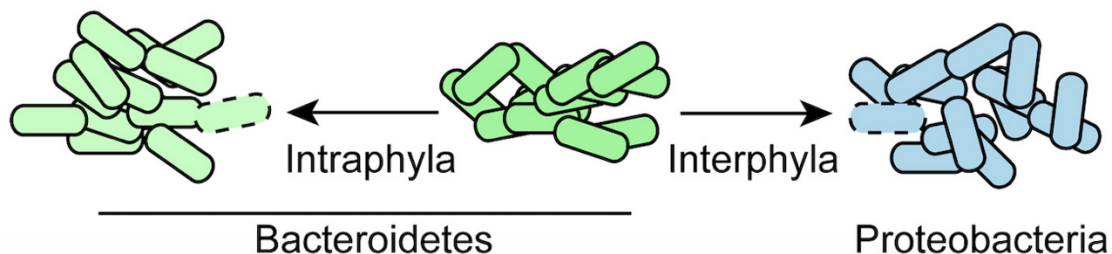


Figure. 1.3¹⁷: Type VI secretion system (T6SS) of *Bacteroidetes* mediates interbacterial killing. It was previously demonstrated that the T6SS of *Bacteroidetes* species are dedicated to intraphyla, which specifically only targets other species of bacteria within the phyla *Bacteroidetes*.

However, microbes also often engage in cooperative interactions which are beneficial to neighbouring cells and the overall community. For example, microbes within a community may cooperate and function as a single unit to perform complex metabolic processes such as nitrogen fixation¹⁸. Bacteria in the wild also commonly engage in symbiotic social interactions such as nutrient sharing: secreting and sharing metabolites including nutrient chelators¹⁹, digestive enzymes²⁰, and various signalling molecules²¹,

which minimizes the investment of energy required for cellular metabolism. These types of interactions often serve as the basis for the maintenance of biodiversity within a general community²². Although symbiotic interactions leading to coexistence within the nature are often well characterized, these cases of coexistences were never reproduced within laboratory settings¹⁸. As bacterial communities in the nature are often spatially organized, it is hypothesized that spatial organization of bacteria within a community plays crucial roles in mediating social interaction and subsequently the biodiversity of the community (Fig. 1.4)²³.

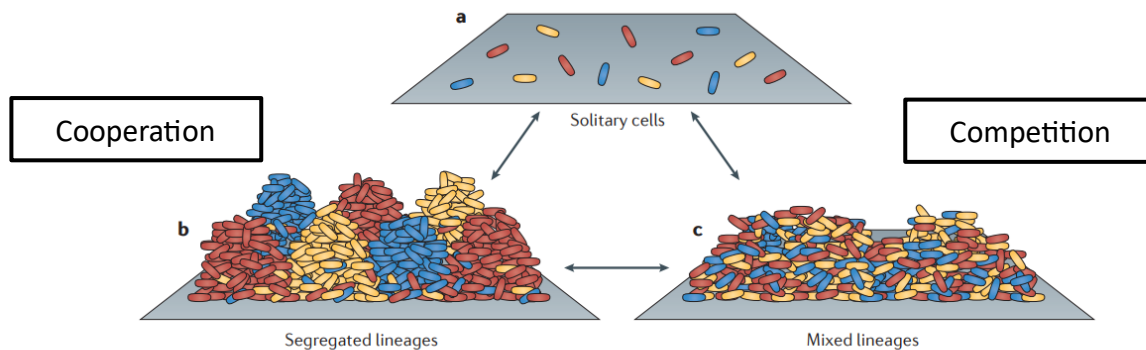


Figure. 1.4²³: Biofilms promote interspecies interactions. The extent of interspecies interactions is dependent on the structure of the biofilms, which in turn feeds back to affect interspecies interactions within the biofilm. In spatially structured biofilm communities with segregated lineages, commensalistic behaviours such as nutrient sharing dominates the community. However, in well-mixed biofilms of very dense populations, antagonism behaviours tend to be the most dominant form of social interaction.

Early computational and simulation efforts suggested spatial organizations as a key contributor to the maintenance of biodiversity within a community (Fig. 1.5)²⁴. It was also later confirmed through experimental works that spatial parameters such as interaction ranges²⁵ and spatial separations¹⁸ are crucial in the maintenance of biodiversity within a

community. Therefore, having a greater understanding of cell-cell interactions at the spatial scale may provide insight regarding the underlying mechanisms of how cells spatially organize, and how spatial organization feeds back to mediate interactions between cells, which may impact the biodiversity within the community.

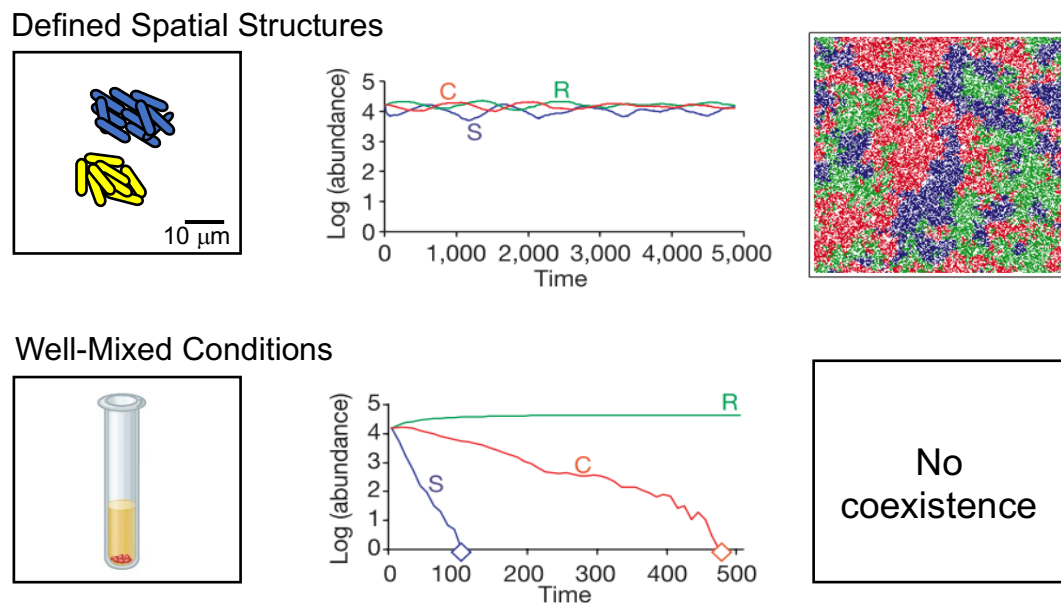


Figure 1.5²⁴: Simulation results indicate the importance of spatial organizations in the maintenance of biodiversity. (A) Simulated growth of an initially spatially organized neighbourhood resulted in stable co-existence between metabolically interacting species within the non-transitive community. (B) Simulated growth of a spatially disorganized system which resembles test tube conditions led to overall destabilization of the community and eventually loss of biodiversity.

1.3 Fluid flow and social interactions

To survive in the physical nature, bacteria would often have to interact with various environmental forces such as fluid flow. Physical forces likely play a key role in shaping the fitness of bacterial colonies through the introduction of mechanical stresses and redistribution of shared common goods²⁶. In the absence of fluid flow, nutrient access is strictly governed by diffusion. However, in the presence of flow, secreted metabolites

will be transported in the direction of flow, leading to changes in the chemical landscape of the ecosystem, which alters nutrient availability of secreted metabolites in the community (Fig. 1.6). Therefore, the physics of the environment would likely have an impact on the fitness of individual cells within a community.

Advances in technologies such as metagenomics provided insights regarding interactions between bacteria²³. However, information at the spatial scale are simply ignored due to technical difficulties associated with mimicking natural growth conditions in the lab setting. Therefore, little is known regarding how fluid flow impact social interactions and spatial organization between bacteria in nature. One common assumption is that metabolic and physical constraints are two independent variables driving bacterial evolution and regulation. Since it is known that local nutrient access is one of the key parameters for mediating stability in a bacterial community, where physical forces then act to alter such parameter, it is likely that fluid flow also plays an important role in mediating social interactions between microbes, therefore shaping the overall fitness of the community.

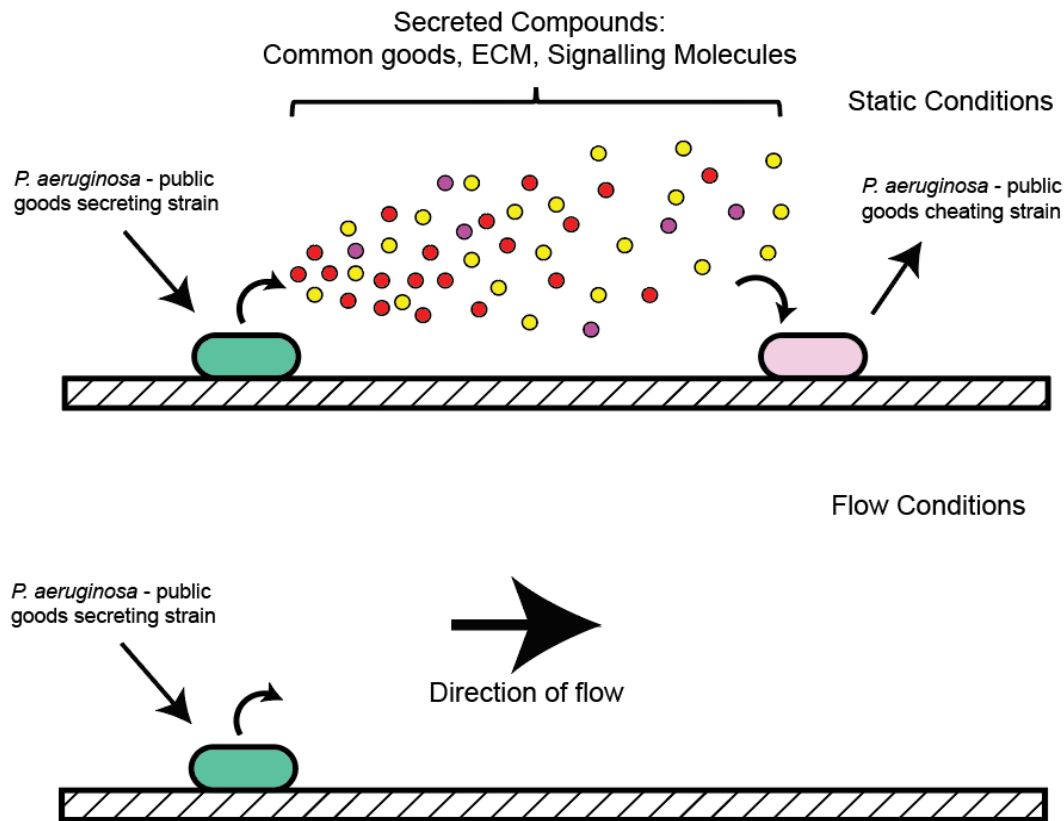


Figure 1.6: Fluid flow act to redistribute the concentration of common goods within the community. The redistribution of common goods leads to altering patterns of nutrient access and social interactions between microbes, which likely leads to differences in the spatial organization of the overall community.

1.4 Human gut microbiota

The human gastrointestinal (GI) tract is home to 10-100 trillion microorganisms termed the gut microbiota²⁷. The gut microbiota consists of various bacteria, archaea, fungi, and bacteriophages which are living in symbiosis with the human host²⁸. Recent advances in technologies including shotgun sequencing and bioinformatics toolboxes have made it possible to gain comprehensive insights of the overall composition of the gut community and their functional potentials²⁹. These large-scale omics studies revealed that in fact the gut microbiota plays important roles in host health: providing important microbial metabolites as signalling molecules³⁰ and energy source³¹ to the host, aid in complex

fibre digestion³² and training host immunity³³. Therefore, it is crucial to maintain a health composition of the gut microbiota.

The human microbiome of infants originate from birth, where it is predominantly passed on by the mother to infants³⁴. The maternally acquired microbiome is then further shaped by many environmental factors such as methods of milk feeding, weaning and the extent of antibiotic use³⁵. In the case of a healthy adult, the most abundant members of a healthy gut microbiota are bacteria from the genus *Prevotella* and *Bacteroides*³⁶. While the microbiota of healthy individuals tend to follow similar trends within families, the gut microbiota composition is also known to differ significantly across healthy individuals of differing geographic space and culture³⁷. These differences are believed to arise as a result of differences in environmental factors such as lifestyle and diet³⁷.

Diet is a key factor influencing the composition and diversity of the gut microbiota, shifting the microbiota towards populations which favours selected nutrients³⁸. For example, diets containing high fibre content increases the abundance of *Bacteroides spp.*, which are prominent complex fibre degraders³⁹. While high fat diets in general leads to the decrease in *Bacteroidetes* and an increase in *Firmicutes* abundance, which is a marker for dysbiosis, a term used to describe an imbalanced gut microbiota, often associated with chronic diseases such as obesity (Fig. 1.7)⁴⁰. Therefore, to ensure the proper functioning of the gut microbiota which confers to host health, it is important to maintain both a healthy lifestyle and diet.

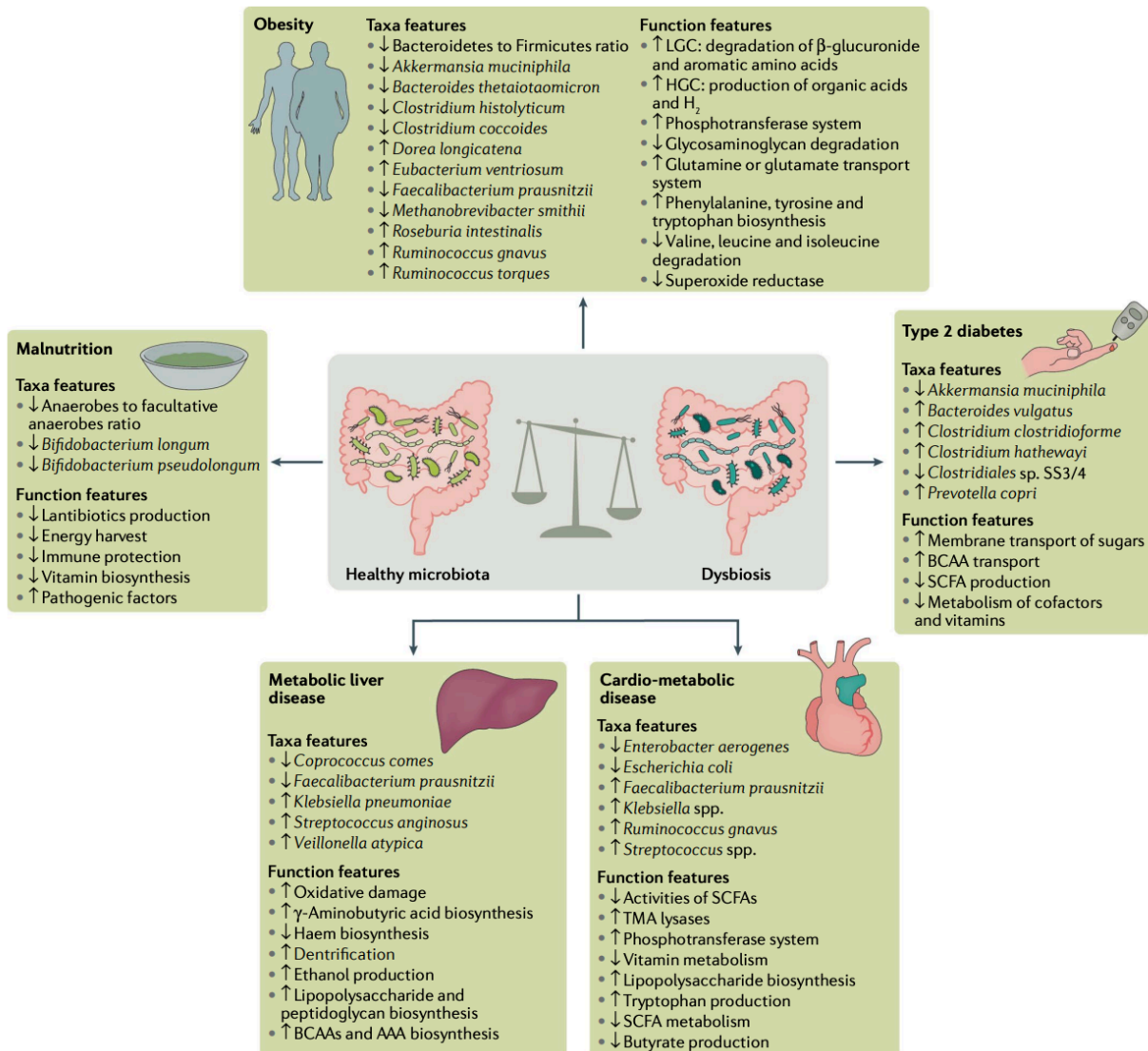


Figure 1.7²⁹: Gut microbiota and diseases associated with dysbiosis. Unhealthy lifestyles and diet may lead to dysbiosis, an imbalance in microbial population of the gut microbiota, which are associated with diseases such as malnutrition, obesity, type 2 diabetes, metabolic liver disease and cardio-metabolic disease.

1.5 Motivation and aims of the thesis

Bacteria have evolved to colonize almost every single surface possible on earth through the formation of biofilms. For example, gut commensals have evolved to colonize the biologically and physically complex mucosal environment. Since bacteria survive in the

physical nature, they would often have to interact with various environmental forces such as fluid flow in the colon. Physical forces likely play a key role in shaping the fitness of bacterial colonies through the introduction of mechanical stresses and redistribution of shared common goods in nutrient sharing communities. However, an overall understanding to how commensal bacteria form biofilms and how mechanical forces such as fluid flow define the composition and organization of the gut community is lacking, which likely has a significant role in defining host health.

During my PhD, I first studied the biofilm formation capabilities of commensal gut microbes in fluid flow. To achieve this goal, I developed an anaerobic microfluidics based technique which allowed for the growth of biofilms under anaerobic environments. I then used 4 model gut microbiota *Bacteroides* species: *Bt*, *Bf*, *Bo* and *Bv* as my model organisms for anaerobic biofilm formation, tested their biofilm formation capabilities and studied their varying morphologies in my microfluidics setup. I then attempted to understand further the mechanisms behind the biofilm formation of these anaerobic biofilms by proteome and transcriptome analysis. Finally, I also studied the impact of environmental factors such as carbon source on the morphologies of *Bacteroides* biofilms. All experiments and detailed results are outlined in **Chapter 2** of this thesis.

Since the *Bacteroides* attached to surfaces and formed biofilms *in-vitro* under anaerobic conditions, I then proceeded to study the possibilities of nutrient sharing within the gut microbiota community. To achieve this goal, I constructed a model gut microbiota consisting of two species: *Bt* and *Bf* and performed polysaccharide screening for complex carbohydrate conditions where nutrient sharing may happen between these two species. I identified a candidate polysaccharide in dextran, which is readily utilized by *Bt* but not *Bf*, where I analyzed the metabolic by-products released by *Bt* dextran metabolism, along with the common good molecule which is shared to *Bf*. I then studied how fluid flow may impact the organization of a nutrient sharing community by subjecting *Bt-Bf* co-culture biofilms in dextran to various flow rates and studying their

spatial organizations. All experiments and detailed results are outlined in **Chapter 3** of this thesis.

I then sought to further understand the molecular mechanisms of dextran utilization and nutrient sharing by *Bt*. To achieve this, I analyzed the proteome of *Bt* grown in dextran versus in glucose and identified a cluster of proteins belonging to polysaccharide utilization locus 48 (PUL48) which were significantly upregulated in dextran growth. I then generated a mutant library of *Bt*, consisting of genetic knockouts of these genes and assessed the growth of individual mutants in dextrans of various sizes to determine the impacts of individual proteins and initial dextran polymer size on *Bt* dextran metabolism. Finally, I wanted to explore how individual PUL48 associated proteins impact the nutrient sharing from *Bt* to *Bf* and whether *Bf* contributes back to *Bt* for the shared nutrients. In this direction, I co-cultured *Bt* mutants with *Bf* and analyzed the abundance of *Bf* through a microscopy-based cell counting assay. I then performed proteome analysis of *Bf* grown in *Bt* spent medium, which may provide insights to metabolic and phenotypic changes of *Bf* under conditions of nutrient sharing. More detailed descriptions of these results are available in **Chapter 4** of the thesis.

Overall, throughout my PhD, I developed a platform which allowed for the growth and observation of biofilms grown under anaerobic conditions. I successfully cultured the gut microbiota *Bacteroides* species *in-vitro* as biofilms, studied their morphologies and identified potential target genes which may contribute to the biofilm formation and structure maintenance of these anaerobes. I then confirmed the presence of nutrient sharing between two gut microbiota species, *Bt* and *Bf*, and illustrated how physical forces such as fluid flow may impact the organization of nutrient sharing biofilm communities through the distribution of public goods. At the molecular level, I examined the roles of individual PUL48 proteins and initial polysaccharide polymer size on *Bt* dextran utilization and subsequent nutrient sharing.

Chapter 2. Biofilm formation by the gut microbiota

Bacteroides

This chapter focuses on the development of methodology for the growth of bacterial biofilms in anaerobic conditions using *Bacteroides* as our model organisms. The potential of biofilm formation by these gut commensals were then assessed, along with the structures and morphologies of biofilms formed by different *Bacteroides* species.

2.1 Abstract

In the nature, bacteria often colonize surfaces as communities embedded in a self-produced matrix known as biofilms. Biofilms are known to play important roles in maintaining the stability of the overall microbial community through the promotion of interspecies co-metabolism and offering protection against antibiotics. The human gut microbiota is an ecosystem which is densely populated by commensal microbes which are crucial for host health. Although the roles of the gut microbiota had been immensely studied in recent years, these studies often focused on the impact of host nutrition on the composition of the gut microbiota and its impact on the host, often neglecting the question of how these bacteria colonize and form mucous associated biofilms in the gut. Therefore, in this work, we developed a method for the growth of anaerobic biofilms with the aim of further understanding the surface colonization and biofilm formation dynamics of anaerobic gut commensals. Using the *Bacteroides*, a family of highly abundant gut microbes as our model organism, we observed that these anaerobic bacteria attaches to surfaces and forms biofilms of highly varying structures which are species and nutrient specific.

2.2 Additional background

In the wild, microorganisms often co-colonize surfaces, forming complex surface attached communities termed biofilms²³. Within biofilms, various residence species often function as a unit owing to their abilities to socially interact with one another⁴¹. Often embedded in a self-secreted extracellular polymeric matrix, the biofilm lifestyle also offer residence bacteria advantages including protection against external threats such as antibiotics¹. Due to this reason, biofilms are of serious global health concern due to their abilities to tolerate antibiotics, playing crucial roles in persistent chronic infections in hospitals^{42,43}, a major problem in modern day society.

Due to its role in antibiotic resistance, many research efforts have been made with the goal of further understand the mechanisms behind biofilm formation by pathogenic bacteria. One of the model organism for biofilm formation is the pathogen

Pseudomonas aeruginosa, which commonly infects the lungs of cystic fibrosis patients⁴⁴. *P. aeruginosa* utilizes extracellular appendages called type IV pili to initially attach to and colonize surfaces⁴⁵. Upon initial attachment, this signal is then transduced and amplified through a chemosensory system which alters the metabolism of the cell, leading to the transcription of various virulence genes and biofilm inducing pathways⁴⁶. *P. aeruginosa* also secrete at least 3 extracellular polysaccharides alginate, Pel and Psl, which plays critical roles in the surface attachment and structural development of *P. aeruginosa* biofilms^{47,48}. Similarly, it had been previously demonstrated that pili plays important roles in the biofilm formation by other pathogens such as *Escherichia coli*^{49,50}, and *Clostridium difficile*⁵¹, whereas the production of extracellular matrix components are important for the architecture of *Vibrio cholerae* biofilms⁵². The overall architecture and structure of biofilms also plays an important role in antibiotic susceptibility, where in *P. aeruginosa*, dome shaped biofilms were more resistant to antibiotics in comparison to biofilms which are more flat⁵³.

Although a lot is known regarding biofilm formation by pathogenic species, in contrast, very little research has been performed to date regarding biofilm formation mechanisms by symbionts. The human gastrointestinal (GI) tract hosts dense communities of symbiotic microorganisms termed the gut microbiota, which contributes significantly to the human physiology, playing critical roles in host metabolism, nutrient absorption and resistance to diseases^{54,55}. Despite our current knowledge on the importance of diet⁵⁶ in the regulation these commensal bacteria which confers host health, little is known regarding the roles of initial attachment, colonization and biofilm formation by these commensals on the relative abundance and composition of the gut microbiota. One of the most abundant genus of bacteria residing in the human colon are the *Bacteroides*³⁶. Just like most pathogenic bacteria, the *Bacteroides* also possess cell-surface associated appendages including pili and fimbriae⁵⁷. These pili had been structurally characterized to be distinct from typical Type IV pili⁵⁸, and was previously shown to contribute to the biofilm forming capacity by *Bacteroides thetaiotaomicron*⁵⁹. However, the overall role of various pili and fimbriae in the adhesion and subsequent biofilm formation by *Bacteroides* remain unclear. On the cell surface, *Bacteroides* also produce

capsular polysaccharides (CPS), which plays important roles in protecting the bacteria from host immune responses and antibiotic perturbations, offering them an advantage in the colonization of the host environment⁶⁰. It has also been previously demonstrated that CPS has potential roles in mediating biofilm formation *in-vitro*⁶¹. In this work, we sort to further understand the mechanisms of surface colonization and biofilm formation by anaerobic gut microbes. Using four species of *Bacteroides* as our model organisms: *Bacteroides thetaiotaomicron*, *Bacteroides fragilis*, *Bacteroides ovatus* and *Bacteroides vulgatus* with the combination of fluorescence microscopy and proteome/ transcriptome analysis, we identified that different members of the *Bacteroides* formed biofilms of highly varying architecture *in-vitro*. We also observed the upregulation of various fimbriae in both *Bt* and *Bf* biofilms, which highlights the potential importance of extracellular appendages in the biofilm formation by gut microbes.

2.3 Results

2.3.1 *Bacteroides* form unique biofilms in TYG medium

To characterize the biofilm formation capabilities of *Bacteroides* species in flow, we assembled microfluidic growth devices inside the anaerobic chamber. We first seeded *Bt* constitutively expressing sfGFP in the microchannels, flushed unattached cells and initiated growth for 3 days under constant flow of Tryptone – Yeast Extract – Glucose (TYG) medium (Fig. 2.1A). To visualize colonization patterns, we imaged the biofilms using spinning disc confocal microscopy after 2 hours of aerobic incubation. *Bt* formed tightly packed, surface attached comet like multicellular structures in the presence of flow in TYG medium (Fig 2.1A). At the head of the comets, these biofilms extends roughly 10-15 μm above the coverslip surface. With the same setup, we then seeded *B. ovatus* (*Bo*) constitutively expressing sfGFP in our microfluidic device and allowed the biofilm to grow anaerobically for 3 days. We observe that like *Bt*, *Bo* also could colonize the glass coverslip surface and formed a biofilm. The biofilm of *Bo* appeared more elliptical in shape in comparison to *Bt*, and the *Bo* aggregates seem to be packed less tightly in comparison to *Bt* (Fig 2.1B).

We then further extended our biofilm growth protocol to two other species of *Bacteroides*: *Bacteroides vulgatus* (*Bv*) and *Bacteroides fragilis* (*Bf*). We observed that the biofilms of *Bv* are drastically different in comparison to *Bt* and *Bo* in TYG medium. Instead of forming clump like aggregates, *Bv* attaches to surfaces and forms unique, elongated barbwire like structures (Fig 2.1C). Zoomed in images show that these barbwires are formed as a result of cell-cell adhesion between subsequent *Bv* cells (Fig 2.1D), leading to a formation of large, thin, and elongated “barbwire” features which have not been previously observed. In the case of *Bf*, we observed again that *Bf* form unique biofilms in TYG medium under flow in comparison to *Bo*, *Bt* and *Bv*. *Bf* biofilms appear shockingly as thick bundles of filaments. Confocal fluorescence imaging reveals that these biofilms attach to a small area on the glass surface and extends 3-dimensionally as thick bundles of thick filaments (Fig 2.1E).

Overall, our data suggest that members of the *Bacteroides*: *Bt*, *Bo*, *Bv* and *Bf* all have the potential of attaching to surfaces and forming biofilms under the constant flow of the nutrient rich TYG medium. With our microfluidics based anaerobic biofilm growth set-up, we were also able to assess the morphologies of different anaerobic *Bacteroides* biofilms and observed that *Bt*, *Bo*, *Bv* and *Bf* all formed biofilms of unique and exotic morphologies, where *Bv* and *Bf* formed surface attached biofilms which resembled elongated barbwires and bundles of filaments respectively. The differences in morphologies suggest highly varying mechanisms in biofilm formation across different species within the *Bacteroides* genus of gut commensal bacteria, and such differences may have a potential impact on the overall colonization and abundance of different bacteria within the gut microbiota which in turn can have a major impact on the overall ecology of the ecosystem.

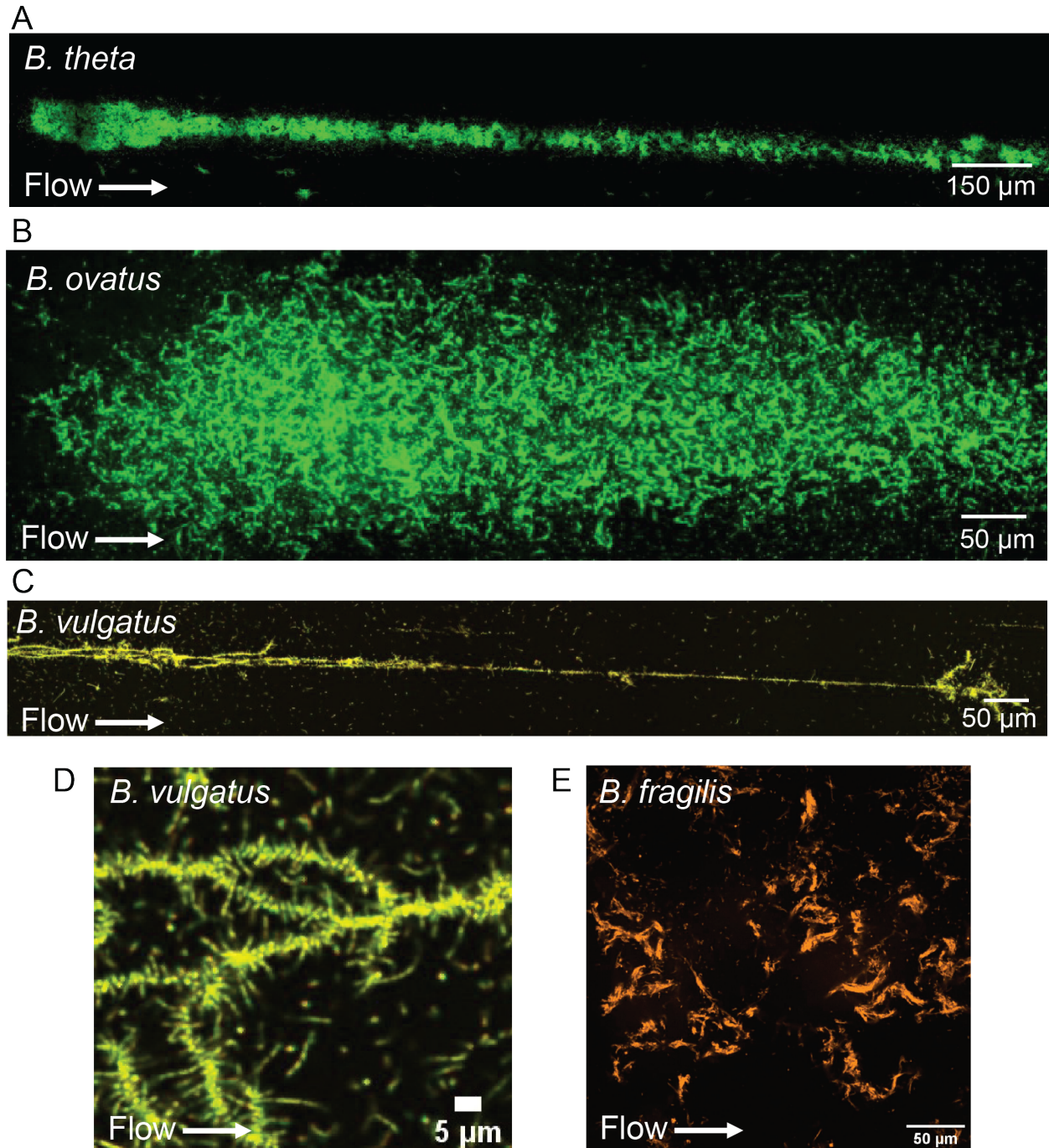


Figure 2.1: *Bacteroides* species form biofilms in flow under nutrient rich conditions. (A) Biofilm from *Bt* constitutively expressing sfGFP. (B) Biofilm from *Bo* constitutively expressing sfGFP. (C) Biofilm from *Bv* constitutively expressing sfGFP and mCherry. (D) Close-up view of *Bv* biofilms show the cell-to-cell adhesion by *Bv* which leads to the formation of barbwire like features. (E) Biofilm from *Bf* constitutively

expressing mCherry show large *Bf* aggregates in the form of large filaments which extends in the third dimension. All biofilms were grown anaerobically for 3 days under flow of TYG medium. All biofilms were grown anaerobically for 3 days at the flow rate of 2 μ L/min.

2.3.2 Proteins upregulated in biofilm formation by *Bt*

It has been previously demonstrated that cellular components such as pili and fimbriae potentially contribute to the cohesion of *Bt* and *Bf* biofilms⁶². However, these studies were performed only on defined pili gene targets and an overall picture of the gene expression profile of *Bt* in biofilm state is still lacking. With the goal of further understanding the proteins important for biofilm formation by *Bt*. We therefore compared the proteomes of *Bt* growing in liquid cultures versus as a flow-cell biofilm in TYG medium. Differential expression analysis shows that *Bt* upregulates a group of proteins when grown in the form of a biofilm (Fig. 2.2). These proteins are all encoded in a defined region of the *Bt* genome (from BT4226 to BT4236). Some of these upregulated proteins include BT4226 (FimB-like protein), BT4227 (FimC like protein), BT4233 (DUF3868 domain-containing protein), BT4236 (CheY like protein) and BT4234 (FimX like protein). These data suggest that *Bt* upregulates the production of extracellular fimbriae which potentially promotes surface adhesion and biofilm formation. The presence of the two-component system sensor histidine kinase/response regulator CheY like protein also suggests the existence of signal sensing and transduction upon surface binding in *Bt*.

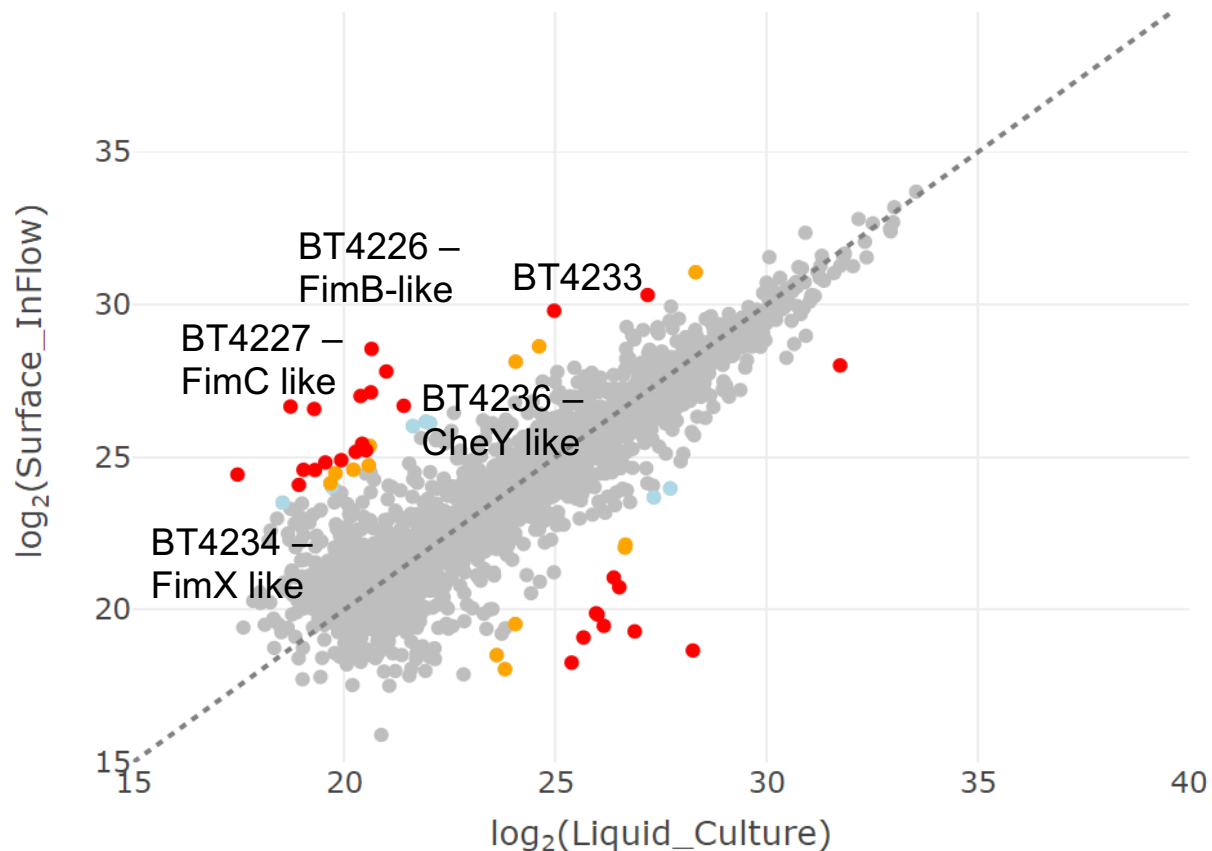


Figure 2.2: Proteomic analysis of *Bt* growing as a biofilm versus in liquid culture in TYG medium. We identified a cluster of genes between BT4226 and BT4236 which were upregulated in *Bt* biofilms. ($N = 1$)

2.3.3 Mechanisms of biofilm filamentation by *Bf*

Recall, *Bf* forms biofilms which resembles thick bundles of filaments extending in the third dimension (Fig. 2.1E), which are strikingly different in comparison to *Bt* and *Bo* biofilms. This raised the question of what contributes to such drastic differences in terms of biofilm morphology between *Bt* and *Bf*. We hypothesized based on the appearance of the *Bf* filamentous biofilms that *Bf* forms thick bundles of filaments through the promotion of cell-to-cell adhesion. Therefore, just like with *Bt*, we performed differential analysis on the proteome of *Bf* grown as filamentous biofilms versus as a liquid culture (Fig. 2.3A). We again observed a series of proteins belonging to a similar region of the

Bf genome which is highly upregulated when it is grown as a biofilm (BF9343_1395-1420). The functions of these individual proteins are highlighted in the supplementary information (Fig. S1.1). Unfortunately, the genome of *Bf* NCTC-9343 is nowhere as well annotated as the *Bt* genome, but based on current available annotations, many of these proteins have predicted functions of either as conjugal transfer proteins (BF9343_1413 and BF9343_1417) or as fimbrillin family proteins (BF9343_1407-1410). Interestingly, the proteins BF9343_1407 and BF9343_1408 resembles the structure of fimbrillin subunit proteins, and BF9343_1409 resembles the structure of a fimbrillin tip protein, along with a glycan binding domain. These data suggest that *Bf*, like *Bt*, also upregulates the production of extracellular fimbriae under conditions of biofilm formation. In the case of *Bf*, the upregulation of proteins responsible for conjugal transfer and fimbriae suggests a potential mechanism to filament formation by *Bf*, where it utilizes fimbriae dedicated to DNA transfer for the adhesion to subsequent *Bf* cells while growing as a biofilm, promoting the formation of thick bundles of fibres through cell-cell adhesion, and the transfer of DNA across the subpopulation of *Bf* cells growing as a biofilm.

To further confirm that these upregulated genes are indeed upregulated in the process of biofilm formation, we performed RNA sequencing (RNAseq) to compare the transcriptome of *Bf* grown as a biofilm versus in liquid culture as RNAseq also provides the opportunity for higher sequence coverage. We then compared our RNAseq data with the proteomics data and observed the exact same cluster of proteins being highly upregulated when *Bf* was grown as a flow-cell biofilm (Fig. 2.3B). Therefore, these data further confirms that the proteins BF9343_1395-1420 are indeed upregulated in *Bf* biofilms. Overall, our results suggest a potential mechanism in biofilm formation by *Bf*, where it assembles into thick bundles of filament via the upregulation of a series of fimbrillin proteins which promotes cell-cell adhesion.

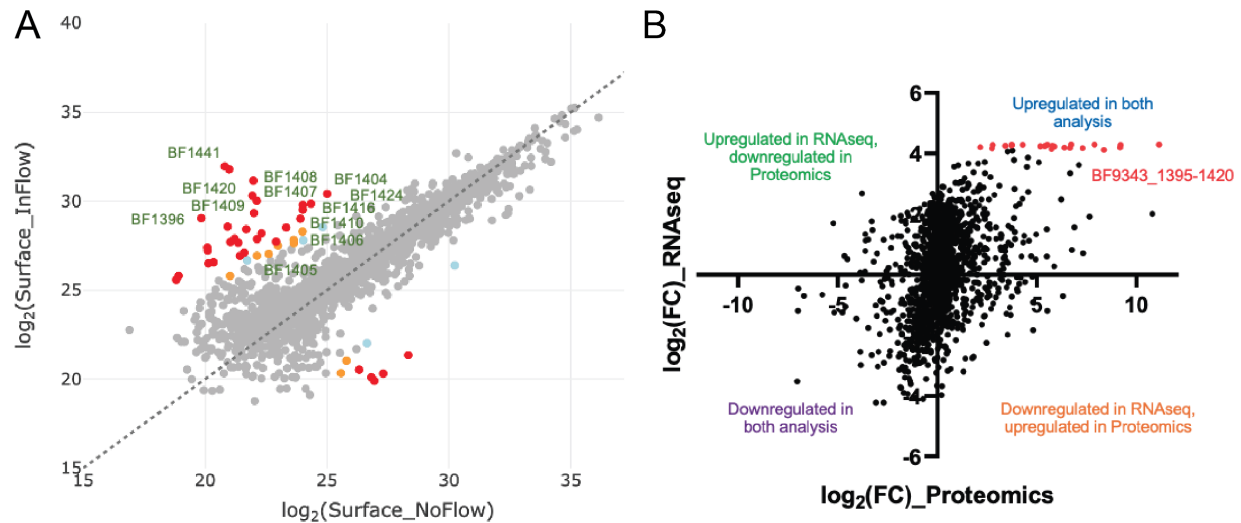


Figure 2.3: Differential expression analysis of *Bf* growing as a biofilm versus in liquid culture in TYG medium. (A) We identified a cluster of genes between BF9343_1395-1420 which were upregulated in *Bf* biofilms by proteomic analysis. (B) Comparison of differential expression profiles of *Bf* biofilm growth versus liquid growth through proteomics and RNAseq. BF9343_1395-1420 were identified as targets upregulated in *Bf* biofilms in both LC-MS based proteomic and RNAseq experiments. ($N = 1$)

2.3.4 Duo-species *Bacteroides* biofilms in TYG medium

We then wondered how these species assemble into stable multi-species biofilm communities which resembles the gut environment. Based on the species specific and unique biofilms we observed in our mono-species biofilm data we hypothesize that these species will retain these growth features and grow independently in the presence of other species in nutrient rich settings, where the sole limitation to growth being the competition for space. To test this hypothesis, we grew duo-species biofilms of various combinations of *Bt*, *Bf* and *Bo* in TYG medium.

First, we mixed *Bt* sfGFP and *Bf* mCherry at a 1:1 ratio and allowed the biofilm to grow anaerobically in flow for 3 days. We then imaged the biofilm from the inlet towards the outlet, covering the full length of a single elongated *Bt* biofilm (Fig. 2.4A). We observe

that *Bt* and *Bf* tend to grow individually with minimal mixing (Fig. 2.4A). We then zoomed into a region of interest covering the interface between *Bt* and *Bf* biofilms and observed that *Bf* barely mixes with *Bt* as a coculture in TYG medium as a boundary between the two species is clear (Fig. 2.4B). Interestingly, *Bt* and *Bf* both retain their biofilm morphology as a mono-species biofilm under a coculture setting, where *Bt* forms comet like elongated biofilms, where *Bf* filaments and extends in the third-dimension. Although a growth boundary between *Bt* and *Bf* is clear, *Bf* appear to be capable of adhering to the edges of the tightly packed *Bt* biofilm. To study this, we further zoomed in on the coculture biofilm at the single single-cell level by imaging the biofilm with the 100x objective with the confocal fluorescence microscope. We observed clearly that *Bf* filaments are formed as a result of *Bf*-*Bf* cell-to-cell adhesion (Fig. 2.4C). We also observed *Bf* localizing to the edges of *Bt* single cells, suggesting that *Bf* are not only capable of adhering to adjacent *Bf* cells, but they may also adhere to neighbouring *Bt* cells (Fig. 2.4C). Overall, our results demonstrate that *Bt* and *Bf* grows independently of each other under the nutrient rich TYG medium.

In a similar manner, we then attempted to mix *Bt* mCherry and *Bo* sfGFP in a one to one ratio and cocultured these species together a duo-species biofilm (Fig 2.4D). Again, we observe that *Bt* and *Bo* do not mix when grown in the nutrient rich TYG medium, where growth boundaries between *Bt* and *Bo* are again apparent. *Bo* was observed to be less abundant in comparison to *Bt* and surrounded completely by *Bt* cells. This may be attributed to a higher growth rate in *Bt*, which puts *Bt* at an advantage in terms of space competition. Finally, we grew a duo-species biofilm consisting of *Bf* mCherry and *Bo* sfGFP. We observe that *Bo* forms a loose carpet biofilm close to the surface, where *Bf* forms bundles of thick filaments which extends in the third-dimension (Fig. 2.4E). Overall, our results suggest that *Bacteroides* species grows independently on one another as a co-culture under a nutrient rich setting, where inter-species mixing is minimal. The growth morphology of independent species is also conserved under a co-culture setting, suggesting that the presence of other species have minimal impact on how these bacteria form biofilms individually. Finally, the abundance and distribution of individual species are also defined by the competition for space, where the faster

growers outcompete slower growers in the case of *Bt Bo* co-cultures. The unique ability of *Bf* forming long filament which extends 3D may provide them with an advantage to competition for space and nutrients.

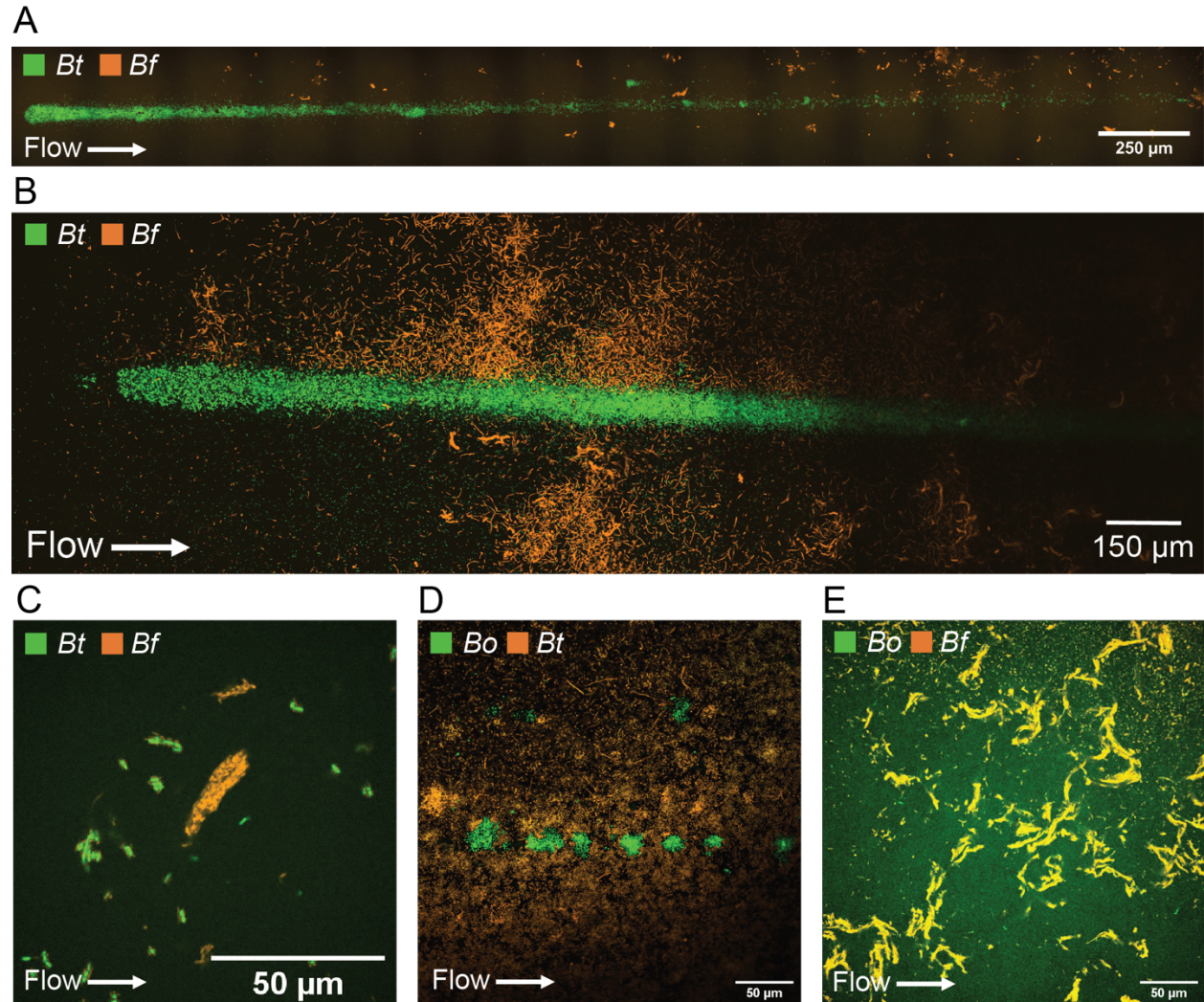


Figure 2.4: Duo species *Bacteroides* biofilms in flow under nutrient rich conditions. (A) Full biofilm view of a *Bt Bf* co-culture biofilm (B) Zoomed in view of a *Bt Bf* co-culture biofilm. A boundary between *Bt* and *Bf* growth was observed. (C) Single cell imaging of a *Bt Bf* co-culture biofilm. *Bf* cells not only adhere to each other to form filaments, but they can also localize to *Bt* cells. (D) *Bt Bo* co-culture biofilm. The degree of mixing between *Bt* and *Bo* is minimal, where *Bt* outcompetes *Bo* in terms of competition for space, leading to *Bo* colonies being completely surrounded by *Bt* (E) *Bf*

Bo co-culture biofilm. *Bo* localizes to the surface, forming loose carpets, where large filaments of *Bf* attach on top and grows in the third dimension. All biofilms were grown anaerobically for 3 days under flow of TYG medium. All biofilms were grown anaerobically for 3 days at the flow rate of 2 μ L/min.

2.3.5 Nutrient source impacts biofilm morphology

As we observed no changes to individual species' biofilm morphology when grown under co-culture conditions, we then wondered whether nutrient sources may have an impact on the biofilm morphology and abundance of *Bacteroides* species. As these bacteria are wide-range polysaccharide utilizers, we decided to test this hypothesis by growing biofilms in *Bacteroides* Minimal Medium (BMM) supplemented with various polysaccharide sources and observing the final biofilm morphologies by confocal fluorescence microscopy. With our anaerobic microfluidics-based biofilm setup, we first grew *Bt*, *Bf* and *Bo* as mono-culture biofilms in BMM supplemented with the simple monosaccharide glucose. We observe that *Bt* grows into dense, elongated biofilms of similar morphology to those grown in TYG medium which also contains glucose as a carbon source (Fig. 2.1A and 2.5A). *Bo* also grows into a biofilm in BMM glucose resembling the morphology of that which is grown in TYG medium (Fig. 2.1C and 2.5B). Based on the results from *Bt* and *Bo*, we then expected *Bf* to also form filamentous biofilms in BMMG like that observed in TYG medium. However, this was not the case. Instead, *Bf* formed surface attached comet-like biofilms which resembles that of *Bt* in BMMG and TYG medium (Fig. 2.5C). These results together suggest that the impact of carbon source on *Bacteroides* biofilm growth and structures is species dependent. Based on the biofilm morphologies of *Bf* observed in TYG medium and BMMG, carbohydrate sources are not the sole contributor to changes in biofilm morphologies as *Bf* formed filamentous biofilms in TYG medium but did not do so in BMMG.

We then proceeded to increase the complexity of the carbohydrate source to test whether *Bacteroides* species can form biofilms under conditions with complex polysaccharides being the main nutrient source, resembling the gut environment upon

host diet. We chose to work with the complex carbohydrate arabinan to test this hypothesis as arabinan is isolated from sugar-beets which resembles dietary fibre and it is relatively soluble in water in comparison to other complex carbohydrates. Therefore, we substituted the glucose in BMMG with arabinan from sugar-beet to generate the BMMA medium, which we then used to culture *Bt* and *Bf* as monocultures anaerobically for 3 days. We observed that *Bt* can form biofilms in arabinan, consistent with previous works which demonstrated the presence of an arabinan utilization locus in *Bt*⁶³. *Bt* biofilms in arabinan appear to be more clumpy and less elongated in comparison to BMMG and TYG growth (Fig. 2.5D). *Bf* on the other hand, failed to grow into a biofilm in arabinan although minimal growth was observed perhaps to due small molecule contaminations within the arabinan source (Fig. 2.5E). These results together demonstrate that carbohydrate sources not only have an impact on the overall abundance of individual species within a biofilm community due to utilization capabilities but can also introduce changes to biofilm morphologies.

As we observed *Bt* growth in the form of a biofilm in BMMA, but not of *Bf*, we then wondered whether there is the possibility of nutrient sharing through *Bt*'s metabolism of arabinan to *Bf*. To test this hypothesis, we mixed *Bt* and *Bf* at a 1:1 ratio and cultured them for 3 days anaerobically in BMMA. In the co-culture biofilm, we observed *Bt* being the dominant species, along with several minor *Bf* colonies with no significant increase in abundance compared to the mono-species growth (Fig. 2.5F). Overall, our results demonstrate the importance of carbohydrate sources in defining the abundance of species within a *Bacteroides* biofilm community along with the overall biofilm structures and morphologies. We also demonstrate through *Bt* arabinan utilization and biofilm formation that nutrient sharing is not guaranteed between *Bacteroides* species.

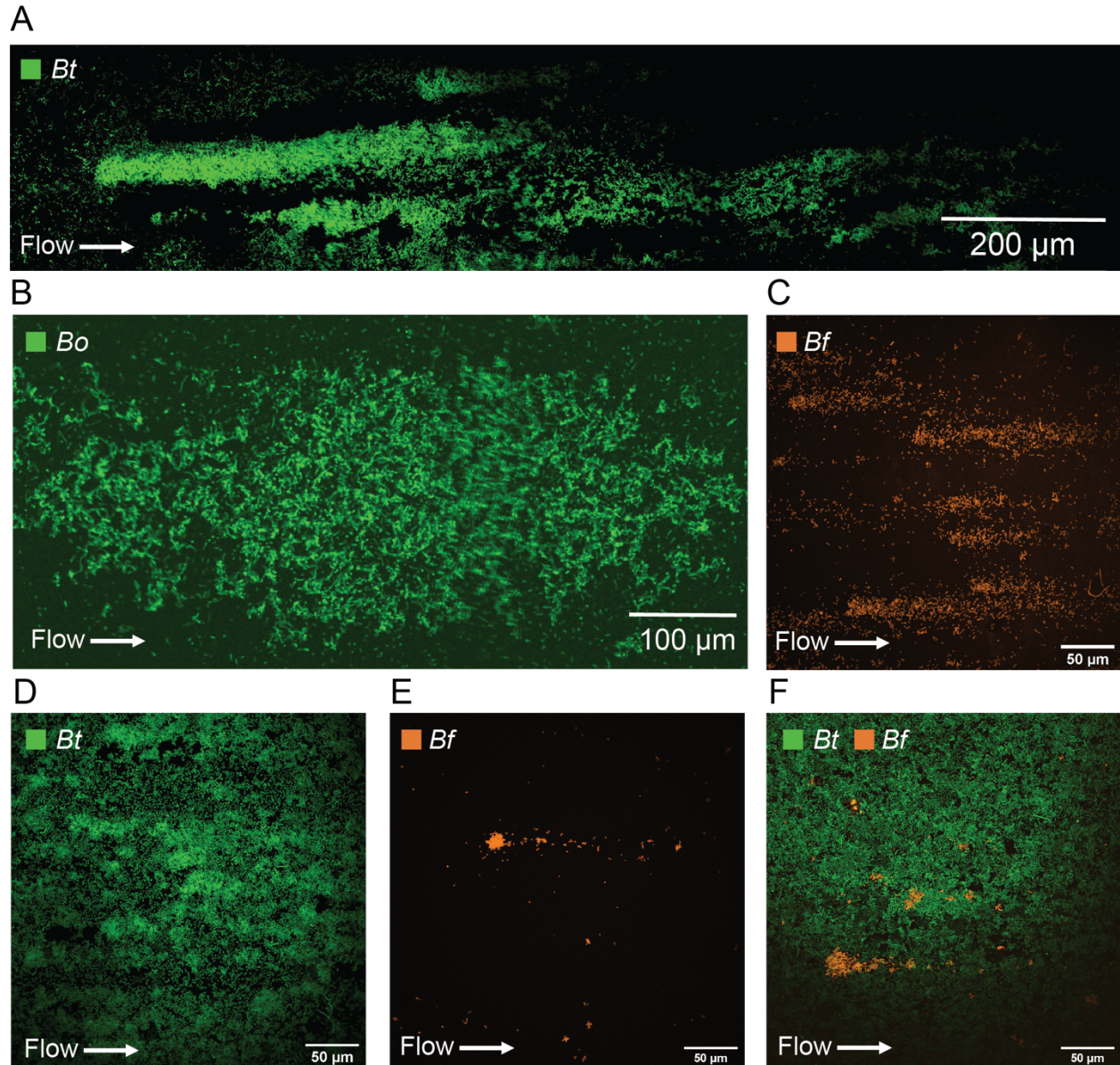


Figure 2.5: *Bacteroides* biofilms in flow under minimal medium conditions with various carbohydrate sources. (A) Biofilm of *Bt* in BMM-glucose. (B) Biofilm of *Bo* in BMM-glucose. (C) Biofilm of *Bt* in BMM-glucose. Bundles of filaments observed in TYG medium growth were not observed under minimal medium conditions. (D) *Bt* forms biofilms in BMM-arabinan. (E) *Bf* fails to form biofilms in BMM-arabinan. (F) *Bt*-*Bf* co-culture biofilm in BMM-arabinan. *Bf* growth is not rescued by the presence of *Bt*, suggesting the absence of nutrient sharing from *Bt* to *Bf* in arabinan. All biofilms were grown anaerobically for 3 days under flow of BMMG or BMMA medium. All biofilms were grown anaerobically for 3 days at the flow rate of 2 μ L/min.

2.4 Discussion

In the intestine, commensals form dense and organized communities associated with the mucosal surface⁶⁴. Amongst the high variety of bacteria present in the gut, the *Bacteroidetes* emerge as one of the most abundant phyla of bacteria found in the human gut microbiota⁶⁵. Although the overall mechanisms behind their high abundance in the human hosts remain unclear, it is believed that their strong evolutionary adaptation to the gut environment: the ability to utilize host- and plant- derived complex glycans⁶⁶ and the ability to establish long-term mutualistic relationship with the host⁶⁷ plays important roles in their colonization success. However, one factor which is overlooked is the surface colonization and biofilm formation capabilities of these bacteria under flow conditions resembling the human colon. As differences in surface attachment and biofilm formation can have a direct impact on the abundance and fitness of a species within a community, we sort to investigate biofilm formation by *Bacteroides* species. To address this problem, we developed an anaerobic microfluidics biofilm growth protocol which allowed us to grow and study the biofilm formation by anaerobic species such as the *Bacteroides* under conditions of controlled flow rates. With our system, we were able to for the first time show *in-vitro* biofilm formation by 4 of the most common *Bacteroides* species found in our gut: *Bt*, *Bf*, *Bo*, *Bv*, highlighting the capabilities of these anaerobes colonizing surfaces and forming biofilms of highly varying morphologies.

In nature, bacteria form biofilms of highly varying architectures and phenotypes under different nutrient sources and growth conditions⁶⁸. Such differences in biofilm morphology and architecture often confers to the fitness of the community. In *Pseudomonas aeruginosa*, the formation of dome shaped biofilms decreases susceptibility against antibiotics⁵³, whereas in *Vibrio cholerae*, the formation of filamentous biofilms offer advantages in the colonization and spreading on chitin particles⁶⁹. Out of the four different *Bacteroides* strains we tested, we found that *Bv* and *Bf* formed barbwire like and filamentous biofilms respectively unlike *Bt* and *Bo*, which formed surface-associated monolayer biofilms under nutrient rich conditions. These highly differing morphologies may account for the ecological fitness of each species

within the environment of growth. For instance, *Bv*'s formation of barbwire like biofilms through cell-cell entanglement may offer it an advantage to colonization under fluid flow conditions. On the other hand, *Bf*'s formation of thick filaments which extends in the third dimension may offer it an advantage to further nutrient access away from the surface, and growth space as it is not solely limited to growing directly on top of a surface. We also identified that the filamentation phenotype of *Bf* biofilms were lost upon growth in minimal medium supplemented with specific carbon sources, demonstrating the role of nutrient source on the overall architecture of anaerobic biofilms. However, to better picture the impact of different growth morphologies on the fitness of individual species within a microbial community, co-culture experiments must be performed.

Bacterial biofilm communities in the wild are typically composed of many species¹. Within these communities, member bacteria often engage in symbiotic social interactions which have positive impacts on the fitness and metabolism of neighbouring cells such as nutrient sharing²³. It has been previously demonstrated that *Bt*, an arabinan utilizer, can nutrient share arabinan based degradation by-products to *Bo* in solution⁷⁰. We demonstrate here that nutrient sharing is not always granted as *Bt*, which grew into a biofilm as a monoculture, failed to rescue the growth of *Bf*, a non-utilizer, in the case of a coculture biofilm. On the other hand, within these communities, bacteria also often engage in fierce competition with neighbours for nutrient source and space⁷¹. Therefore, individual colonization strategies by member strains may have an impact on the overall composition of the biofilm community. Under nutrient rich conditions where competition for space and resources dominate, we observe that co-cultures of any combinations of *Bt*, *Bo* and *Bf* resulted in biofilms where individual growth characteristics were conserved. This may be a result of the lack of nutrient competition present in these growth conditions as a constant flux of the nutrient rich TYG medium was provided, which supported the growth of each species individually. A good example of competition for space would be the co-cultures of *Bt* and *Bo*, where both these species favour the formation of surface attached monolayers. In this case, we observe that *Bt* outcompetes *Bo* on the surface, which can likely be due to a combination of *Bt*

having a higher growth rate and surface attachment capabilities compared to *Bo*. To study whether the filament formation by *Bf* confers to *Bf* competition in a co-culture setting, we cocultured *Bf* with *Bt* and *Bo* individually. In both cases, we observed *Bt* and *Bo* adhering to the surface and forming surface associated biofilms, whereas *Bf* formed filaments which extended high up in the third dimension. Unlike the *Bt-Bo* co-culture biofilms where *Bo* was clearly out competed by *Bt*, *Bf* abundance was not reduced in either co-culture with *Bt* or *Bo* in comparison to mono-species growth. Therefore, the filamentation architecture by *Bf* increases the fitness of *Bf* in the community by offering *Bf* an alternative to competition for surface space through extension of filaments in the third dimension.

As *Bt* and *Bf* exhibit drastically different strategies in surface colonization and biofilm formation, it would be interesting to understand the mechanisms of biofilm formation by these anaerobes, which leads to such differing biofilm morphologies. Previous studies have shown that bacterial extracellular appendages such as pili and fimbriae plays crucial roles in the initial surface attachment and biofilm formation in *P. aeruginosa*^{46,72}, *E. coli*^{49,50}, and *C. difficile*⁵¹. Although very little is known regarding the mechanisms of surface adhesion and biofilm formation by non-pathogenic bacteria, the genome of *Bf* encode for many proteins dedicated to the production of surface adhesins such as fimbriae and pili⁵⁷. We then wondered whether these adhesins in *Bacteroides* potentially play a role in their biofilm formation. We profiled the transcriptome and proteome of surface grown versus liquid cultured *Bf* and identified a series of genes likely encoding a conjugative pilus (BF9343_1395-1420). The tip pilin protein BF9343_1409 also encodes for a Bacteroidetes-Associated Carbohydrate-binding Often N-terminal (BACON) domain, likely responsible for the initial binding to surface glycans of *Bf* cells, where the conjugative pilus then connects neighbouring cells, allowing for DNA transfer between cells, ultimately leading to the formation of thick filaments of *Bf* in the form of a biofilm. Interestingly, we observed that *Bf* cells may also localize to the surface of *Bt* cells, potentially providing another advantage to *Bf* colonization where in the presence of *Bt*, *Bf* may easily adhere and colonize the surroundings. As we were interested in the differences in the mechanisms of biofilm formation between *Bf* and *Bt*, we also profiled

the proteome of surface grown versus liquid culture *Bt*. We identified a series of genes from BT4226-4236 which are upregulated in surface grown biofilms. Four of these proteins correspond to a FimB-like, a FimC like, a FimX like and a CheY like protein. In *E. coli*, FimB and FimC are proteins responsible for regulating the transcription⁵⁰ and assembly⁷³ of the type 1 fimbriae in *E. coli*. CheY is a chemotaxis signalling protein which controls the direction of flagellar rotation in *E. coli*⁷⁴, whereas FimX is known to be a signal transduction protein connecting environmental signals to surface twitching motility in *P. aeruginosa*⁷⁵. These results suggest the potential importance of a type 1 fimbriae in the biofilm formation by *Bt*, and the presence of signal transduction proteins FimX and CheY suggests the potential presence of surface sensing mechanisms in *Bt*. Overall, having an understanding behind the mechanisms of biofilm formation by symbiotic anaerobes such as *Bt* and *Bf* may provide an explanation regarding their dynamics and abundance within the gut microbiota community, which have a major impact on host health.

2.5 Methods

2.5.1 Strains and culture media

Bacteroides thetaiotaomicron VPI-5482 sfGFP and *Bacteroides fragilis* NCTC-9343 mCherry, *Bacteroides ovatus* ATCC-8483 sfGFP and *Bacteroides vulgatus* ATCC-8482 sfGFP-mCherry⁷⁶ were used for experiments in this work. TYG medium and *Bacteroides* minimal medium (BMM) supplemented with the indicated carbon source were used in all experiments.

For TYG medium, 10g tryptone, 5g yeast extract, 2.5g D-glucose and 0.5g L-Cysteine were dissolved in 465 mL of ddH₂O. The resulting solution was then immediately autoclaved and allowed to cool down to room temperature. In the meantime, Salt Solution A was prepared by mixing 0.26g of CaCl₂ and 0.48g of MgSO₄ in 300 mL of ddH₂O until fully dissolved where 500 mL of ddH₂O was then added. 1g KH₂PO₄, 1g K₂HPO₄ and 2g of NaCl were then added to the solution and stirred at room temperature until all salts are fully dissolved followed by the addition of 200 mL of

ddH₂O to top up the volume. The salt solution was then stored at 4°C for future use. A 10% (w/v) NaHCO₃ solution was prepared by dissolve 50g of NaHCO₃ into 500 mL of ddH₂O followed by filter sterilization with a 0.22 µm filter. A 1.9 mM Hematin – 0.2M Histidine solution was prepared by dissolving 60.18 mg of hematin in 1 mL of 1M NaOH until fully solubilized, then neutralized with 1 mL of 1M HCl. In a separate beaker, 1.55 g of L-Histidine was dissolved in 48 mL of ddH₂O. The histidine solution was then combined with the hematin solution, filter sterilized with a 0.22 µm filter and stored at 4°C for future usage. 5 mL of hematin-histidine solution and 10 mL of 10% NaHCO₃ solution were added to the TYG base medium with a 0.22 µm filter. With a separate 0.22 µm filter, 20 mL of Salt Solution A was then added. The resulting complete TYG medium was then stored at 4°C for future usage.

The BMM medium was prepared as previously described^{77,78}. Briefly, a 10x medium stock containing 1 M KH₂PO₄, 150 mM NaCl and 85 mM (NH₄)₂SO₄ was first prepared and adjusted to a pH of 7.2. Solutions of 1 mg/mL vitamin K₃, 0.4 mg/mL FeSO₄, 0.1 M MgCl₂, 0.8% (w/v) CaCl₂, 0.01 mg/mL vitamin B₁₂ and 1.9 mM hematin–0.2 M histidine solutions were prepared separately. To prepare 100 mL of BMM, 10 mL of the 10x salts were mixed with 0.1 g of L-cysteine, 50 µL of vitamin B₁₂ solution, and 100 µL of each vitamin K₃, FeSO₄, MgCl₂, CaCl₂ and hematin-histidine solution. All carbon sources were added to a final concentration of 5 mg/mL. The media were filter-sterilized using a 0.22 µm filter unit and degassed in the anaerobic chamber overnight. All bacteria were cultured at 37 °C under anaerobic conditions in a vinyl anaerobic chamber (COY) inflated with a gas mix of approximately 5% carbon dioxide, 90% nitrogen and 5% hydrogen (CarbaGas). Bacteria were first streaked on brain heart infusion plates (SigmaAldrich) containing 10% sheep blood (TCS BioSciences). Single colonies were then inoculated in BMM and grown overnight.

2.5.2 Microchannels fabrication

Microchannels were fabricated by standard soft-lithography as previously described⁷⁹. Simple channels with dimensions of 2 cm-length, 2 mm-width and 300µm-height were used in all biofilm experiments. Upon cutting out the cured PDMS (Sylgard 184, Dow

Corning) channels, 1 mm inlet and outlet, along with a 3 mm holes were punched immediately downstream of the inlet. The PDMS was then bound to sonicated glass coverslips without plasma treatment. Microfluidics chips were then fabricated by loading medium through the inlet until the 3 mm hole was filled up, where a piece of PDMS was then placed on top to seal the hole, serving as the bubble trap of the resulting channel. Medium was then loaded until the channel was filled.

2.5.3 Biofilm growth and microscopy

All biofilm growth experiments were performed in TYG medium, BMM-glucose or BMM-arabinan. Arabinan from sugar-beet (Megazyme) was used for all experiments involving arabinan. Overnight monocultures of *Bt* and *Bf* were grown in either TYG medium or BMMG according to the medium used for the subsequent biofilm experiments. To initiate biofilm formation in flow, cell cultures were diluted to a final OD of 0.1 where 5 μ L of the diluted bacterial culture was then loaded into the microchannels through the outlet and incubated for 15 minutes for initial attachment. The inlet was then connected to a 10 mL disposable syringe (BD Plastipak) filled with the medium and mounted onto a syringe pump (KD Scientific), using a 1.09 mm outer diameter polyethylene tube (Instech) and a 27G needle (Instech). All biofilms were then grown anaerobically for 3 days at room temperature under the volume flow rate of 2.0 μ L/min. Upon 3 days of growth, the tubings were carefully disconnected. The biofilms were then removed from the anaerobic chamber and incubated in an oxygenated environment for 2 hours to allow for fluorescent protein folding while maintaining biofilm integrity. The biofilms were then imaged by fluorescence confocal microscopy. Imaging were performed with the 40x APOChromat water immersion objective with a numerical aperture (N.A.) of 0.95 and the 100x oil immersion objective with an N.A. of 1.45. Fiji was then used for the display of all images.

2.5.4 Sample preparation for proteomics

Bt or *Bf* were grown 3 days anaerobically into biofilms in TYG medium. Resulting biofilms were then unplugged from the inlet tubings, where 200 μ L of lysis buffer

containing 2% SDS, 100 mM HEPES pH 8.0 was used to flush out cells within the channels and collected through the outlet. The resulting mixture was then used to flush out cells from 2 other biofilms, to generate enough protein for subsequent mass spectrometry analysis. The PDMS was then carefully disconnected from the glass coverslip, where a sterile blade was used to scrape off cells which remain attached to the glass surface. Resulting pellets were then resuspended in the 200 μ L of lysis buffer containing cells which had been successfully flushed out. BCA assays were then performed to determine the total concentration of protein present in the cell lysates, where an aliquot containing 20 μ g of protein content were collected for downstream mass spectrometry analysis. For detailed downstream steps, refer to section 2.5.9.

2.5.5 Sample preparation, RNAseq and data analysis

Bf biofilms were grown 3 days anaerobically at room temperature. The resulting biofilms were unplugged and cells were harvested and lysed as samples prepared for proteomics experiments. Trizol and chloroform were then added to the harvested cells according to the manufacturer's protocol (ThermoFisher Scientific) and centrifuged at 12000 rcf, 4°C for 15 mins. Total RNA was then isolated through the transfer of the aqueous phase to a new Eppendorf tube. RNA was then precipitated through the addition of isopropanol and centrifuged at 12000 rcf, 4°C for 10 mins. The supernatant was then discarded and the RNA pellet was washed with 75% ethanol and centrifuged at 7500 rcf, 4°C for 5 mins. The resulting supernatant was discarded and the RNA pellet was vacuum dried, followed by resuspension in 50 μ L of RNase-free water. RNA was further purified with a Nucleic Acid Concentrator Column (Zymo Research), where the concentration and quality of the total RNA was tested by Nanodrop and Tapestation. rRNA depletion was then performed on RNA samples with the Pan-Bacteria riboPOOL kit (SiTOOLs Biotech) based on the detailed protocol provided by the supplier. gDNA were then removed from the depleted RNA samples with the Heat&Run gDNA removal kit (ArcticZymes). Library prep was then performed with the NEBnext ultra II directional RNA kit (New England Biolabs), and RNAseq was performed with the Nexteq PE75 with 130mio reads.

Transcriptomics analysis was done using usegalaxy.org. Briefly, the .fastq raw data from RNAseq was imported into galaxy, along with the chromosomal DNA sequence of *B. fragilis* NCTC-9343. HISAT2 was then used for mapping reads to the genome. The resulting mapped reads and a gene description file (.gff) were fed to HTseq-Count, where the number of reads per gene were counted. Differential expression across two conditions were then analyzed by DEseq2, followed by annotation of all genes by Annotate.

2.6 Supplementary information appendix

2.6.1 Supplementary figures

Locus tag	Description	log2(FC)
BF9343_1441	hypothetical protein	4.2982709
BF9343_1409	fimbrillin family protein	4.2941517
BF9343_1413	conjugal transfer protein	4.2934788
BF9343_1406	hypothetical protein	4.2904585
BF9343_1394	DUF4373 domain-containing protein	4.2904502
BF9343_1440	hypothetical protein	4.2854021
BF9343_1397	DUF2786 domain-containing protein	4.2842235
BF9343_1395	hypothetical protein	4.2814494
BF9343_1396	toprim domain-containing protein	4.2776856
BF9343_1417	conjugal transposon protein TraM	4.2734336
BF9343_1415	hypothetical protein	4.2550108
BF9343_1416	membrane protein	4.2546544
BF9343_1404	DUF3127 domain-containing protein	4.2511155
BF9343_1410	fimbrillin family protein	4.2418331
BF9343_1430	NA	4.2317821
BF9343_1407	hypothetical protein	4.2286652
BF9343_1421	M23 family metalloproteinase	4.2150322
BF9343_1400	hypothetical protein	4.2101099
BF9343_1408	fimbrillin family protein	4.2019525
BF9343_1391	hypothetical protein	4.1927374
BF9343_1398	hypothetical protein	4.1909119
BF9343_1392	NA	4.1894324

BF9343_1393	DUF4373 domain-containing protein	4.1872427
BF9343_1405	DUF3575 domain-containing protein	4.1858336
BF9343_1429	DNA adenine methylase	4.1779252
BF9343_1399	hypothetical protein	4.1732542
BF9343_1411	hypothetical protein	4.1695642
BF9343_1422	hypothetical protein	4.167513
BF9343_1401	NA	4.1576394
BF9343_1389	hypothetical protein	4.146028
BF9343_1420	conjugative transposon protein TraN	4.1240819
BF9343_1403	hypothetical protein	4.0943763
BF9343_1443	hypothetical protein	4.066954
BF9343_1412	NA	4.003478
BF9343_3304	hypothetical protein	-4.031547
BF9343_0168	magnesium-translocating P-type ATPase	-4.0609429
BF9343_4125	NA	-4.0850182
BF9343_0854	RagB/SusD family nutrient uptake outer membrane protein	-4.0966554
BF9343_2294	hypothetical protein	-4.105407
BF9343_2262	winged helix-turn-helix domain-containing protein	-4.1565293
BF9343_2565	Hsp20/alpha crystallin family protein	-4.2213729
BF9343_1151	DUF4890 domain-containing protein	-4.224523
BF9343_3337	NA	-4.2247098
BF9343_3257	hypothetical protein	-4.2729762

Figure S2.1: Genes significantly upregulated or downregulated in *Bf* biofilms from RNAseq differential expression analysis. All genes with a $\log_2(\text{FC})$ of greater than ± 4 are listed. ($N = 1$)

Chapter 3. Fluid flow structures gut microbiota biofilm communities by distributing public goods

This chapter focuses on the effect of fluid flow on the organization and composition of nutrient sharing biofilm communities. It has been published in PNAS in May 2023, as:

Jeremy P. H. Wong, Michaela Fischer-Stettler, Samuel C. Zeeman, Tom J. Battin & Alexandre Persat*, *Fluid flow structures gut microbiota biofilm communities by distributing public goods.*

<https://doi.org/10.1073/pnas.2217577120>

Author contributions:

J.P.H.W., T.J.B., and A.P. designed research, J.P.H.W. and M.F.-S. performed research, S.C.Z., T.J.B., and A.P. contributed new reagents/analytic tools, J.P.H.W. analyzed data, and J.P.H.W. and A.P. wrote the paper.

3.1 Abstract

Bacterial gut commensals experience a biologically and physically complex mucosal environment. While many chemical factors mediate the composition and structure of these microbial communities, less is known about the role of mechanics. Here, we demonstrate that fluid flow impacts the spatial organization and composition of gut biofilm communities by shaping how different species interact metabolically. We first demonstrate that a model community composed of *Bacteroides thetaiotaomicron* (*Bt*) and *Bacteroides fragilis* (*Bf*), two representative human commensals, can form robust biofilms in flow. We identified dextran as a polysaccharide readily metabolized by *Bt* but not *Bf*, but whose fermentation generates a public good enabling *Bf* growth. By combining simulations with experiments, we demonstrate that in flow, *Bt* biofilms share dextran metabolic by-products, promoting *Bf* biofilm formation. By transporting this public good, flow structures the spatial organization of the community, positioning the *Bf* population downstream from *Bt*. We show that sufficiently strong flows abolish *Bf* biofilm formation by limiting the effective public good concentration at the surface. Physical factors such as flow may therefore contribute to the composition of intestinal microbial communities, potentially impacting host health.

3.2 Additional background

Bacterial commensals colonize the physically-complex environment of the gastrointestinal (GI) tract as dense mixed communities. While most species tend to compete for resources and space, they can also engage in positive interactions that promote diversity. Many bacteria secrete compounds such as nutrient chelators⁸⁰, digestive enzymes⁸¹, and signalling molecules⁸² that promote the fitness of neighboring cells, either from the same or another taxon. The spatial arrangements of different species within biofilms influences how these competitive or cooperative interactions are enforced⁸³, ultimately shaping the composition and function of the bacterial community⁸⁴. Spatial structure of communities is however often overlooked in investigations of microbiota, both *in vivo* and *in vitro*.

Interspecies interactions involving public goods are often studied in liquid cultures⁸⁵, where cells, metabolites and secreted molecules are well-mixed. In the GI tract, commensals however grow as spatially-structured, dense communities exposed to fluid flow⁸⁶. Forces generated by flow can impact the positioning of single cells in biofilms and transport soluble molecules^{87,88}. As a result, advective transport shapes the distribution of molecules secreted by surface-associated bacteria. For example, flow transports signaling molecules, ultimately structuring gene expression in an isogenic community⁸⁹. By mixing metabolic by-products, flow stabilizes the co-existence of *Vibrio cholerae* producers and engineered cheaters⁹⁰. In a similar way, intestinal-like flows impact the composition of an engineered *Escherichia coli* cross-feeding community growing in microchannels⁹¹. Based on these results, we postulate that hydrodynamic forces shape the structure of anaerobic gut communities commonly found in the GI tract, thereby influencing microbiota composition and metabolic output. Technical challenges, including the dearth of methodologies enabling biophysical investigations of microbiota biofilms, have so far limited our ability to probe these questions. As a result, how metabolic and mechanical factors together mediate the composition and spatial structure of a realistic gut microbiota communities is not entirely understood.

Bacteroides spp. are among the most abundant commensals found in the human bowel⁹². *Bacteroides thetaiotaomicron* (*Bt*) is beneficial to human hosts: it confers colonization resistance and produces metabolically-accessible short-chain and organic acids⁹³. *Bacteroides fragilis* (*Bf*) also commonly colonizes the human large intestine, conferring health benefits, but can also opportunistically turn pathogenic⁵⁷. *Bf* and *Bt* leverage polysaccharide utilization loci (PULs) to metabolize a wide range of complex glycans. PUL-encoded proteins process complex polysaccharides into metabolically-accessible sugars^{94–98}. The genomes of *Bacteroidetes* species frequently encode hundreds of PULs⁹⁹, allowing these commensals to grow on a broad range of dietary or host-derived glycans^{94,95,97,100}.

PULs are often composed of a carbohydrate sensor/transcriptional regulator, various surface glycan-binding proteins, a TonB-dependent transporter, and carbohydrate active enzymes such as glycosylhydrolases (GHs), polysaccharide lyases and carbohydrate

esterases¹⁰¹. Complex fibres often bind to the cell surface where surface-associated GHs then initiate cleavage of the bulky polysaccharides. Resulting oligosaccharides can subsequently enter the cell⁹⁶, but are also released in the extracellular environment as metabolic by-products^{101,102}, thereby constituting a public good accessible to the rest of the community. Thus, a species otherwise unable to utilize the original polysaccharide could grow by utilizing this public good¹⁰³. Consistent with this scenario, *Bacteroides* species share metabolic by-product glycans with other species in liquid cultures^{103,104}. In the context of the GI tract, flow could transport these metabolites, affecting their distribution and access to other commensals. These changes would impact the spatial growth pattern of secondary degraders. Despite their relevance to human health and the evidence for metabolic-sharing, the spatial organization of *Bacteroides* species has never been explored experimentally.

We hypothesize that flow impacts the spatial organization of syntrophic microbiota communities by transporting metabolic by-product public goods. To demonstrate this, we investigated nutrient sharing between *Bt* and *Bf* biofilms. We show that both species can form robust surface-associated biofilms in flow environments. We found that when degrading dextran, a common food additive¹⁰⁵, *Bt* sustains *Bf* growth in co-culture by sharing a metabolic by-product. We found that fluid flows which resemble the ones these species experience in the human colon strongly impact the spatial organization and composition of these syntrophic *Bacteroides* biofilm communities.

3.3 Results

3.3.1 *B. theta* and *B. fragilis* form biofilms in flow

In the intestine, commensals form dense and organized communities associated with the mucosal surface⁶⁴. *Bt* isolates have variable abilities to form biofilm-like macroscale multicellular structures¹⁰⁶. Several cellular components such as pili are susceptible to contribute to the cohesion of *Bt* and *Bf* biofilms⁶². Whether these multicellular structures are sufficiently cohesive and resistant to flow is unclear¹⁰⁷. To characterize *Bt*'s ability to form biofilms in flow conditions that replicate the fluidic environment of the intestine, we

implemented a microfluidic-based anaerobic biofilm assay for single-cell resolution microscopy. We initially seeded *Bt* constitutively expressing sfGFP in microchannels, flushed unattached cells and initiated growth for 4 days under constant flow of Bacteroides Minimal Medium (BMM) supplemented with glucose (Fig. 3.1A). To visualize colonization patterns, we imaged the surface-associated population using spinning disc confocal microscopy outside of the anaerobic chamber.

Bt formed cohesive multicellular structures that remained attached to the surface in the face of flow (Fig. 3.1B). Visualizations at the single-cell level showed that bacterial cells grew contiguously (Fig. 3.1C). These multicellular structures extended in the depth of the channel, roughly 10-15 μm above the coverslip surface. *Bf* constitutively expressing mCherry also formed dense surface-associated communities of contiguous cells with an architecture resembling the one of *Bt* (Fig. 3.1B, C). These observations show that *Bt* and *Bf* can form surface-attached biofilms that resist shear forces generated by flow (Fig. 3.1B, C). As a result, we postulate that flows surrounding *Bt* and *Bf* biofilms impacts the distribution of secreted molecule, including metabolites, in a way that could impact community composition and organization. To test this hypothesis, we investigated how a biofilm community composed of *Bt* and *Bf* self-organizes when sharing or competing for nutrients in flow.

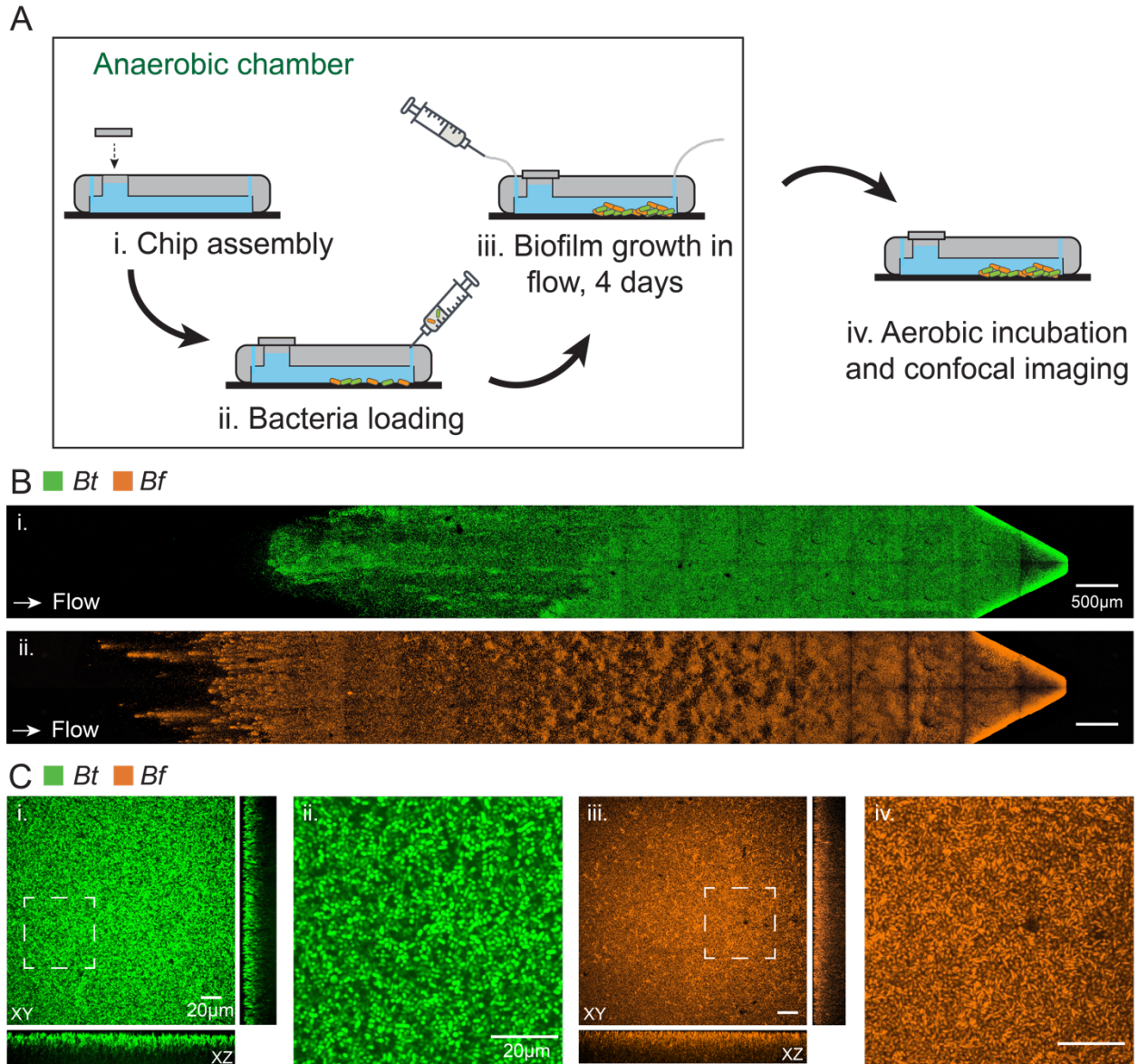


Figure 3.1: *Bacteroides thetaiotaomicron* (*Bt*) and *Bacteroides fragilis* (*Bf*) form biofilms in flow. (A) Schematic of experimental procedure for anaerobic biofilm growth in flow. (B) Full-channel view of biofilm from (i) *Bt* constitutively expressing sfGFP and (ii) *Bf* constitutively expressing mCherry. (C) Three-dimensional and close-up view of (i, ii) *Bt* and (iii, iv) *Bf* biofilms show the tight packing of single cells and growth in the channel depth. All biofilms were grown anaerobically for 4 days under flow of *Bacteroides* Minimal Medium (BMM) supplemented with glucose. All biofilms were grown anaerobically for 4 days at the flow rate of 0.1 μL/min.

3.3.2 Cross-feeding between *B. theta* and *B. fragilis*

Bacteroides species possess dedicated PULs that permits growth on a wide-range of polysaccharides¹⁰⁸. *Bt* and *Bf* are versatile utilizers with 84 and 57 predicted PULs, respectively¹⁰⁹. Some of these systems process the same polysaccharides in *Bt* and *Bf*, so that *Bt* and *Bf* can compete for a single dietary fiber. Others are specific, in principle promoting the growth of only one of the two species. However, polysaccharide degradation can release metabolic by-products accessible to the second species. We therefore searched for nutrient-sharing conditions by identifying a polysaccharide that *Bt* or *Bf* alone can metabolize to generate a by-product that can sustain growth of the other. Based on previous measurements of *Bacteroides* growth under various nutrient conditions, we selected three candidate polysaccharides susceptible to induce nutrient-sharing: dextran, arabinan and inulin^{95,110–112}.

We assessed the growth of *Bt* and *Bf* in test tubes as mono- and co-cultures in BMM media supplemented with each polysaccharide. *Bt* efficiently grew on dextran and arabinan, while *Bf* could not (Fig. 3.2A). Conversely, *Bf* grew on inulin, but not *Bt*. These nutrients therefore promote the exclusive growth of a single species out of the two, illustrating specificity in polysaccharide utilization by *Bt* and *Bf*. To investigate whether utilization of one of the three candidate glycans could stimulate nutrient sharing, we co-cultured *Bt* and *Bf* in BMM supplemented with either inulin, arabinan or dextran. We mixed *Bf*-mCherry and *Bt*-sfGFP at a 1:1 ratio in the initial inoculum. To identify nutrient sharing conditions, we quantified the relative population of *Bt* and *Bf* in these cultures using fluorescence microscopy. After 1 and 2 days of growth in anaerobic conditions, we sampled the cultures, incubated them at atmospheric conditions, imaged to count mCherry- and sfGFP- positive cells, and finally computed the *Bf* fraction. In competition for glucose, *Bt* and *Bf* grew roughly in balance, with only a slight advantage for *Bf*. In arabinan, the fraction of *Bf* dropped after 1 day, showing it is likely unable to utilize *Bt*'s arabinan metabolic by-products (Fig. 3.2B). Conversely, *Bf* showed a strong growth advantage over *Bt* in inulin, suggesting that *Bf* does not produce glycans accessible to *Bt*. The consortium showed a striking difference in dextran: the fraction of each species

in co-culture remained close to 50% throughout the 2 days of growth. Growth was balanced in dextran of low and high molecular weight alike, suggesting that *Bf*'s capability of utilizing dextran is independent of the polymer's structure¹¹³. These results suggest that, while it is unable to grow alone, *Bf* can benefit from *Bt*'s growth in dextran during co-culture. Consistent with this scenario, *Bf* grows in *Bt* spent dextran medium (Fig. S3.1).

To verify that *Bf* grows through exploitation of a public good, we investigated *Bt*'s physiology during dextran fermentation. We first compared the proteomes of *Bt* growing in dextran and glucose. Differential expression analysis shows that *Bt* strongly upregulates a group of proteins in dextran (Fig. 3.2C). These proteins are encoded in an operon (BT3086-BT3090) predicted to belong to the PUL48 of *Bt*¹⁰⁹. These genes encode for homologues to the nutrient binding protein SusD, the importer protein SusC, a SusE homologue and 2 GHs: α -glucosidase II and dextranase. This operon had previously been identified as essential for *Bt*'s growth in dextran in a transposon screen¹¹⁴. Alongside PUL48, we also identified a sole GH, BT4581, encoding for an α -glucosidase which is also highly upregulated in dextran growth. Dextran is a polyglucan with α -1,6 and α -1,3 glycosidic linkages. Since the dextranase BT3087 and α -glucosidases are known to liberate glucose as a product^{115,116}, we therefore hypothesized that *Bt* degrades dextran into glucose or small gluco-oligosaccharides which promote *Bf* growth.

To expose the mechanisms of nutrient sharing, we analyzed the metabolites released by *Bt* during dextran metabolism. We performed High-Performance Anion Exchange Chromatography - Pulsed Amperometric Detection (HPAEC-PAD) analysis of BMM-dextran growth media. Chromatograms of sterile BMM supplemented with glucose and dextran showed dense peaks at short and long retention times, respectively. The chromatograms of supernatant from *Bt* cultures in BMM- dextran showed an increased density of peaks at short retention times compared to the negative control (Fig. 3.2D). The most prevalent peak induced by *Bt* growth matched the retention time of the glucose standard, and was clearly distinct from disaccharide peaks (Fig. S3.2). To test

whether *Bf* utilizes glucose produced by *Bt* as public good, we inoculated *Bf* into *Bt* spent medium and analyzed the supernatant after 20 h and 44 h of incubation (Fig. 3.2E). HPAEC-PAD analysis showed that the glucose peak decreases in amplitude after *Bf* growth. We estimated glucose utilization from spent medium by integrating the glucose peak area. Peak area decreased sharply as a function of time of *Bf* incubation, in comparison to the isomaltose peak (Fig. 3.2E, F). Our results show that when metabolizing dextran, *Bt* releases glucose which cross-feeds *Bf* (Fig. 3.2F, G). Therefore, *Bf*-*Bt* co-culture in dextran therefore represents a realistic model for investigating the feedback between spatial structure and flow during public good sharing between microbiota biofilms.

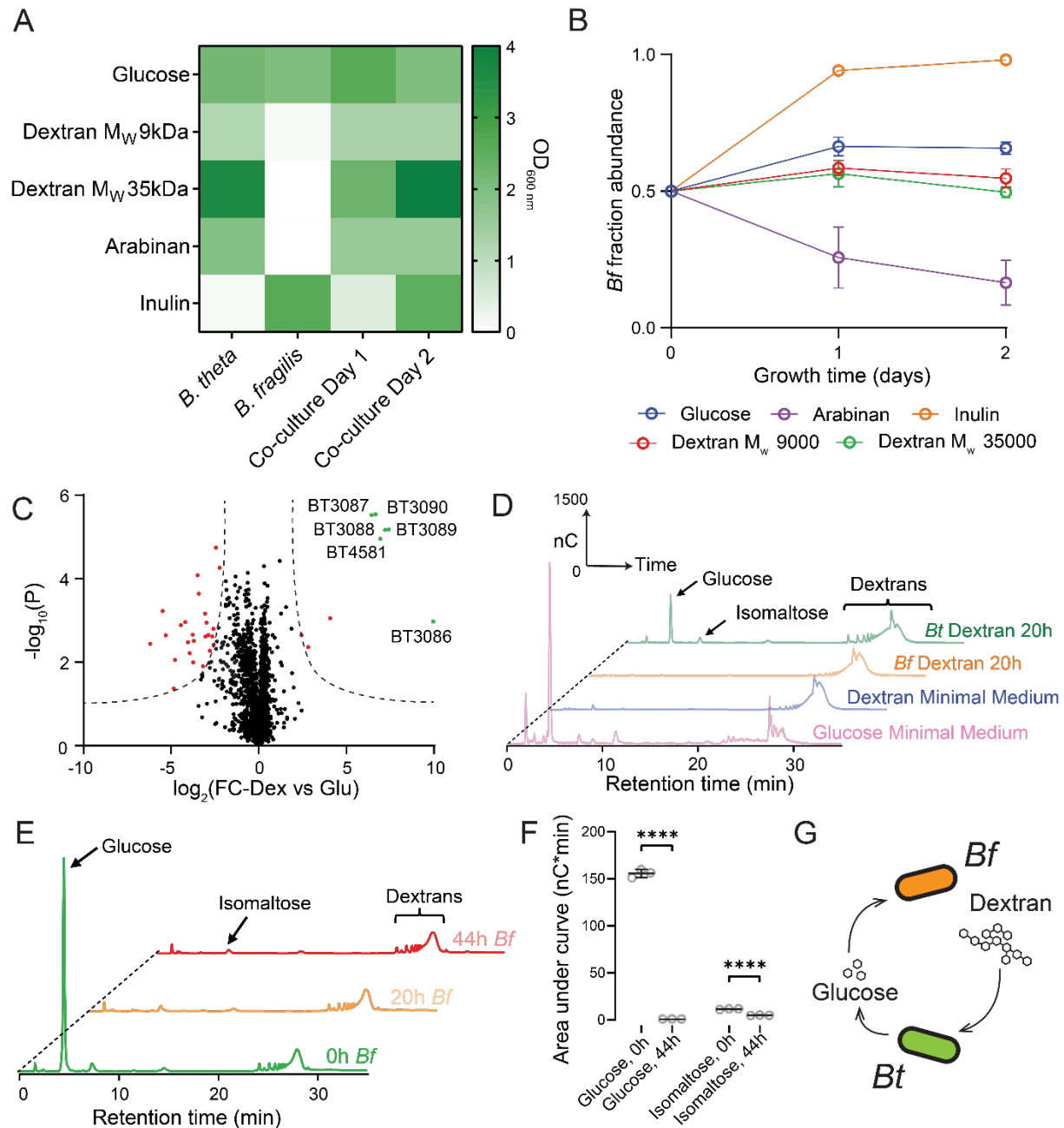


Figure 3.2: *Bt* shares a dextran degradation by-product that enables *Bf* growth in co-cultures. (A) *Bt*, *Bf* growth in mono- and co-cultures in dextran, arabinan and inulin. We measured optical density (OD) after 2 days. (B) Fraction of *Bf* in co-culture with *Bt* in the different glycan sources measured by fluorescence imaging ($N = 3$, error bars: standard deviation). (C) Proteomic analysis of *Bt* growing in dextran. We generated the volcano plot based on fold-change in dextran relative to culture in glucose ($N = 3$). Red

and green dots correspond to proteins with statistically significant different fold changes (S_0 value of 1.0 and FDR cut-off of 0.01). Proteins from genes encoding for PUL48 are strongly upregulated (green dots). (D) HPAEC-PAD analysis of the metabolic output of *Bt* and *Bf* liquid monocultures in dextran. *Bt* growth in dextran produces metabolites whose retention times.

3.3.3 Nutrient sharing structures *Bacteroides* biofilms

In any fluidic environment, molecules secreted by biofilm-dwelling bacteria diffuse and go with the flow. The relative contributions of these two transport mechanisms impacts distribution of these solutes, and ultimately their effective concentration near biofilms. We therefore compared the architectures of *Bt-Bf* biofilm communities sharing public goods in the absence and presence of flow. We observed that *Bt* formed biofilms under flow of dextran with similar density and architecture as in glucose (Fig. 3.3A). By contrast, *Bf* alone attached to the channel surface but failed to grow into biofilms (Fig. 3.3B), as expected from the undetectable growth in liquid culture. However, *Bf* formed biofilms in dextran when co-cultured with *Bt* (Fig. 3.3C). While *Bt* uniformly colonized the surface in both dextran and glucose, the local spatial arrangement of *Bt* and *Bf* cells in dextran-grown biofilms was markedly different from conditions without cross-feeding (Fig. 3.3C, D). In particular, the mean nearest neighbour distance from *Bf* to *Bt*, which is a local measurement of how far a *Bt* cell is from a *Bf* cell, is larger in dextran than glucose (Fig. 3.3C). The short interspecies distance measured in glucose indicates a higher degree of mixing. This is likely due to the simultaneous growth of *Bf* and *Bt* from an initially well-mixed surface-attached population. In this case, *Bt* and *Bf* compete for space under nutrient excess to rapidly colonize the surface. In dextran, *Bt* is excluded from *Bf* biofilms, thereby increasing nearest neighbour distance. In this case, nutrient limitations explain the increase in lineage segregation¹¹⁷. To test whether sharing nutrients reduced *Bt* fitness, we quantified how the presence of *Bf* influenced *Bt* biofilm growth. We compared *Bt* biomass accumulation in the presence and absence of *Bf*. We could not distinguish any difference in *Bt* colonization between those two conditions,

showing *Bt* does not pay a marked fitness penalty for sharing metabolic by-products (Fig. S3.3).

Bf microcolonies only noticeably grew after 3 days of co-culture while *Bt* already formed biofilms early on (Fig. S3.4). This suggests that the *Bt* population must reach a critical density to produce sufficient metabolic by-products to enable *Bf* growth. Consistent with this sequence, *Bf* biofilms mainly grew on top of *Bt* biofilms, whereas in glucose they tend to grow on the glass surface (Fig. 3.3D). Layered growth could be a consequence of the competition for space at the microchannel surface, thereby contributing to the large interspecies distance (Fig. 3.3C). In summary, sharing nutrients imposes spatial and temporal constraints on biofilm growth in the presence of flow. To reveal the contributions of flow in shaping the structure of *Bt-Bf* communities, we imaged the same biofilms grown in the absence of flow. The two-species biofilms also formed, but with a more heterogeneous architecture at the single cell level. Again, the nearest neighbour distance between *Bf* and *Bt* is higher in dextran than glucose, but the difference between the two conditions is lower than in flow conditions (Fig. 3.3C, E). We conclude that flow plays a crucial role in shaping the architecture of the *Bacteroidetes* biofilm communities. We therefore suspect that flow mediates the organization and composition of this community by distributing public goods at the global scale of the community.

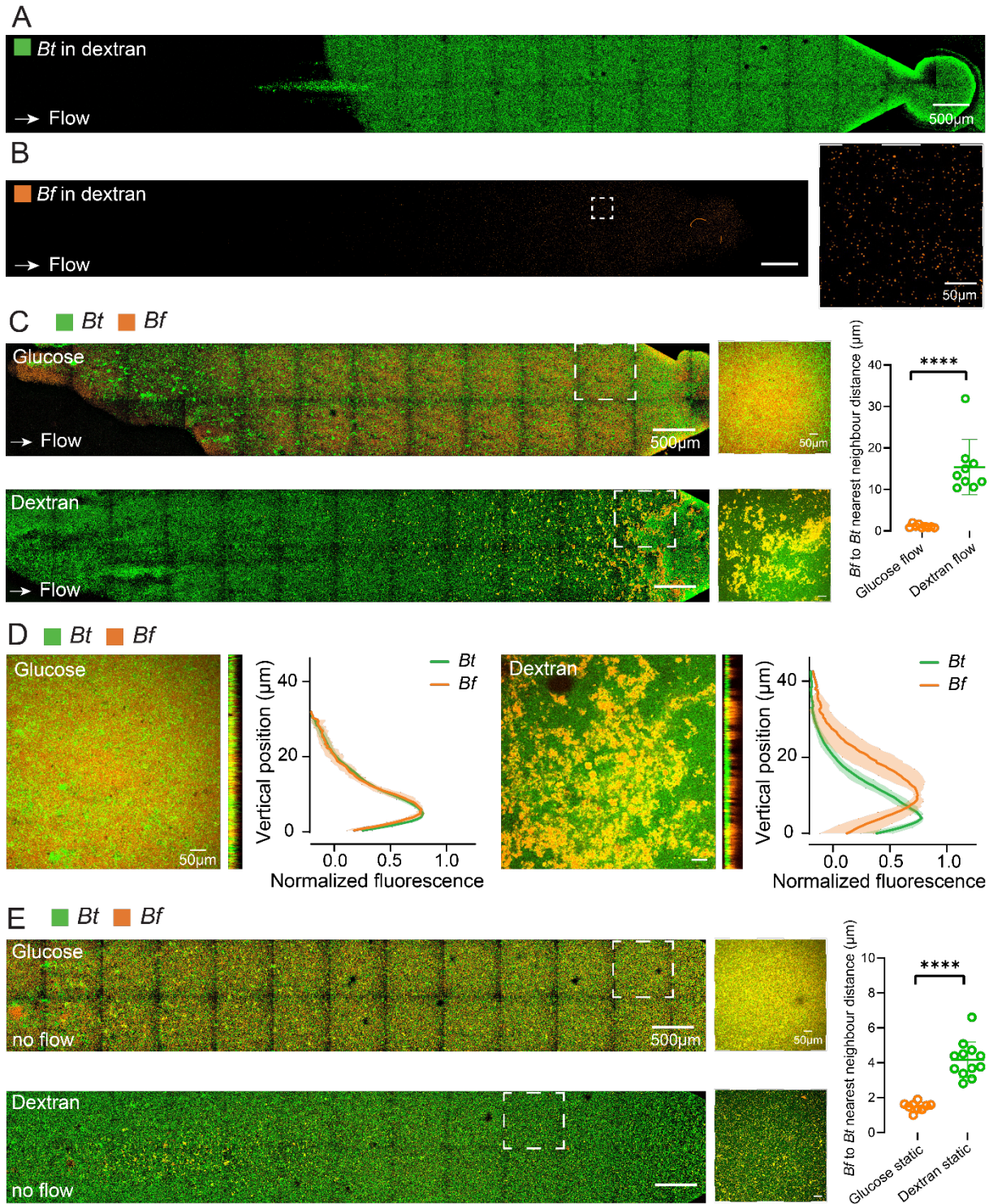


Figure 3.3: Flow structures syntrophic *Bt-Bf* biofilm communities at the microscale. (A) *Bt* biofilm growing in dextran. (B) *Bf* does not form biofilms in dextran. However, individual cells still remain attached to the glass surface during the 4 days of incubation in flow (close-up view on the right). (C) 4-day *Bt-Bf* mixed biofilms in flow of

glucose (top) and dextran (bottom). Nearest neighbour analysis between *Bf* and *Bt* of coculture growth in dextran and glucose show increased segregation during cross-feeding. (D) Three-dimensional structure of 4-day co-culture biofilm in glucose and dextran in flow. We computed the fluorescence profile of the biofilm as a function of height. In glucose, *Bt* and *Bf* grow at the coverslip surface, while *Bf* grows on top of *Bt* biofilms in dextran ($N = 3$, shaded regions: standard deviation across replicates). (E) 4-day *Bt-Bf* mixed biofilms of in glucose and dextran without flow. Nearest neighbour analysis between *Bf* and *Bt* of coculture growth in dextran and glucose again show increased segregation during cross-feeding. However, the degree of segregation difference between the two conditions is less compared to in the presence of flow. All biofilms were grown anaerobically for 4 days at the flow rate of 0.1 $\mu\text{L}/\text{min}$. All images are representative ($N = 9$). See figure 4 for quantification and statistical significance.

3.3.4 Flow impacts biofilm community organizations by transporting public goods

In the absence of flow, *Bf* and *Bt* co-colonized the entire channel surface (Fig. 3.4A). In flow, *Bt* also formed uniform biofilms but the overall *Bf* population shifted downstream (Fig. 3.4B). This observation is consistent with a mechanism where flow transports *Bt*-produced public goods. We quantified the downstream population shift of *Bf* by defining λ as the distance between growth fronts of *Bt* and *Bf* populations. We calculated λ by first averaging each the fluorescent intensities for each species across the channel, computing the position at which each population fluorescence reaches a specified threshold to ultimately take the difference between these two distances (Fig. 3.4C). In the absence of flow, we found no difference between the population shift in glucose and dextran. By contrast, λ increased under flow of dextran, while it had a mild opposite effect in flow of glucose (Fig. 3.4D). Our results are consistent with a mechanism where fluid flow transports a public good downstream as it is produced by *Bt* upstream. The effective concentration of secreted glucose would thus increase along the channel in the direction of flow⁸⁹. This allows a secondary utilizer to grow, but in a niche separate from the primary utilizer. Without flow, dextran utilization by *Bt* produces free glucose that

diffuses around biofilms, slowly accumulating to promote isotropic growth of *Bf*. Only when *Bt* biofilms reach a sufficient density will they produce an amount of glucose promoting *Bf* biofilm growth.

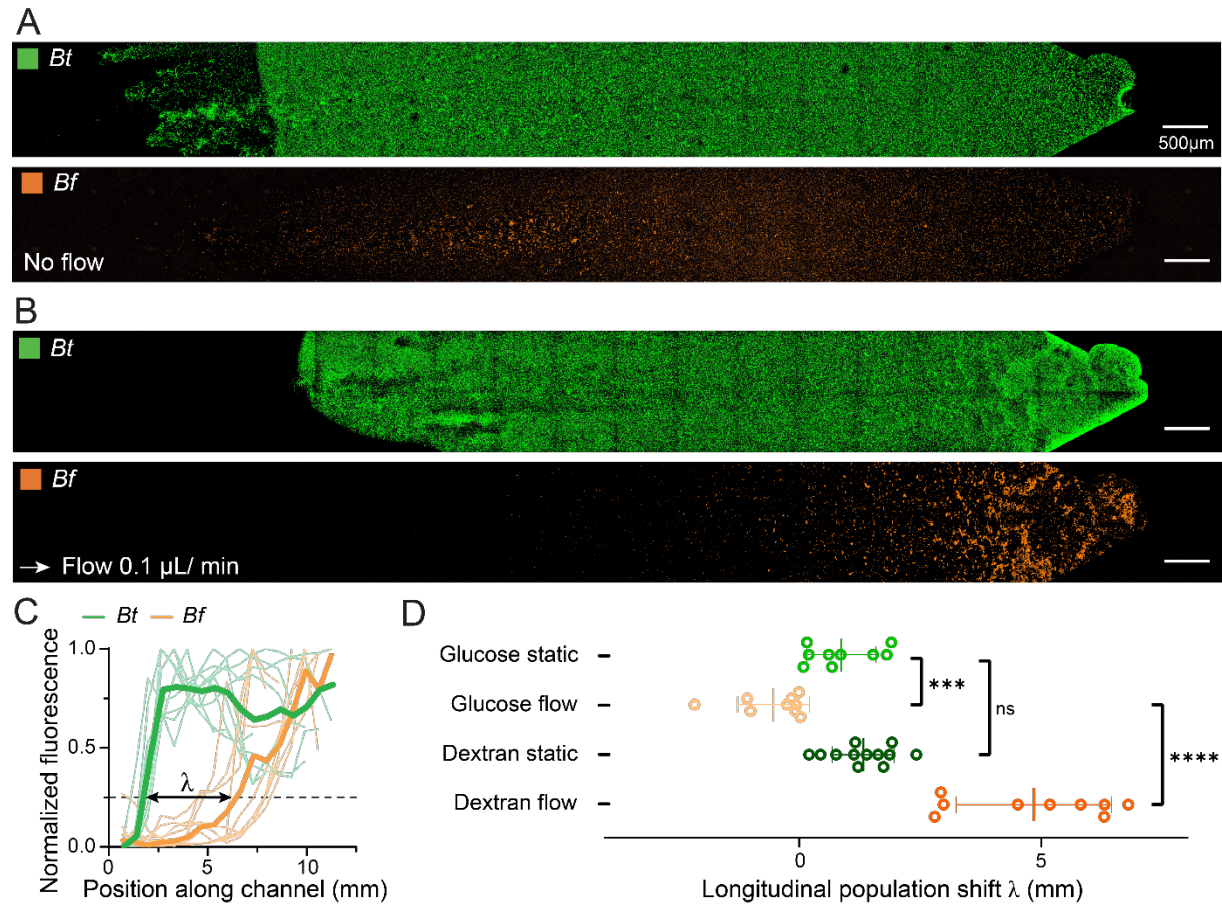


Figure 3.4: Flow impacts biofilm community organization by transporting public goods. *Bf* and *Bt* biofilms in co-culture grown in dextran for 4 days (A) without flow and (B) with flow (flow rate = 0.1 µL/min). (C) Cross-sectional averaged fluorescence intensity profiles of *Bf* and *Bt* biofilms along the microchannel. Each line corresponds to a biofilm from a single co-culture experiment. Bold lines correspond to the average of 9 replicates. We define the longitudinal population shift λ as the x-position difference between the *Bt* and *Bf* population across the channel at 25% of the maximal normalized fluorescence intensity. (D) *Bf* longitudinal shift (λ) of co-culture biofilms grown in dextran or glucose, in the presence and absence of flow. Statistical test: unpaired t-tests, *** 0.001 < p < 0.0001 and **** p < 0.0001.

3.3.5 Small geometrical feature have a local impact on community organization

The intestinal epithelium surface is decorated with crypts that can host bacteria. Crypt-shaped structures can have an impact on cell-cell communication by affecting the transport of quorum sensing signaling molecules⁸⁹. As a result, we wondered whether crypt-shaped feature would influence the transport of shared metabolites and ultimately affect the spatial organization of *Bt-Bf* biofilms. To characterize this, we replicated the geometry of the colon by fabricating microfluidic channels decorated with lateral crypt-like features. We grew *Bt-Bf* biofilms in these channels at a flow rate identical to the one applied in straight channels (Fig. 3.5A). We observed that both *Bt* and *Bf* co-colonized lumen and crypts in both glucose and dextran. The spatial organization of the resulting mixed biofilms were qualitatively similar to the ones observed in straight channels (Fig. 3.5A). *Bt* and *Bf* were well-mixed when growing in glucose, both in the lumen and in the crypts. We found no growth differences for *Bf* between the two locations (Fig. S3.5A, B). In dextran, *Bt* uniformly colonized lumen and crypts. *Bf* grew into biofilms with a downstream shift as in the simple channels, both in the lumen and in the crypts (Fig. 3.5A, B). We could not distinguish any global difference in *Bf* colonization in the crypts relative to the lumen. We however observed that very locally, *Bf* tends to colonize the tip of the crypt features in dextran more densely (Fig. 3.5A). We therefore quantified the abundance of *Bf* at the tip of the crypt relative to the lumen, which confirmed that in the downstream regions of the channel where *Bf* grows the most, its density is highest at the crypt ends (Fig. 3.5C). Overall, our results show the importance of transport of nutrient from the upstream *Bt* population within the lumen. Flow patterns impact that global spatial organization of the mixed community, whereas small geometrical feature only have a local impact on the organization of the community.

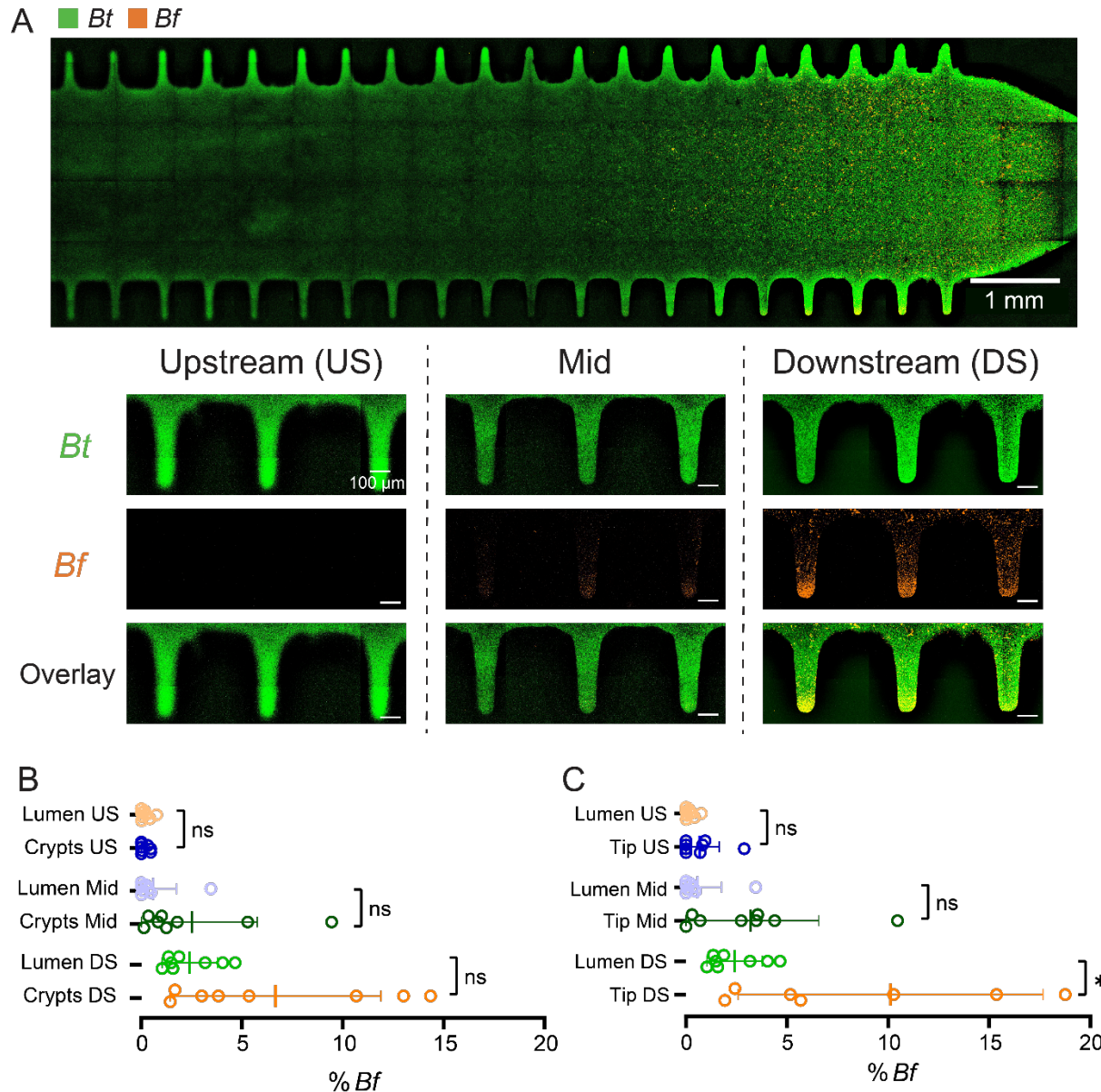


Figure 3.5: Spatial organization of *Bt-Bf* biofilms in crypt-like features. (A) Full channel view of a *Bf-Bt* co-culture biofilm in dextran grown in channels decorated with crypts (top). Close-up images of colonized crypts at upstream, mid and downstream positions of the biofilm (bottom). (B) Proportion of *Bf* in dextran co-culture biofilms inside the lumen and crypts. *Bf* population favours colonization at downstream positions within in lumen. No significant differences in *Bf* population was observed between the lumen and crypt structures. (C) Proportion of *Bf* in dextran co-culture biofilms at crypt tips compared to the lumen. In downstream locations, *Bf* abundance is higher at the tip of the crypts. Statistical test: unpaired t-tests, * $p < 0.05$.

3.3.6 Simulating glucose transport predicts *Bf* biofilm growth

The distribution of a public good depends on its diffusion and on transport by flow. The non-dimensional Péclet number (Pe) estimates the relative contribution of these two transport mechanisms⁸⁷. In the case of glucose, we calculated that $Pe \sim 6$ for the flow rates applied in our experiments. In physiological conditions, gut contents enter the proximal colon under an estimated flow speed of $30 \mu\text{m/s}$ ¹¹⁸. Flow velocity decreases to about $5 \mu\text{m/s}$ by the end of the ascending colon¹¹⁹. This in turn enforces Pe in a range between 1 and 100. We anticipate that glucose distribution, and ultimately the spatial arrangement of *Bt-Bf* biofilms, will consequently strongly depend on Pe . We therefore explored the distribution of public goods *in silico* using finite element simulations for the transport of glucose in the fluidic system.

We performed 2D simulations under a laminar flow to compute the glucose concentration profile. We assumed a constant flux boundary condition at the channel base that models the secretion of glucose by a uniform *Bt* biofilm degrading dextran. By first running these simulations in 2 cm-long channels, we observed that the concentration profile shifts in the direction of the flow (Fig. 3.6A, S3.6A). Further increasing the flow to reach $Pe \sim 100$ strongly reduced the glucose concentration across the channel, creating a boundary layer of secreted glucose near the channel surface. We then computed the glucose concentration profiles near the bottom-surface of the channels. We identified a boundary condition that permits *Bf* growth within the channel (Fig. S3.6B). The effective glucose concentration at any given location of the channel decreases with increasing Pe , as glucose is being depleted by stronger flows. Thus, a glucose concentration enabling *Bf* growth would be encountered further downstream, increasing the population shift. To highlight the dependence of λ on Pe , we computed the position along the channel that yields a 1 mM of glucose concentration (Fig 3.6B). We find that λ increases with Pe (Fig. 3.6C). The absolute values were consistent with the shift we measured at $Pe \sim 6$.

These simulations confirm that flow can promote the population shifts we observed experimentally. Moreover, they predict that further increasing the flow would shift the *Bf*

population further downstream. To experimentally validate this prediction, we fabricated ~7 cm-long microfluidic channels that would enable visualization at the simulated length-scale. We grew *Bt-Bf* biofilms at $Pe \sim 60$ in these channels (Fig. S3.7). We observed growth of *Bf* at positions that were much farther downstream than in lower flow regimes (Fig. 3.6D, E). Consistent with our simulations, λ increased in comparison with lower Pe experiments (Fig. 3.5F) and nearly matched the prediction from simulations (Fig. 3.6C). These experimental results further demonstrate that flow shapes the landscape of public good availability. We note that the *Bf* biofilms grew less dense in the stronger flow conditions (Fig. S3.8). This could be likely caused by a reduction in nutrient concentration induced by flow, and/or by the increased shear stress eroding biofilms, which also causes noticeable changes in biofilm morphology (Fig. S3.8, S3.9).

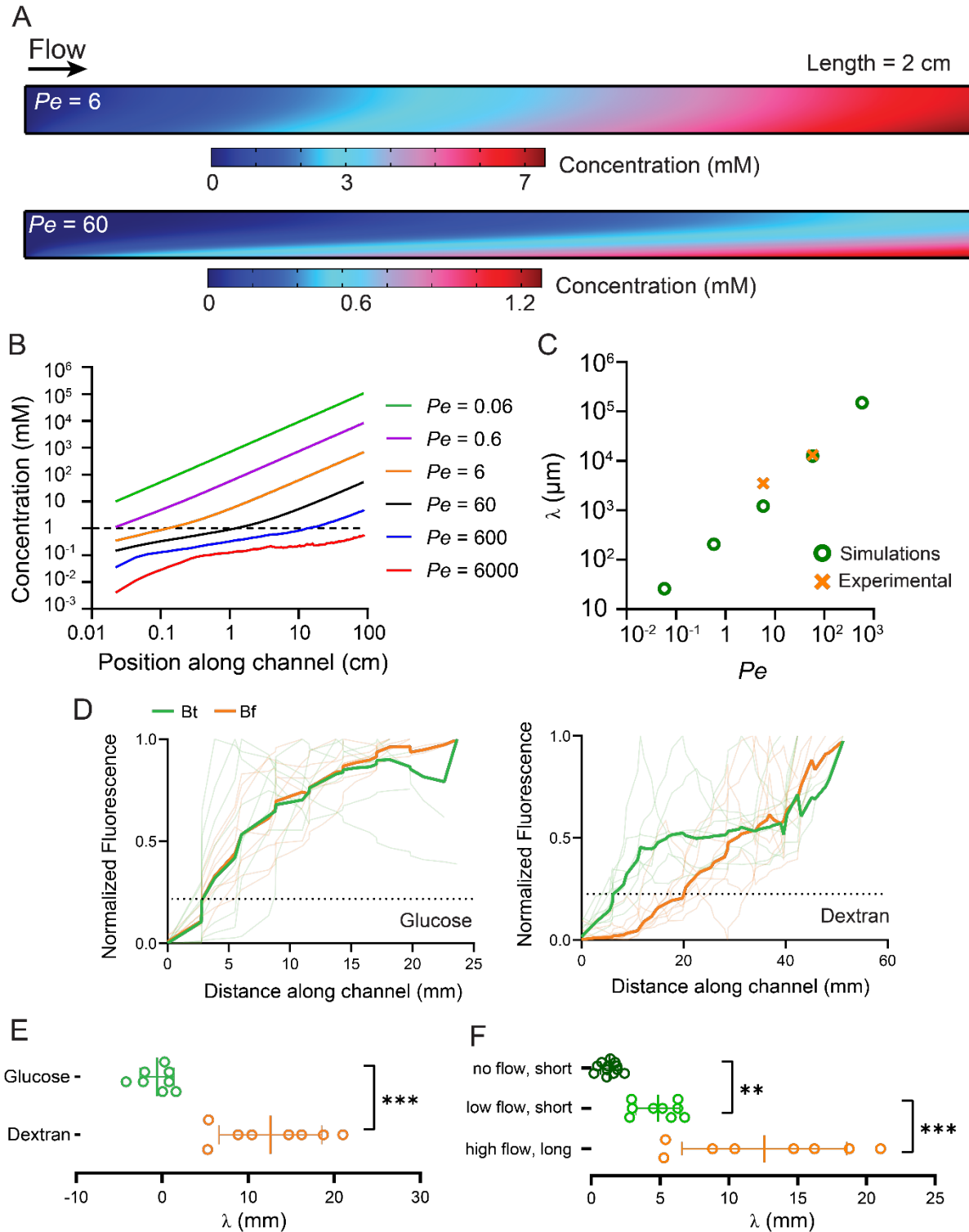


Figure 3.6. Flow impacts community organization by distributing metabolic by-products.

(A) Simulated concentration gradient of glucose along a 2 cm-long channel at $Pe = 6$ and $Pe = 60$. (B) Simulated glucose concentration profiles along a 1m long channel under various Pe regimes with constant flux boundary condition. We define the populational shift λ as the x-

position where the glucose concentration reaches 1 mM. (C) Populational shift λ increases with Pe in simulations and experimental data. (D) Cross-sectional averaged fluorescence intensity profiles of *Bf* and *Bt* biofilms along 10 cm-long microchannel at $Pe = 60$. Each line corresponds to a biofilm from a single co-culture experiment. Bold lines correspond to the average of 7 replicates. (E) *Bf* longitudinal shift (λ) of co-culture biofilms grown in dextran or glucose under high flow ($Pe = 60$) in long microchannels. (F) *Bf* longitudinal shifts (λ) of co-culture biofilms grown in dextran under no flow, low flow and high flow conditions. The λ of the high flow condition is obtained using the long channels.

3.3.7 Flow impacts community composition

Our simulations and experiments show that flow can shift *Bf* population downstream. In a channel of finite length, sufficiently strong flow could push *Bf* outside of the fluidic system, thereby affecting community composition. To explore this catastrophic possibility, we tested whether a fluidic system whose length is shorter than λ could abolish *Bf* growth. To test this hypothesis, we applied a strong flow in a 2 cm-long channel (1 μ l/min, $Pe = 60$, predicting $\lambda = 12$ mm). Consistent with our predictions, *Bf* failed to grow as biofilms while single cells remained attached to the surface (Fig. 3.7A). We quantified the effect of flow on the stability of *Bf* by computing the relative abundance of *Bf* and *Bt* at all flow intensities. Both species grew equally in glucose irrespective of flow intensity, ruling out a possible effect of adhesion strength differences between *Bt* and *Bf* (Fig. 3.7B). In dextran, the *Bf* fraction was however lower than *Bt*, and decreased as flow increased (Fig. 3.7B), so that the *Bf* population in the biofilm at the highest flow rate was negligible (Fig. 3.7A). Overall, this result demonstrates the strong impact of flow and channel geometry on biofilm community composition during nutrient sharing.

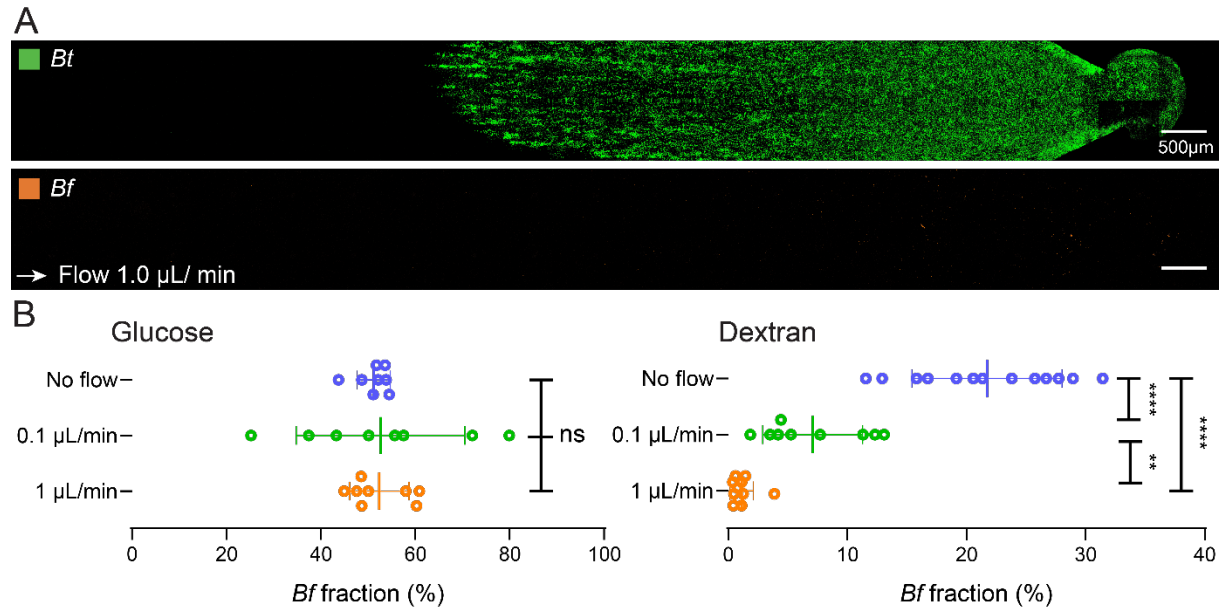


Figure 3.7: Flow impacts community composition during nutrient sharing. (A)

Confocal images of *Bt* and *Bf* co-culture biofilms grown in dextran for 4 days in high flow (flow rate, 1 $\mu\text{L}/\text{min}$). (B) Fraction of *Bf* in co-culture biofilms grown in glucose or dextran at different flow rates. *Bf* fraction decreases with flow in dextran cross-feeding conditions, while it remains insensitive to flow in glucose. Error bars show standard deviation across replicates. Statistical test: unpaired t-tests, ** $0.01 < p < 0.001$, *** $0.001 < p < 0.0001$ and **** $p < 0.0001$.

3.4 Discussion

In well-mixed liquid cultures of multiple species, social interactions impact the growth of each member of the community, ultimately directing ecosystem dynamics. Metabolic interactions are common among microbiota species and provide immediate benefits to the community and the host. For example, commensals share acetate and butyrate, the end-products of carbohydrate metabolism¹²⁰. *In vitro*, *Bacteroides ovatus* produces enzymes which degrades complex polysaccharides into oligosaccharides released at the cell surface, which can be subsequently utilized by surrounding bacteria¹⁰³. We here found that *Bt* can share dextran metabolic by-products with *Bf*, identifying an orthogonal syntrophic interaction between gut microbiota species from a common food additive.

In the context of biofilms, population structure mediates social interactions between different clones or species⁸³. Diffusible solutes such as metabolites and signaling molecules frequently mediate these interactions. Recent developments in imaging, microfluidics and theoretical biophysics have identified how fluid flow can impact the spatial structure and genotypic or phenotypic heterogeneity of biofilms^{90,91}.

Experimental demonstrations typically employ strains with engineered syntrophic interactions. For example, *V. cholerae* degrades chitin into metabolically-accessible saccharides. A mutant lacking a chitinase gene behaves as a cheater when mixed with a wild type population in chitin, thereby creating a fitness penalty for the producer. Fluid flow relaxes this penalty by dispersing the common good, enabling co-existence⁹⁰.

Surface-attached biofilm communities in the GI tract also experience mechanical forces generated by the flow of gut content and mucus, which in principle should impact spatial organization and community composition. Theory predicts that intestinal flow and peristaltic mixing can have a strong impact on microbiota diversity and spatial organization, and has been validated with an engineered cross-feeding community of *Escherichia coli*⁹¹. Still, the mechanisms by which anaerobic microbiota species interact in metabolically in a mechanically-realistic environment have yet to be demonstrated, in particular in the context of biofilms, a lifestyle that has been overlooked in investigations of the human gut microbiota.

We showed that *Bt* shares public goods with *Bf* in a flow-dependent manner which enables co-existence in a structured community. These flows replicate the ones which the microbiota experiences in the proximal and distal colon. Intermediate flow shifts *Bf* populations downstream from *Bt* biofilms. In stronger flow in short channels, advection reduces the local concentration of metabolic by-product to such an extent that it abolishes *Bf* colonization. Thus, by influencing the transport of signalling molecules or public goods, fluid flow mediates social interactions and ultimately microbiota biofilm community composition (Fig. 3.8)¹²¹. We showed that physiological fluid flow impacts the organization and stability of a cross-feeding community composed of two physiologically-relevant human microbiota wild-type species. Our results therefore

mechanistically demonstrate with physiologically-relevant microbiota members the predictions from theory and engineered communities^{91,119,122}.

By controlling the physical and chemical environment of the mucosa, the host creates distinct ecological niches along the GI tract¹²³, each of which is colonized by a specific set of species¹²⁴. Thus, gradients of pH, oxygen or mucus production from the stomach to the colon impose local selective pressures that drive the spatial organization of the microbiota. We showed that flow-dependent transport alone can create such gradients. The resulting spatial organization of bacteria produces chemical gradients of metabolites and signalling molecules that in turn can impact host physiology, ultimately shaping mucosal environment. The spatial structure of microbiota communities thus mediates a feedback between host and commensals, ultimately influencing intestinal homeostasis and host health.

We postulate that fluid flow mediates the spatial organization of bacteria along the human colon in part by influencing the distribution of carbohydrates which constitute major metabolic substrates for cross-feeding. Commensals capable of utilizing complex polysaccharides have a selective advantage in colonizing the proximal colon. Utilizers of simpler glycans produced by primary fermenters would thus colonize the more distal colonic regions. Consistent with this, the overall microbial abundance and diversity increases from the proximal to the distal colon⁸⁶. By transporting metabolites downstream of primary fermenters, flow strongly impacts community composition and can even abolish the growth of a secondary utilizer. Therefore, the biofilm lifestyle and flow are crucial factors to consider in investigations of microbiota composition and stability.

With a realistic model microbiota that integrates polysaccharide utilization and cross-feeding in biofilms, we demonstrated that flows at physiologically-relevant velocities influence the architecture and composition of microbiota biofilms. We therefore postulate that hydrodynamic perturbations induced by changes in intestinal flows or viscosity in the GI tract will impact metabolic interactions between commensals, thereby

modulating community structure and host physiology. The mechanisms that mediate the spatial organization of more complex microbiota communities are still not comprehensively understood, but likely combine biochemical and physical factors. As an illustration, our observation of enrichment of *Bf* at the tips of crypts-like features is reminiscent of *in-vivo* experiments that identified a gene associated with preferential crypt colonization¹²⁵. Advances *in vivo* imaging methodologies of microbial communities have the potential to provide a high-resolution perspective on these complex communities and on the biological and physical forces driving their assembly at the host mucosal surface. A mechanistic understanding of these principles will however require combining animal studies with *in vitro* experimentations like the one we present here. The development of organoid-based host models that integrate *in vivo* parameters critical to host-microbiome interactions such as the mucus layer or even peristaltic motion will these studies to produce a comprehensive understanding of the elementary principles shaping gut microbiota composition and organization^{126–128}.

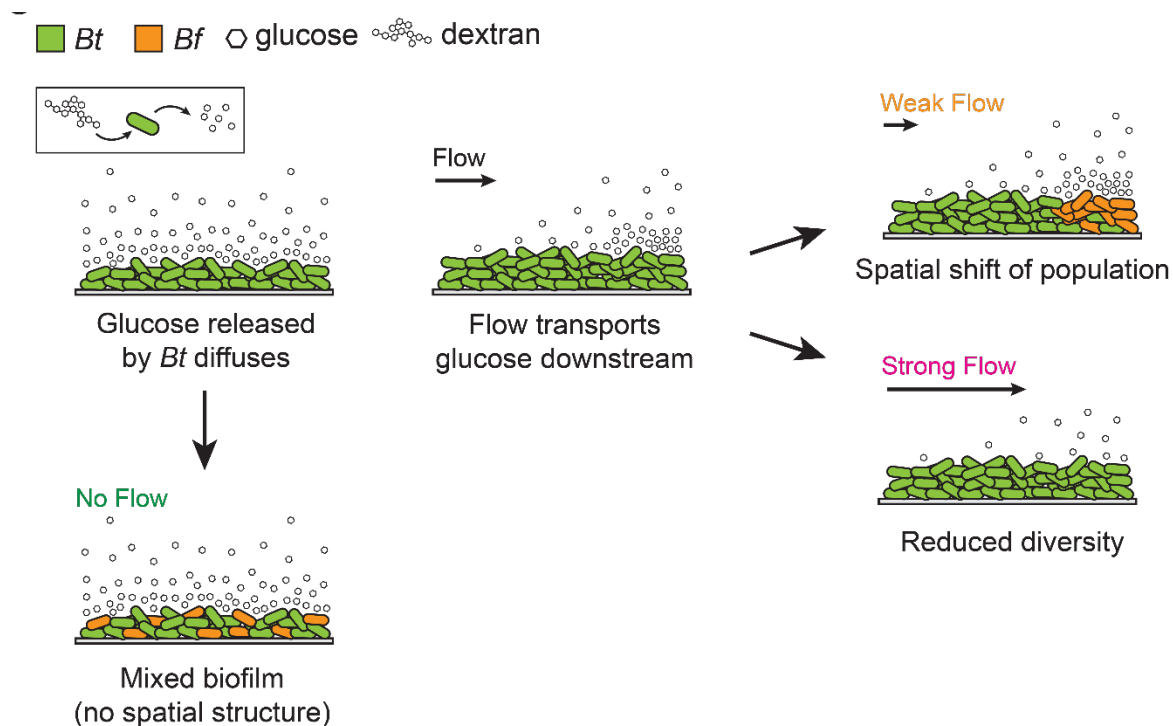


Figure 3.8. Overview of how fluid flow structures nutrient sharing microbial communities. *Bt* releases glucose when metabolizing dextran. Without flow, glucose

diffuses anisotropically. Fluid flow transports glucose downstream, generating a concentration gradient along the channel. *Bf* grows downstream in regions with high glucose concentration. In sufficiently strong flow, glucose concentration is not sufficient to sustain *Bf* growth. Thus, flow impacts community composition by shaping the chemical landscape of public goods.

3.5 Methods

3.5.1 Strains and culture media

Bacteroides thetaiotaomicron VPI-5482 sfGFP and *Bacteroides fragilis* NCTC-9343 mCherry⁷⁶ were used for all experiments in this work. *Bacteroides* minimal medium (BMM) supplemented with the indicated carbon source was used in all experiments. The medium was prepared as previously described⁷⁷. Briefly, a 10x medium stock containing 1 M KH₂PO₄, 150 mM NaCl and 85 mM (NH₄)₂SO₄ was first prepared and adjusted to a pH of 7.2. Solutions of 1 mg/mL vitamin K₃, 0.4 mg/mL FeSO₄, 0.1 M MgCl₂, 0.8% (w/v) CaCl₂, 0.01 mg/mL vitamin B₁₂ and 1.9 mM hematin–0.2 M histidine solutions were prepared separately. To prepare 100 mL of BMM, 10 mL of the 10x salts were mixed with 0.1 g of L-cysteine, 50 µL of vitamin B₁₂ solution, and 100 µL of each vitamin K₃, FeSO₄, MgCl₂, CaCl₂ and hematin-histidine solution. All carbon sources were added to a final concentration of 5 mg/mL. The media were filter-sterilized using a 0.22 µm filter unit and degassed in the anaerobic chamber overnight. All bacteria were cultured at 37 °C under anaerobic conditions in a vinyl anaerobic chamber (COY) inflated with a gas mix of approximately 5% carbon dioxide, 90% nitrogen and 5% hydrogen (CarbaGas). Bacteria were first streaked on brain heart infusion plates (SigmaAldrich) containing 10% sheep blood (TCS BioSciences). Single colonies were then inoculated in BMM and grown overnight.

3.5.2 Microchannels fabrication

Microchannels were fabricated by standard soft-lithography as previously described⁷⁹ with slight modifications. Three different types of channels were fabricated in this study: the simple short channels which are 2 cm-long, 2 mm-wide channels and 300µm-deep,

the crypted short channels, which are short channels containing crypt features 500 μ m-long and 50 μ m-wide and the long channels which are ~7 cm long (6 cm-long straight channels and 2 turns of roughly 0.33 cm-long respectively), 2 mm-wide channels and 300 μ m-deep. Upon cutting out the cured PDMS (Sylgard 184, Dow Corning) channels, 1 mm inlet and outlet, along with a 6 mm hole were punched immediately downstream of the inlet. The PDMS was then bound to cleaned glass without plasma treatment. Medium was then loaded through the inlet until the 6 mm hole was filled up, where a piece of PDMS was then used to seal the hole. This hole served as the bubble trap of the microchannel. Medium was then loaded until the channel was filled.

3.5.3 Biofilm growth

All dextran biofilm growth experiments were performed in BMM-dextran (M_w 35000-45000 Da). For glucose co-cultures, overnight monocultures of *Bt* and *Bf* in glucose were mixed at a 1:1 ratio upon OD measurements and appropriate initial dilutions. For dextran co-cultures, *Bt* and *Bf* were mixed at a 1:1 ratio to a final OD of 0.1 and grown as a co-culture overnight. To initiate biofilm formation in flow, cell cultures were diluted to a final OD of 0.01. 4 μ L of the diluted bacterial culture was then loaded into the microchannels through the outlet and statically incubated for 15 minutes promoting initial attachment. The inlet was then connected to a 10 mL disposable syringe (BD Plastipak) filled with the medium and mounted onto a syringe pump (KD Scientific), using a 1.09 mm outer diameter polyethylene tube (Instech) and a 27G needle (Instech). All biofilms were then grown anaerobically for 4 days at 37°C under the volume flow rates of 1.0 μ L/min or 0.1 μ L/min, which corresponds to the flow velocities of roughly 28 μ m/s and 2.8 μ m/s respectively. These values were chosen as they fall into the physiological range of flow velocities between the proximal and the end of the ascending colon: approximately 30 μ m/s¹¹⁸ and 5 μ m/s¹¹⁹. The procedure was identical for biofilms growing in no flow conditions so that nutrients can diffuse from syringes. Upon 4 days of growth, the tubings were carefully disconnected. For biofilm growth in the absence of flow, cells were cultured, and seeded as mentioned above. 10 μ L of medium was then injected slowly through the inlet to flush away unattached cells. 100 μ L droplets of medium was then carefully deposited on top of the inlet and outlet to

prevent the channel from drying. The biofilms were then removed from the anaerobic chamber and incubated in an oxygenated environment for 2 hours to allow for fluorescent protein folding while maintaining biofilm integrity. The biofilms were then imaged by fluorescence confocal microscopy.

3.5.4 Calculation of Péclet numbers (Pe)

Péclet numbers (Pe) of glucose in each of our flow conditions were calculated based on experimental diffusion coefficients glucose in water at 37 °C¹²⁹. We then computed $Pe = (v * h)/D$, where h is the microchannel height, v the mean flow velocity and D the diffusion coefficient of glucose. The Pe of glucose under high flow conditions is 8.76 and 0.88 under low flow conditions.

3.5.5 Microscopy

All biofilm imaging were performed using a Nikon Eclipse Ti2-E inverted microscope coupled with a Yokogawa CSU W2 confocal spinning disk unit and equipped with a Prime 95B sCMOS camera (Photometrics). The two objectives used for imaging were the 20x APOChromat water immersion objective with a numerical aperture (N.A.) of 0.95 and the 60x water immersion objective with an N.A. of 1.20. Z-stacks were recorded at a 0.5 µm step-height. Fiji was then used for the display of all images. For the visualization of the full biofilm, frames were taken across the xy-plane and stitched together upon background subtraction as described in the image analysis section. All single cell counting experiments in liquid cultures were performed using the Nikon TiE epifluorescence microscope coupled with a Hamamatsu ORCA Flash 4 camera and a 40 x Plan APO NA 0.9 objective. Fiji was then used to display the images.

3.5.6 Image Analysis

To acquire images of biofilms along the entire channel, tile imaging was performed and images were subsequently stitched together using the 'make montage' function upon background subtraction in Fiji. The relative abundance of *Bt* and *Bf* in biofilms were calculated by computing the area of coverage by each strain in Fiji. To quantify the 1st

nearest neighbor distance between *Bf* and *Bt*, we selected 4000 random pixels in the segmented sfGFP picture for each stitched biofilm images. We then calculated the distance between the selected pixels and their nearest neighbor pixels in the corresponding segmented mCherry picture. This way we obtained an average 1st nearest neighbor distance for each stitched biofilm images. For each biofilm, the highest 1st nearest neighbour distance value was filtered out and a mean value of the remaining stacks was calculated. To quantify the relative positioning of *Bf* and *Bt*, we computed the fluorescence intensity along the channel for each 660 μm -wide field of view upon background subtraction. The fluorescent intensity of frames corresponding to the same x positions were then averaged. This was then used to generate fluorescent intensity profiles for *Bt* and *Bf*. For each, the biofilm edge was computed as the x-position at which the fluorescence reached 25% of the maximum intensity. The difference between *Bt* and *Bf* upstream edge positions were then calculated to measure the positional shift between *Bt* and *Bf*, denoted as λ . A similar procedure without averaging the fluorescent intensity of frames corresponding to the same x-positions was used to quantify the relative distribution of *Bt* and *Bf* as a function of biofilm height.

For *Bf* abundance in channels containing crypts, we first divided the channel into 6 zones: upstream lumen, upstream crypts, mid lumen, mid crypts, downstream lumen and downstream crypts. Within the lumen, the average fluorescence intensity of *Bt* and *Bf* were measured, where we then calculated the average number of cells of *Bt* and *Bf* in each respectively by dividing the average intensity of the zone by the average fluorescence of individual cells within individual channels. We then sum the number of *Bt* and *Bf* cells in order to back calculate the % abundance of *Bf* in each respective region. The crypts were analyzed in a similar manner, where the number of *Bt* and *Bf* cells were quantified in individual crypts. The % abundance of *Bf* in each individual crypt were calculated, and averaged across all crypts which belong to the same zone.

3.5.7 Simulations of concentration gradients in flow

All simulations were performed in COMSOL Multiphysics 5.4. We defined our channels as rectangles with the size of 2 cm by 0.1cm (short channels) and 1 m by 0.1 cm (long

channels), with the material being water, liquid. We then simulated the flow profiles within our channels under the conditions $T = 310.15$ K and $p = 1$ atm, with defined channel walls, inlet and outlet using the creeping flow module. We then coupled the creeping flow with transport of diluted species, where we defined the initial glucose flux of $J_{0,c} = 1e^{-6}$ mol/(m²s) on the bottom wall of the channels, corresponding to bacteria secreting glucose on the surface of the microfluidic channels. The concentration gradient along the channels were then simulated with mesh size = normal, under steady state.

3.5.8 Competition experiments in test tubes

Bt and *Bf* were cultured in Bacteroides Minimal Medium (BMM) supplied with 5 mg/mL of D(+)- glucose (Carl Roth), dextran M_w 9000-11000 (SigmaAldrich), dextran M_w 35000-45000 (SigmaAldrich), arabinan (Megazyme) and inulin from dahlia tubers (SigmaAldrich). To start competition experiments, *Bt* and *Bf* were grown separately in 1 mL of BMM-glucose overnight. The resulting cultures were then pelleted by centrifugation and washed twice with PBS. The pellets were then resuspended in PBS, where the OD was measured. *Bt* and *Bf* were then mixed at a 1:1 ratio to an initial OD of 0.1 in each of the carbon sources tested. The cultures were then grown anaerobically for 2 days. A microscopy approach was then used to quantify the relative abundances of *Bt* and *Bf* in these cultures. To achieve this, the cultures were mixed well and 10 µL of each cell culture was sampled at day 1 and 2. The cultures were then diluted in PBS and incubated at aerobic conditions. The samples were then spotted onto a glass coverslip and covered by a thin agarose pad prior to fluorescence imaging by widefield fluorescence microscopy. For each sample and replicate, 3 image frames across the agar pad were recorded. The relative abundance of sfGFP- and mCherry-expressing cells in each sample were then quantified using the 'analyze particle' function in Fiji and averaged across the 3 frames.

3.5.9 Sample preparation, mass spectrometry and data analysis for proteomics

Bt was cultured in BMM-glucose and BMM-dextran (M_w 9000-11000) overnight from an initial OD of 0.01. Cells were lysed and lysates containing 20 µg of protein content were collected for further analysis. Cell lysates were digested with trypsin using the Filter-Aided Sample preparation (FASP)¹³⁰ protocol with minor modifications. Proteins were resuspended in 200 µl of 8 M urea; 100 mM Tris-HCl and deposited on top of Microcon-30K devices. Samples were centrifuged at 9391 g at 20°C for 30 min. All subsequent centrifugation steps were performed using the same conditions. An additional 200 µl of 8 M urea 100 mM Tris-HCl was added and devices were centrifuged again. Reduction was performed by adding 100 µl of 10 mM TCEP in 8 M urea, 100 mM Tris-HCl on top of filters followed by 60 min incubation at 37 °C with gentle shaking and protected from light. Reduction solution was removed by centrifugation and filters were washed with 200 µl of 8 M urea, 100 mM Tris-HCl. After removal of washing solution by centrifugation, alkylation was performed by adding 100 µl of 40 mM chloroacetamide in 8 M urea, 100 mM Tris-HCl and incubating the filters at 37 °C for 45 min with gentle shaking and protected from light. The alkylation solution was removed by centrifugation and another washing/centrifugation step with 200 µl of 8 M urea 100 mM Tris-HCl was performed. This last urea buffer washing step was repeated twice followed by three additional washing steps with 100 µl of 5 mM Tris-HCl. Proteolytic digestion was performed overnight at 37 °C by adding 100 µl of Endoproteinase Lys-C and Trypsin Gold in an enzyme/protein ratio of 1:50 (w/w) on top of filters. Resulting peptides were recovered by centrifugation. The devices were then rinsed with 50 µl of 4% trifluoroacetic acid and centrifuged. This step was repeated three times and peptides were finally desalted on SDB-RPS StageTips¹³¹.

For LC-MS/MS analysis, resuspended peptides were separated by reversed phase chromatography on a Dionex Ultimate 3000 RSLC nano UPLC system connected in-line with an Orbitrap Lumos (Thermo Fisher Scientific, Waltham, USA). A capillary precolumn (Acclaim Pepmap C18, 3 µm-100 Å, 2 cm x 75 µm ID) was used for sample trapping

and cleaning. A capillary column (75 μm ID; in-house packed using ReproSil-Pur C18-AQ 1.9 μm silica beads; Dr. Maisch; length 50 cm) was then used for analytical separations at 250 nl/min over 150 min biphasic gradient. Acquisitions were performed through Top Speed Data-Dependent acquisition mode using a 1 second cycle time. First MS scans were acquired at a resolution of 240000 (at 200 m/z) and the most intense parent ions were selected and fragmented by High energy Collision Dissociation (HCD) with a Normalized Collision Energy (NCE) of 30% using an isolation window of 0.7 m/z. Fragmented ion scans were acquired in the ion trap using a fix maximum injection time of 20 ms and selected ions were then excluded for the following 20 s.

Protein identification and label free quantification were performed using MaxQuant 1.6.10.43¹³². The *B. thetaiotaomicron* Uniprot reference proteome database was used for this search. Carbamidomethylation was set as fixed modification, whereas oxidation (M), phosphorylation (S, T, Y) and acetylation (Protein N-term) were considered as variable modifications. A maximum of two missed cleavages were allowed for this search. “Match between runs” was selected. A minimum of 2 peptides were allowed for protein identification and the false discovery rate (FDR) cut-off was set to 0.01 for both peptides and proteins. Label-free quantification and normalisation was performed by Maxquant using the MaxLFQ algorithm, with the standard settings¹³³.

In Perseus¹³⁴, reverse proteins, contaminants and proteins only identified by sites were filtered out. Biological replicates were grouped together and protein groups containing a minimum of two LFQ values in at least one group were conserved. Missing values were imputed with random numbers using a gaussian distribution (width = 0.3, down-shift = 1.8). Two-samples t-test was performed to identify the differentially expressed proteins, followed by a permutation-based correction (False Discovery Rate). Significance curves in the volcano plot corresponded to a S_0 value of 1.0 and FDR cut-off of 0.01.

3.5.10 Glycan analysis using HPAEC-PAD

For culture supernatant analysis experiments, *Bt* or *Bf* was inoculated into 1 mL of BMM-dextran M_w 9000-11000 to a final OD of 0.01. The cultures were then grown

overnight for 20 hours anaerobically. The resulting cultures were pelleted by centrifugation and the supernatant was collected. Cation and anion exchange chromatography with AmberChrom resins (SigmaAldrich) were then used to clean up the samples followed by filtering through a 0.22 μ m sterilization filter prior to analysis. The resulting flow-throughs were then analyzed by HPAEC-PAD. For identification of the carbohydrate cross-fed to *Bf*, we produced *Bt* spent medium from a 30 mL culture grown in BMM-dextran for 20 hours. We pelleted the culture, collected the supernatant, and filtered it using a 0.22 μ m sterilization filter. We cultured *Bf* overnight in BMM glucose, washed and resuspended them in BMM without any carbon source, and then added this to the spent medium at a final OD of 0.01. After 24 and 40 hours of growth, we pelleted the cultures and cleaned up the samples with the exact same procedures used for the supernatant samples. The sugars were separated on a Dionex CarboPac PA-20 column from Thermo Fisher Scientific with the following eluent: A) 100 mM NaOH; B) 150 mM NaOH and 500 mM sodium acetate at a flow rate of 0.4 mL/min. The gradient was 0 to 15 min, 100% A (monosaccharide elution); 15 to 26 min, gradient to 10% A and 90% B (malto-oligosaccharide elution); 26 to 36 min, 10% A, 90% B (column wash step); and 36 to 46 min step to 100% A (column re-equilibration). Peaks were identified by co-elution with known glucose, isomaltose standards using the Chromeleon software. The HPLC data was then exported and replotted with the graphing software GraphPad Prism 8, where area under the curve of peaks of corresponding samples were calculated.

3.6 Supplementary information appendix

3.6.1 Supplementary figures

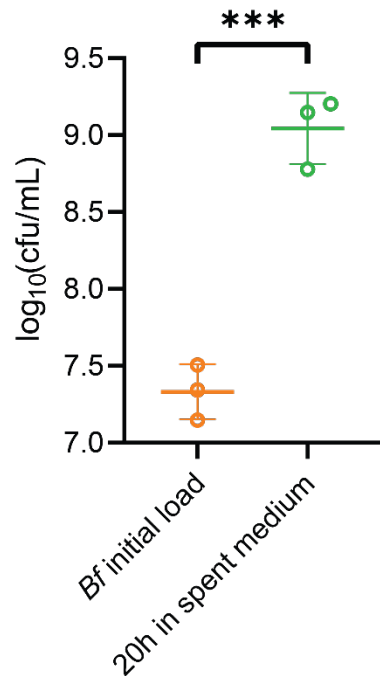


Figure S3.1: *Bt* spent dextran medium supports the growth of *Bf*. We filter-sterilized a *Bt* monoculture in BMM dextran. We then inoculated *Bf* to this spent medium and performed CFU counts at time of inoculation and after 20 h of incubation. *Bf* density increased more than 10-fold, showing that a public good released by *Bt* through dextran degradation supports *Bf* growth. Error bars show standard deviation across replicates. Statistical test: unpaired t-tests, *** $0.001 < p < 0.0001$.

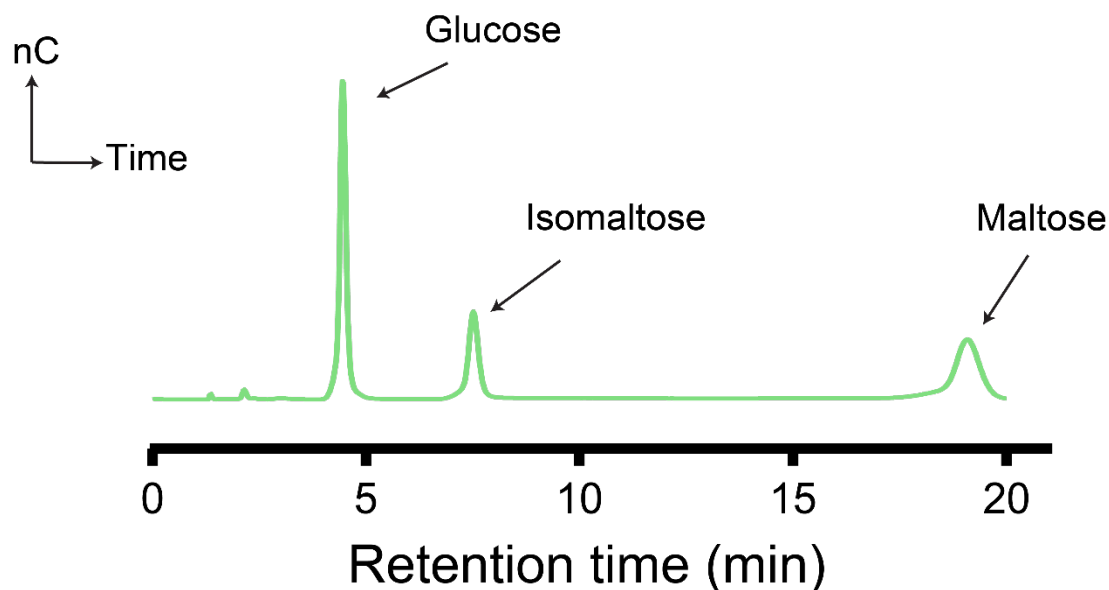


Figure S3.2: HPAEC-PAD standards for sugar identification. A 10 mM standard solution containing glucose, isomaltose and maltose was analyzed by HPAEC-PAD. The retention time of glucose, isomaltose and maltose are ~4.5 min, ~7.5 min and ~19.1 min respectively.

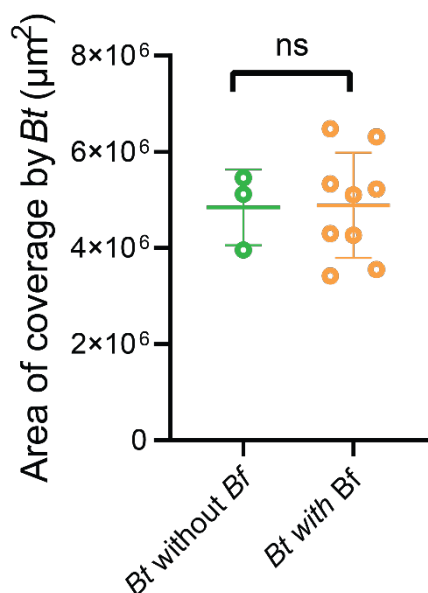


Figure S3.3: *Bt* biofilm growth in dextran is insensitive to the presence of *Bf*. Area of coverage by *Bt* of monoculture and *Bt*-*Bf* co-culture biofilms in dextran reveals no significant changes to *Bt* population induced by the presence of *Bf*. Error bars show standard deviation across replicates. Statistical test: unpaired t-test.

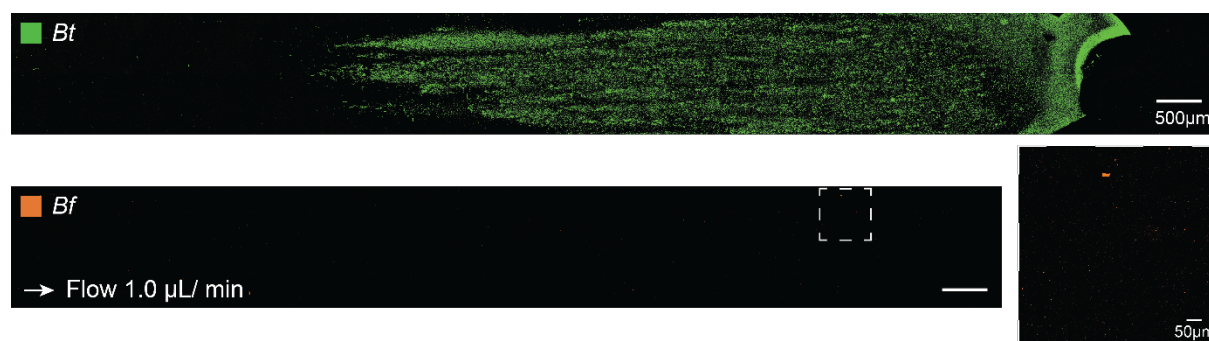


Figure S3.4: *Bf* growth in co-culture biofilms are delayed compared to *Bt*. After 3 days of co-culture biofilm with *Bt*, *Bf* shows no measurable growth. This suggests that

the density of *Bt* biofilms must reach a critical value to produce sufficiently metabolic by-products to enable *Bf* growth.

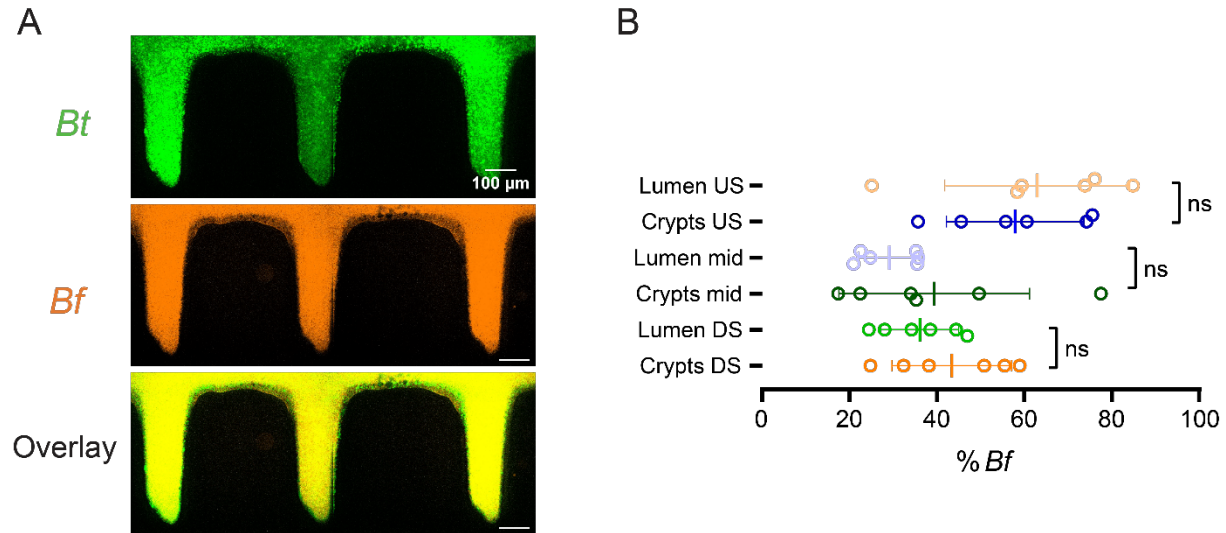


Figure S3.5: Abundance of *Bf* in glucose co-culture biofilms in lumen and crypts.

(A) *Bt* and *Bf* uniformly colonize crypt structures in glucose at high density. (B) *Bf* % abundance in the lumen and crypts. No significant differences in *Bf* abundance were observed between the lumen and crypts.

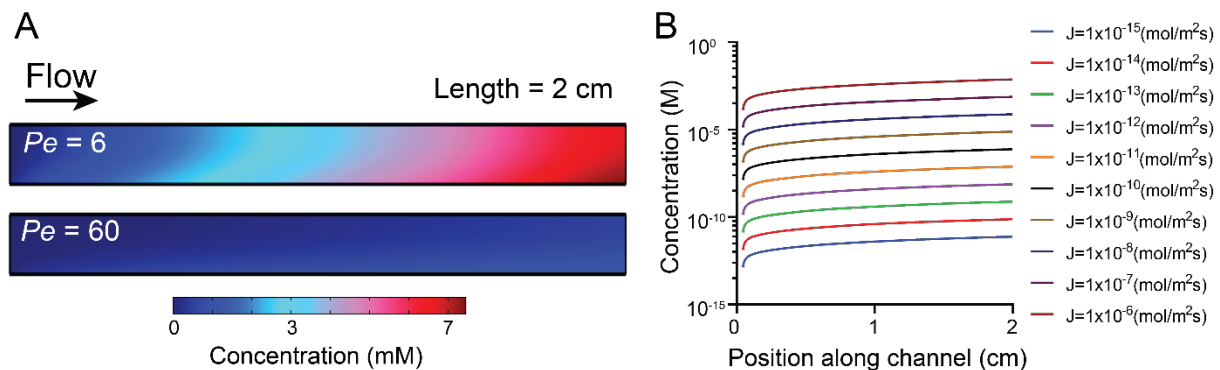


Figure S3.6: Simulation of glucose concentration gradient along channels in the presence of flow. (A) Simulated concentration of glucose along a rectangle with a length of 2 cm under our 2 flow regimes: $Pe \sim 6$ and $Pe \sim 60$. The data is identical to the

one showed in Fig. 6A but displayed with the same concentration scale. (B) Simulated glucose concentrations at the surface of a 2 cm long channel at various initial flux values (J). We defined the critical concentration of glucose required for *Bf* growth to be 1 mM, corresponding to the initial flux $J=1 \times 10^{-6}$ mol/m²s. Therefore, for all subsequent simulations, the J value of 1×10^{-6} mol/m²s is used.

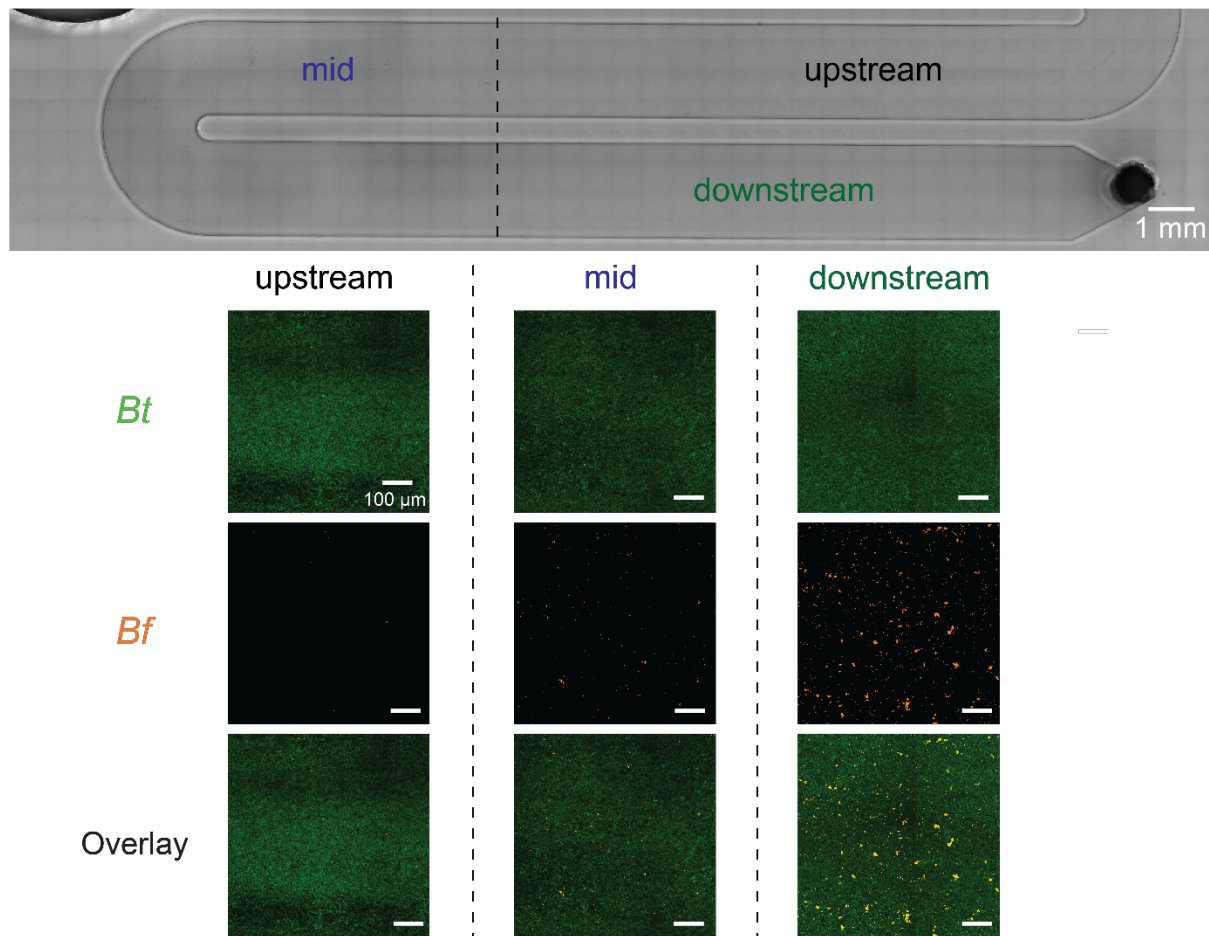


Figure S3.7: *Bf* growth was observed in downstream regions of the long channels under high flow. Brightfield image of the growth channel along with closeup fluorescence images of *Bt*, *Bf* and their overlay from the respective regions of the channel. *Bf* grows into small clusters in positions downstream of the fluid flow.

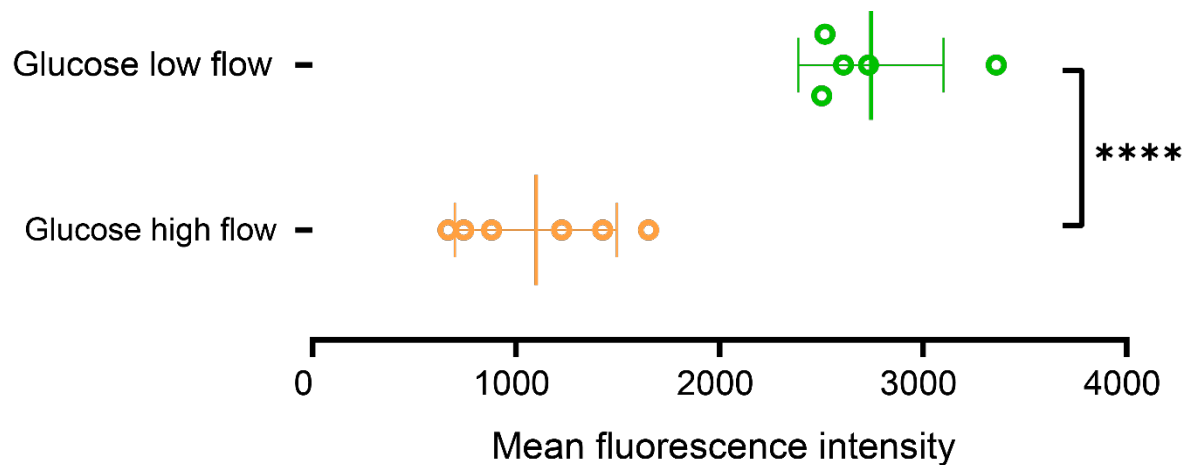


Figure S3.8: Less *Bt* cells were observed in biofilms grown under higher flow conditions. The amount of *Bt* cells present in biofilms grown under high or low flow were assessed by measuring the mean fluorescence intensity of the whole growth channel. More *Bt* cells were present in growth in low flow. Statistical test: unpaired t-test, **** $p < 0.0001$.

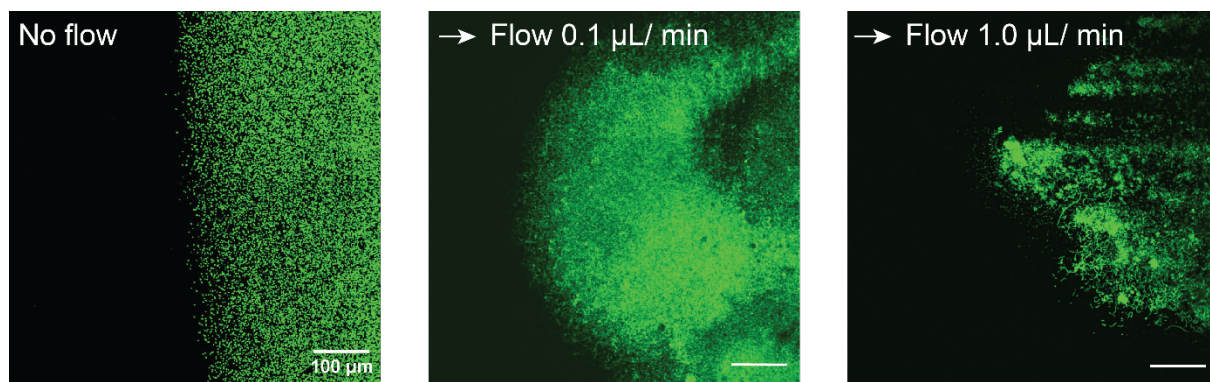


Figure S3.9: Flow produces a comet-like shape *Bt* biofilms at upstream positions. Increasing fluid flow leads to increasingly elongated comet-like tails in upstream positions of *Bt* biofilms, possibly due to increasing erosion of the biofilm as flow increases.

Chapter 4. Size dependent dextran metabolism and nutrient sharing by the gut commensal *B. thetaiotaomicron*

This chapter focuses on how the mechanisms of how gut commensals *B. theta* and *B. fragilis* utilize complex carbohydrate nutrients of various molecular weights and undergo syntrophy. This chapter is a preliminary version of a manuscript that is to be submitted.

Jeremy P. H. Wong, Noémie Chillier, Michaela Fischer-Stettler, Samuel C. Zeeman, Tom J. Battin & Alexandre Persat*, *Bacteroides thetaiotaomicron* metabolic activity decreases with polysaccharide molecular weight.

Author contributions:

J.P.H.W., T.J.B., and A.P. designed research, J.P.H.W., N.C. and M.F.-S. performed research, S.C.Z., T.J.B., and A.P. contributed new reagents/analytic tools, J.P.H.W. analyzed data, and J.P.H.W. and A.P. wrote the paper.

4.1 Abstract

The human colon hosts hundreds of commensal bacterial species, many of which ferment complex dietary carbohydrates. To transform these fibers into metabolically-accessible compounds, microbes often express series of dedicated enzymes homologous to the starch utilization system (*sus*) encoded in polysaccharide utilization loci (PULs). The genome of *Bacteroides thetaiotaomicron* (*Bt*), a common member of the human gut microbiota, encodes nearly 100 PULs, conferring a strong metabolic versatility. While the structures and functions of individual enzymes within the PULs have been investigated, little is known about how polysaccharide complexity impacts the function of *sus*-like systems. We here show that the activity of *sus*-like systems depends on polysaccharide size, ultimately impacting bacterial growth. We demonstrate the effect of size-dependent metabolism in the context of dextran metabolism driven by the specific utilization system PUL48. We find that as molecular weight of dextran increases, *Bt* growth rate decreases and lag time increases. At the enzymatic level, the dextranase BT3087 is the main glycosylhydrolase for dextran utilization and that BT3087 and BT3088 contribute to *Bt* dextran metabolism in a size-dependent manner. Finally, we show that the polysaccharide size-dependent metabolism of *Bt* impacts its metabolic output in a way that modulates the composition of a producer-consumer community it forms with *Bacteroides fragilis*. Altogether, our results expose an overlooked aspect of *Bt* metabolism which can impact the composition and diversity of microbiota.

4.2 Additional background

Polysaccharides are complex, polymeric molecules composed of long chains of monosaccharide subunits linked together through glycosidic linkages¹³⁵. These molecules are essential to life¹³⁶ and are commonly found in our daily diets¹³⁷. Their chemical structures are variable due to differences in monosaccharide compositions and glycosidic linkage patterns¹³⁸. As a result, the degradation of these molecules requires diverse sets of enzymes that generally target specific polysaccharides. While

humans lack the ability to degrade many polysaccharides, their intestinal microbiota contains bacterial commensals that are versatile polysaccharide utilizers. In fact, microbiota species are selected for the ability to forage more or less complex carbohydrates and glycans¹³⁹. Thus, for many gut microbes, the ability to persist in the gut correlates with their ability to utilize dietary fibers and other carbohydrate-based nutrients¹⁴⁰. Therefore, understanding the mechanisms of polysaccharide utilization by gut microbes may provide an understanding to the forces driving the composition of the gut microbiota¹³⁹.

Bacteroides spp. are among the most abundant and well-studied glycan-foraging commensals found in the human bowel⁹². *Bacteroides* can utilize complex carbohydrates through the expression of series of protein systems encoded in polysaccharide utilization loci (PULs)¹⁴¹. PULs encode for proteins which bind, cleave and import complex polysaccharides into simpler, metabolically-accessible sugars^{94–98}. *Bacteroides thetaiotaomicron (Bt)* can utilize many dietary polysaccharides including starch¹⁴², arabinan⁶³, levan¹⁴³, inulin¹⁴⁴, rhamnogalacturonan II¹⁴⁵, complex dietary N-glycans¹⁰⁰, and even glycans derived from its mammalian hosts such as o-linked glycans from mucins and HMO (human milk oligosaccharides)¹⁴⁶.

The starch utilization system (Sus) has served as model system for PUL studies¹⁴². In *Bt*, 8 genes encode Sus (*susRABCDEFGG*). *SusD*, *SusE* and *SusF* are outer membrane lipoproteins which are responsible for the initial binding of oligosaccharides to the cell surface^{142,147}. *SusG* is an outer membrane-associated α -amylase which hydrolyzes the starch into maltooligosaccharides¹⁴⁸. The resulting maltooligosaccharides enter the periplasm thanks to the TonB-dependent transporter *SusC*¹⁴⁹. These sugars are further cleaved by two periplasmic glycosylhydrolases (GHs) *SusA* (neopullulanase) and *SusB* (α -glucosidase)^{150,151}. The inner membrane-spanning sensor-regulator protein *SusR* regulates the expression *Sus* genes in response to periplasmic levels of maltose¹⁵². Other PULs are *Sus* homologs encoding the nutrient binding and importer proteins *SusD* and *SusC*, lipoproteins of similar structures to *SusE* and *SusF*, along with a series of diverse GHs dedicated to a wide range of different complex carbohydrates, which are

regulated by a SusR-like protein¹⁵³. The genome of *Bt* encode 96 different PULs⁹⁹, allowing them to grow on a broad range of dietary or host-derived glycans^{94,95,97,100}.

Although different PULs are dedicated to the degradation of specific polysaccharides with unique glycosidic linkages and monosaccharide compositions, a specific polysaccharide may be found with different complexities such as molecular weight (MW) and degree of branching¹³⁸, as in starch produced by different plants¹⁵⁴. Sus-like systems are composed of multiple surface-exposed components that need to coordinate functions to properly cleave and import degraded oligosaccharides. These must therefore handle polymers with the vastly differing physical attributes which may impact their processability. However, little is known about how MW impacts the efficacy of PULs in producing accessible glycans that act as accessible substrate for growth.

In a previous work¹⁵⁵, we have identified dextran as a polysaccharide readily utilized by *Bt*. Like starch, dextran is a polyglucan consisting of 2 unique glycosidic linkages: an α -1,6 linked backbone along with α -1,3 branches¹⁵⁶. Dextran is a common additive in the food industry¹⁰⁵. Unlike starch, dextran polymers are highly soluble in water. Also, due to their extensive commercial and clinical applications, there exists many purification protocols which produce dextran polymers of defined MW¹⁰⁵. Using *Bt* as model commensal and dextran as model dietary fiber, we investigated the impact of polysaccharide MW on the efficacy of dextran utilization by *Bt*. We found that *Bt* growth rate decreases as dextran MW increased. By studying dextran metabolism with *Bt* mutants containing knockouts of PUL48 genes, we identified protein targets within PUL48 whose importance in dextran utilization is MW-dependent, thereby suggesting a mechanism of size-dependent metabolism. We ultimately demonstrate that size-dependent metabolism has an impact on the composition of a model microbiota community.

4.3 Results

4.3.1 *Bt* uses PUL48 to degrade dextran

Bt exposed to dextran as sole carbon source upregulates proteins belonging to the predicted PUL48 and the α -glucosidase BT4581¹⁵⁵ (Fig. 4.1A). Consistent with this, a functional genomic screen identified genes from PUL48 to be essential for growth in dextran¹⁵⁷. PUL48 comprises of a SusD-like surface associated nutrient binding protein (BT3089), a SusC-like TonB-dependent importer protein (BT3090), a SusR-like sensor-regulator protein (BT3091) and 2 GHs: α -glucosidase II (BT3086) and dextranase (BT3087) (Fig. 4.1A). To study the functions of individual PUL48 proteins in *Bt* dextran metabolism, we generated knockout mutants of PUL48 genes (Table 4.1). We first characterized the essentiality of these genes for growth in dextran. We grew individual mutants in *Bacteroides* Minimal Medium (BMM) supplemented with dextran (MW = 35 kDa) over 3 days (Fig. 4.1B). We observed that *Bt* mutants lacking the α -glucosidase II BT3086 and nutrient binding protein BT3088 (SusE) resulted in marginal growth defects in dextran. Mutants lacking the α -glucosidase BT4581 showed delayed growth. Mutants in nutrient binding protein gene BT3089 (SusD) and importer protein BT3090 (SusC) showed severely impaired growth in dextran in comparison to WT *Bt*. Finally, *Bt* mutants in the regulatory protein BT3091 (SusR) and the dextranase BT3087 were entirely unable to grow in dextran (Fig. 4.1B). We examined the growth profiles of *Bt* mutants lacking several GHs: $\Delta 86,81$ (double deletion of BT3086 and BT4581), $\Delta 87,81$ (double deletion of BT3087 and BT4581), $\Delta 86,87$ (double deletion of BT3086 and BT3087) and $\Delta 86,87,81$ (triple deletion of BT3086, BT3087 and BT4581) also suggest that cell growth is eliminated only in the case of the loss of dextranase BT3087 (Fig. S4.1A). These results suggests that the proteins BT3086, BT3088 and BT4581 are auxiliary proteins which promote but are not essential to dextran fermentation. The proteins BT3089 (SusD) and BT3090 (SusC) are important for the proper growth of *Bt* in dextran. Their absence likely leads to a decrease in nutrient availability to *Bt* through impaired oligosaccharide binding and import.

Given the functional results of the mutants on growth phenotypes, we wanted to further understand the contributions of each individual GHs: BT3086, BT3087 and BT4581 in dextran breakdown. We took an *in-vitro* approach to address this question, where we analysed the degradation products of purified GHs. We first produced the three GHs recombinantly: BT3086 (α -glucosidase II), BT3087 (dextranase) and BT4581 (α -glucosidase), all lacking their signal peptide domains. Individually expressed GH constructs were purified by affinity chromatography and subsequently analyzed by SDS-PAGE (Fig. S4.1B). We then incubated individual GHs in BMM-dextran. We analyzed the resulting digested carbohydrate contents by HPAEC-PAD. HPAEC-PAD chromatograms of BMM dextran treated by each of the three enzymes all showed similar patterns degradations but with quantitative differences (Fig. 4.1C). BT4581 produced glucose as the sole degradation product, whereas BT3086 produced glucose and isomaltose as major degradation products. Finally, BT3087 treatment of dextran not only produced glucose and isomaltose as major degradation products, but also other higher MW oligosaccharides (Fig. 4.1C, D). These data suggest that the enzyme BT3087 is the key GH for the initial debranching of dextran polymers, whereas the enzymes BT3086 and BT4581 plays import roles in liberating glucose from dextran – oligosaccharides, which may be subsequently metabolized by *Bt*.

KO name	Annotation and function
$\Delta BT3086$	Deletion of α -glucosidase II BT3086 (GH)
$\Delta BT3087$	Deletion of dextranase BT3087 (GH)
$\Delta susE$	Deletion of <i>susE</i> like BT3088 (Surface glycan binding protein)
$\Delta susD$	Deletion of <i>susD</i> like BT3089 (Surface glycan binding protein)
$\Delta susC$	Deletion of <i>susC</i> like BT3090 (Oligosaccharide import)
$\Delta susR$	Deletion of <i>susR</i> like BT3091 (transcription regulator)
$\Delta BT4581$	Deletion of α -glucosidase BT4581 (GH)
$\Delta 86,87$	Deletion of BT3086 and BT3086 (GH)
$\Delta 86,81$	Deletion of BT3086 and BT4581 (GH)
$\Delta 87,81$	Deletion of BT3087 and BT4581 (GH)

$\Delta 86,87,81$	Deletion of BT3086, BT3087 and BT4581 (GH)
-------------------	--

Table 4.1. Dextran utilization knockout strains generated for this study.

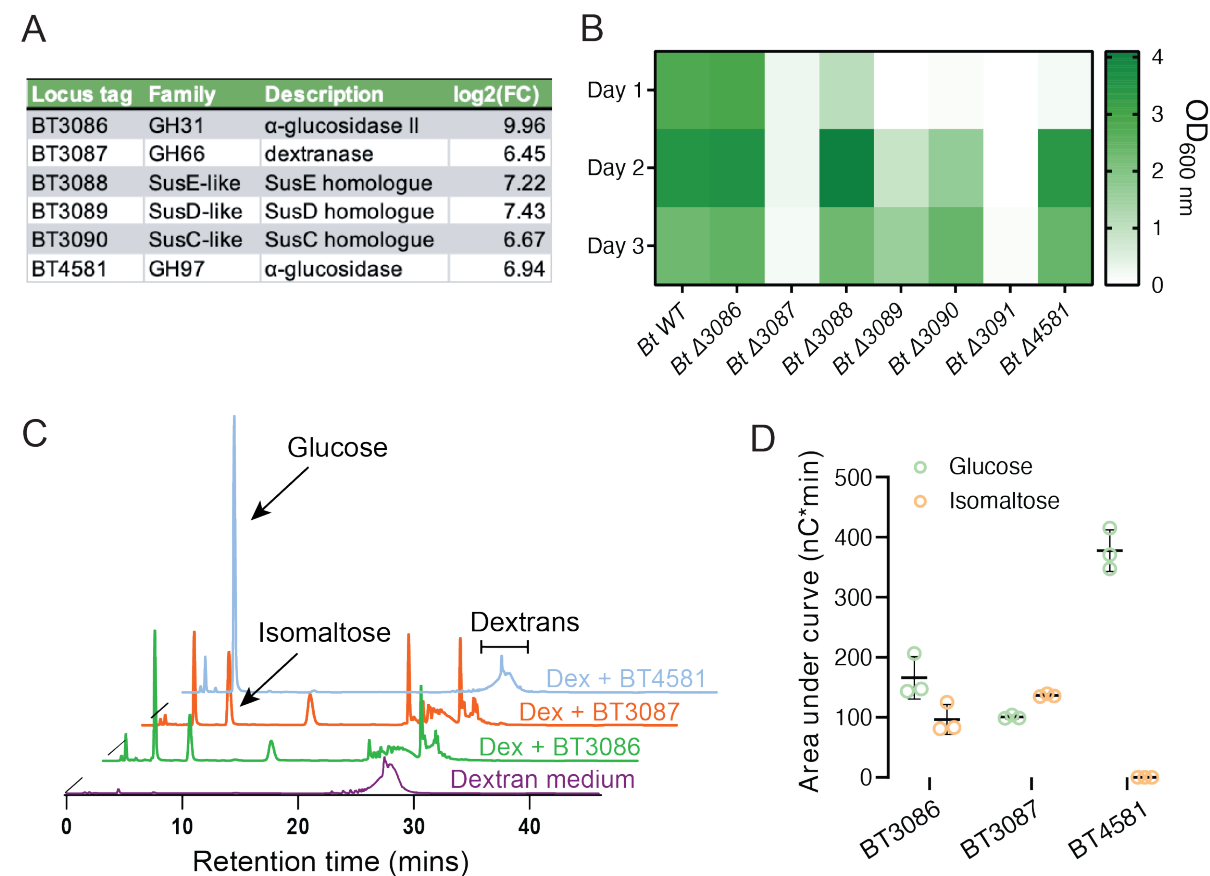


Figure 4.1: The roles of PUL48 proteins in the mechanism of dextran metabolism.

(A) List of proteins (green dots) which are significantly upregulated in dextran along with their functions. These proteins include 6 proteins belonging to the predicted PUL48, along with a sole GH BT4581. (B) Monoculture growths of *Bt* WT and various PUL48 KO mutants in dextran. We measured the optical density (OD) of individual cultures everyday over the course of 3 days. (C) HPAEC-PAD analysis of dextran medium treated overnight with recombinantly expressed GHs: BT3086, BT3087 or BT4581. Violet = no treatment, Green = treatment with BT3086, orange = treatment with BT3087 and blue = treatment with BT4581. (D) Area under the curve analysis of the glucose and isomaltose peaks of dextran treated with BT3086, BT3087 or BT4581. BT3086 and

BT3087 form both glucose and isomaltose as products, whereas BT4581 forms solely glucose. HPAEC-PAD experiments were run in triplicates, we display one representative chromatogram.

4.3.2 *Bt* growth dynamics in dextran is dependent on dextran MW

Dextran polysaccharides exist in a wide range of MW and branching which influence its complexity^{113,158}. We wondered whether the size of the dextran polymer itself may have an influence on the concerted activity of the sus-like enzymes, and therefore on dextran metabolism and subsequent growth dynamics of *Bt*. To explore this possibility, we grew WT *Bt* in dextrans of 3 different MWs: MW = 9 kDa, 35 kDa and 200 kDa (total mass of dextran is equal between conditions). We cultured *Bt* for 3 days while measuring optical density to eventually generate growth curves (Fig. 4.2A). We then quantified maximum OD, lag time and growth rates of individual cultures (Fig. 4.2B). We found that the total biomass *Bt* biomass at its maximum value was independent of dextran MW. However, we found important differences in the dynamics of its growth. First, higher dextran MW tends to increase lag time, thereby delaying recovery from stationary phase. In addition, higher the growth rate of *Bt* is slower in higher MW dextran. Overall, this leads to a delayed growth pattern for *Bt* in higher MW dextran polysaccharide (Fig. 4.2A).

As we have already cultured all PUL48 mutants supplemented with dextran 35 kDa in test tubes (Fig. 4.1B) and observed growth defects in mutants lacking BT3087, BT3089 or BT3090, we then wondered whether changes in dextran MW can further impact the growth dynamics of these *Bt* mutants. To explore this question, we measured the growth of PUL48 gene knockouts supplemented with 3 different MW of dextran polymers with a plate reader (Fig. S4.2). We first quantified and compared the maximum OD of individual mutant cultures in each of the dextran media (Fig. 4.2C, S4.3A). Mutants lacking the GH BT3087 which could not grow in 35 kDa dextran (Fig. 4.1B), did grow well in 10 kDa dextran. By contrast, we observed that *Bt* mutants lacking BT3089 (SusD), BT3090 (SusC) or BT3091 (SusR) were unable to grow in dextran of any

molecular weight. This result suggests that the activity of BT3087 becomes crucial in *Bt* metabolism for growth in high molecular weight dextran. Finally, we observed that the mutant lacking BT3088 (SusE) also grew in all dextran sizes but with weaker growth at 200 kDa, suggesting that this protein also contribute to dextran utilization at high MW.

We wondered whether these changes in biomass were due to perturbations in growth rates or lag time. We thus measured the impact of dextran MW on the growth rate of the various *Bt* mutants by computing the growth rates of all mutants in different sizes of dextran (Fig. 4.2D, S4.3C). Like the case of *Bt* WT, we observed a trend of decreasing *Bt* growth rates as dextran MW increased. The mutants lacking BT3087 all led to a decrease in growth rate as dextran MW increased, confirming that BT3087 is a crucial GH for supporting *Bt* growth in high MW dextrans (Fig. S4.3C). The mutant $\Delta BT3088$ also experienced a sharp decrease in growth rate between growths in dextran 35 kDa and 200 kDa (Fig. 4.2D), suggesting the importance of this enzyme in the metabolism of high MW dextran polymers by *Bt*. Finally, we quantified the lag phases of all mutants in different MW of dextran. We observed a general increase in lag time as the size of dextran increases as in WT *Bt*. (Fig. 4.2E, S4.3B). The mutant $\Delta BT3088$ showed the most drastic increase in lag phase between dextran 35 kDa and 200 kDa.

Overall, our data suggest a dextran size dependent growth pattern in *Bt*. As dextran MW increases, this leads to a decreased growth rate of *Bt*. We identified that three enzymes within PUL48: BT3089 (SusD), BT3090 (SusC) and BT3091 (SusR) which are crucial for *Bt* growth in any dextran size. We also found that BT3087 and BT3088 (SusE) promote *Bt* dextran metabolism at high MW. Interestingly, our data also suggest that large dextran oligosaccharides of 9 kDa can be metabolized by *Bt* without the aid of BT3087.

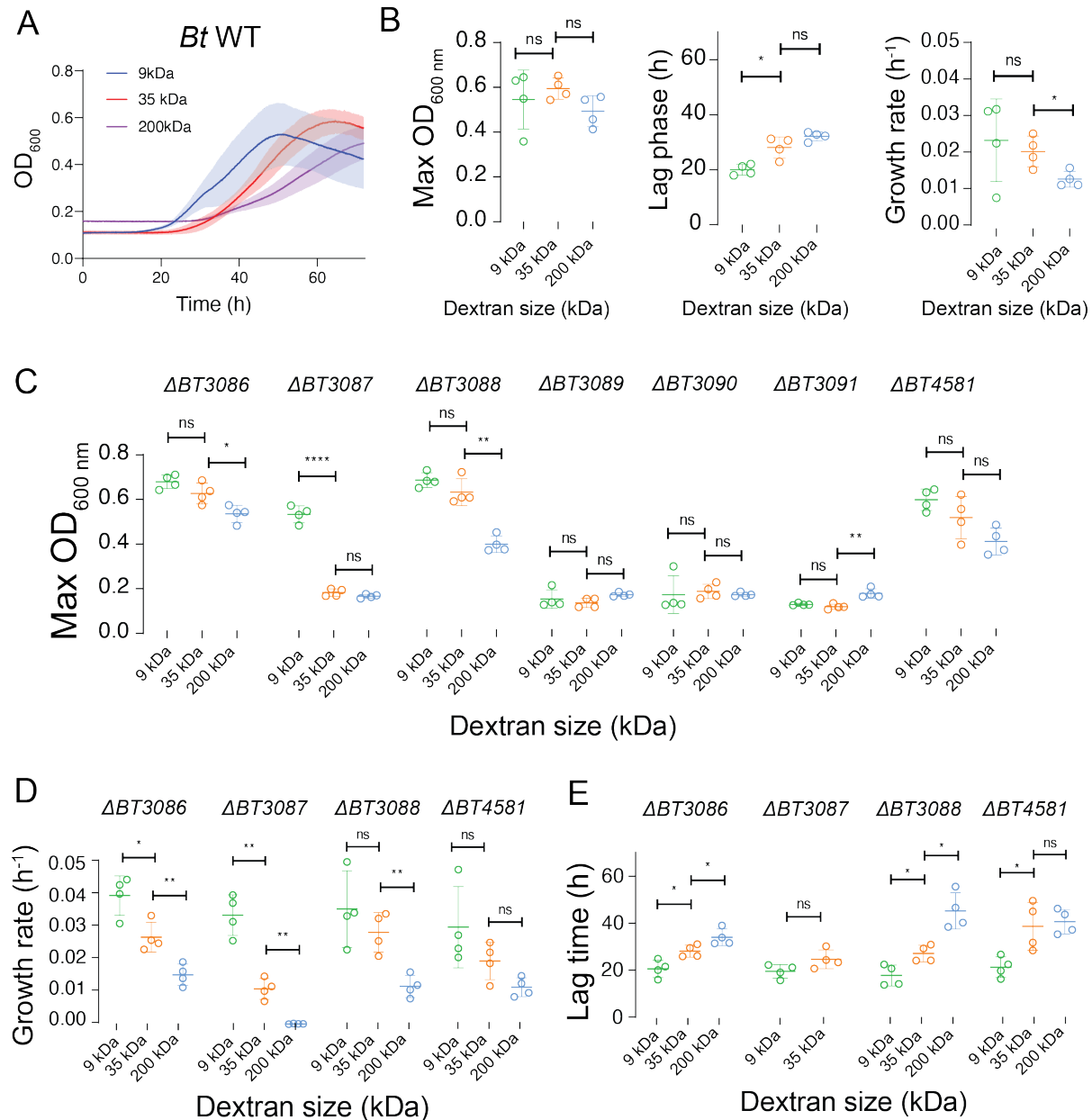


Figure 4.2 Growth profile quantifications from growth curves of various *Bt* mutants in 4 different sizes of dextran. (A) Growth curves of *Bt* WT in 3 different sizes of dextran. $N = 4$. (B) Extracted parameters from wildtype *Bt* growth curves in dextran. We quantified the maximum OD, lag phases and growth rates of *Bt* WT in 3 different sizes of dextran. We observed a general trend where increasing dextran sizes lead to an increase in lag phase and a decrease in growth rate. (C) Maximum OD of each single mutant cultures in 3 different sizes of dextrans. (D) Quantified growth rates of individual mutants in 3 different sizes of dextrans. Mutants which failed to grow were

omitted. (E) Quantified lag time of individual mutant cultures in 3 different sizes of dextrans. Mutants which failed to grow were omitted. (B-E) All growth experiments: $N = 4$, error bars: standard deviation. Statistical test: t -tests were performed between pairs of dextran sizes. ns $p > 0.05$, * $p < 0.05$, ** $0.05 < p < 0.01$, *** $0.001 < p < 0.0001$ and **** $p < 0.0001$.

4.3.3 Tracking dextran binding using fluorescent polymers

To further investigate the mechanisms of binding and import of polysaccharides of various sizes, we designed a fluorescence microscopy-based assay for dextran localization at the surface of *Bt* cells (Fig. 4.3A). We cultured *Bt* cells all expressing the fluorescent protein mCherry constitutively in the following backgrounds: WT, $\Delta BT3088$ (*susE*-), $\Delta BT3089$ (*susD*-) and $\Delta BT3090$ (*susC*-). We grew these strains in BMM containing equal amounts of dextran and glucose. We then diluted the cells in PBS supplemented with fluorescein-conjugated dextran of various sizes. The solution was then incubated aerobically for one hour, washed and imaged by high-resolution fluorescence microscopy. All samples were imaged in both the red and green fluorescence channels, which correspond to *Bt* cells and fluorescent dextrans respectively (Fig. 4.3B, S4.4). Microscopy images of *Bt* incubated with 40 kDa dextran-fluorescein showed a strong localization of green fluorescence signal to WT and $\Delta BT3088$ cells, but not $\Delta BT3089$ and $\Delta BT3090$ cells. These results suggest that mutants lacking *SusD* or *SusC* lose the ability to bind 40 kDa dextran on the cell surface, potentially explaining their inability to grow in dextran (Fig. 4.2C).

We then measured the dextran-binding capacity of each *Bt* strain by quantifying dextran fluorescence per cell normalized to the mCherry fluorescence of the same cell. We then average this for all cells. In the case of *Bt* WT, we could not distinguish differences in the dextran binding capacity across the 4 different sizes of dextran polymers tested (Fig. 4.3C). We then performed the same analysis on PUL48 mutants (Fig. 4.3D-F). First, we observed that the deletion of *BT3089* (*SusD*) or *BT3090* (*SusC*) led to a significant decrease in green fluorescence upon treatment with dextran polymers of MWs higher than 10 kDa (Fig. 4.3D, E), suggesting that these two enzymes are important for the

specific localization of dextran molecules to the cell membrane of *Bt*. Interestingly, the deletion of BT3088 (SusE) led to a decrease in green fluorescence localization upon treatment with dextran polymers greater than 40 kDa in MW (Fig. 4.3F), suggesting that this protein is important in *Bt* dextran binding in a size-dependent manner. Finally, we observed that all 3 deletions led to no significant changes in green fluorescence upon treatment with 10 kDa dextran compared to WT (Fig. S4.5), suggesting that this dextran binds to *Bt*'s cell membrane without the aid of the PUL48 machinery. Together, these data suggest that the PUL48 enzymes BT3088, BT3089 and BT3090 play crucial role in the dextran binding by *Bt*, and that the MW of dextrans itself does not have an impact on the binding capability by WT *Bt* cells.

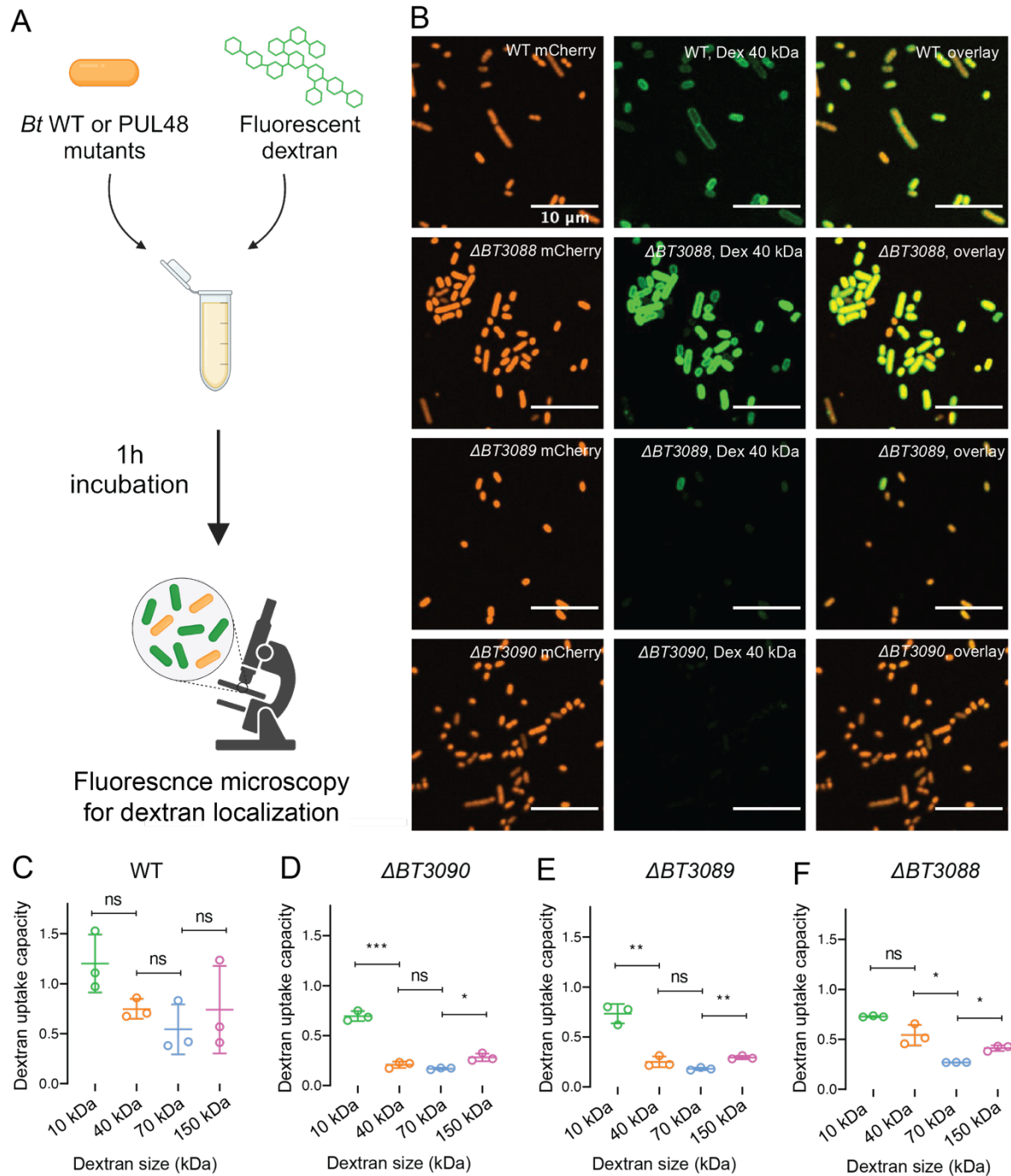


Figure 4.3: Fluorescent dextran localization to *Bt* cells. (A) Schematic of experimental set-up. *Bt* cells constitutively expressing mCherry are incubated with fluorescein-dextran of various molecular weights for 1 hour, washed and imaged by fluorescence microscopy. (B) fluorescence microscopy images of *Bt* wildtype along with various mutants constitutively expressing mCherry incubated in dextran 40 kDa conjugated to fluorescein. Red channel corresponds to *Bt* cells, green channel

corresponds to dextran, and the overlay corresponds to localization of dextran to *Bt* cells. (C) The binding capacity of various *Bt* mutants to varying sizes of dextran molecules. The binding capacity is defined as the ratio between green and red fluorescence signals per individual cells. The ratio for individual cells within a field of view were then averaged and plotted. For all fluorescein dextran binding experiments, $N = 3$. Statistical test: *t*-tests were performed between pairs of dextran sizes. * $p < 0.05$, ** $0.05 < p < 0.01$, *** $0.001 < p < 0.0001$ and **** $p < 0.0001$.

4.3.4 PUL48 proteins and dextran size defines the extent of nutrient sharing by *Bt*

We previously demonstrated that *Bt* can share by-products of dextran metabolism with *Bacteroides fragilis* (*Bf*), ultimately guiding community composition and biofilm spatial organization¹⁵⁵. We thus wondered whether individual PUL48 proteins may influence the nature of nutrient sharing by *Bt* to other members of a community, including in a MW-dependent manner. To answer this question, we grew *Bt-Bf* each constitutively expressing distinct fluorescent proteins in competition and monitored the relative fraction of each species in the community using fluorescence microscopy (Fig. 4.4A). We first quantified overall biomass (via optical density) of the co-cultures after 3 days (Fig. 4.4B). The growth patterns in co-cultures were identical to the *Bt* monocultures in dextran from Fig. 1C: co-cultures containing mutants which lacks the GH BT3087 or the regulator BT3091 failed to grow. We then measured the abundance of *Bf* in each co-culture by sampling each co-culture upon 1, 2, and 3 days of growth under anaerobic conditions. When computing the *Bf* fraction abundance by computing the ratio between mCherry- and sfGFP- positive cells (Fig. 4.4C), we found that with when co-cultured with WT *Bt*, the fraction abundance of *Bf* overtime is maintained at 50%¹⁵⁵. This ratio however decreases in all *Bt* PUL48 mutants which have the ability to grow in dextran: $\Delta BT3086$, $\Delta BT3088$, $\Delta BT3089$, $\Delta BT3090$, $\Delta BT4581$, and $\Delta 86,81$. These results suggest that the deletion of any one of these proteins potentially lead to either a reduction in availability of metabolic by-products like glucose, which ultimately leads to a reduction of nutrient availability for glycolysis in *Bt*.

Finally, based on different metabolic rates of *Bt*, we hypothesized that the size of polysaccharide polymers modulates nutrient sharing to impact community composition. To address this question, we competed *Bt* WT with *Bf* WT at a 1:1 ratio in 3 different sizes of dextran. We sampled these co-cultures after overnight growth (Fig. 4.4D), measured optical density along with the fraction abundance of *Bf* by fluorescence microscopy (Fig. 4.4E). First, we observed that the final OD of co-cultures decrease as the size of dextran polymers increased, consistent with our *Bt* monocultures (Fig. 4.2A). We found that co-cultures grown in higher MW dextran (35 and 200 kDa) have a decrease in *Bf* relative abundance (Fig. 4.4E). These results suggest that the size of polysaccharides impacts *Bt*'s growth rate, where reduced *Bt* growth impacts the amount of glucose metabolites generated at a given time. Increasing dextran MW reduced glucose production rate and secretion which may decrease *Bf* growth. Altogether, these results show that polysaccharide size can impact nutrient sharing in microbial communities, leading to changes in community compositions.

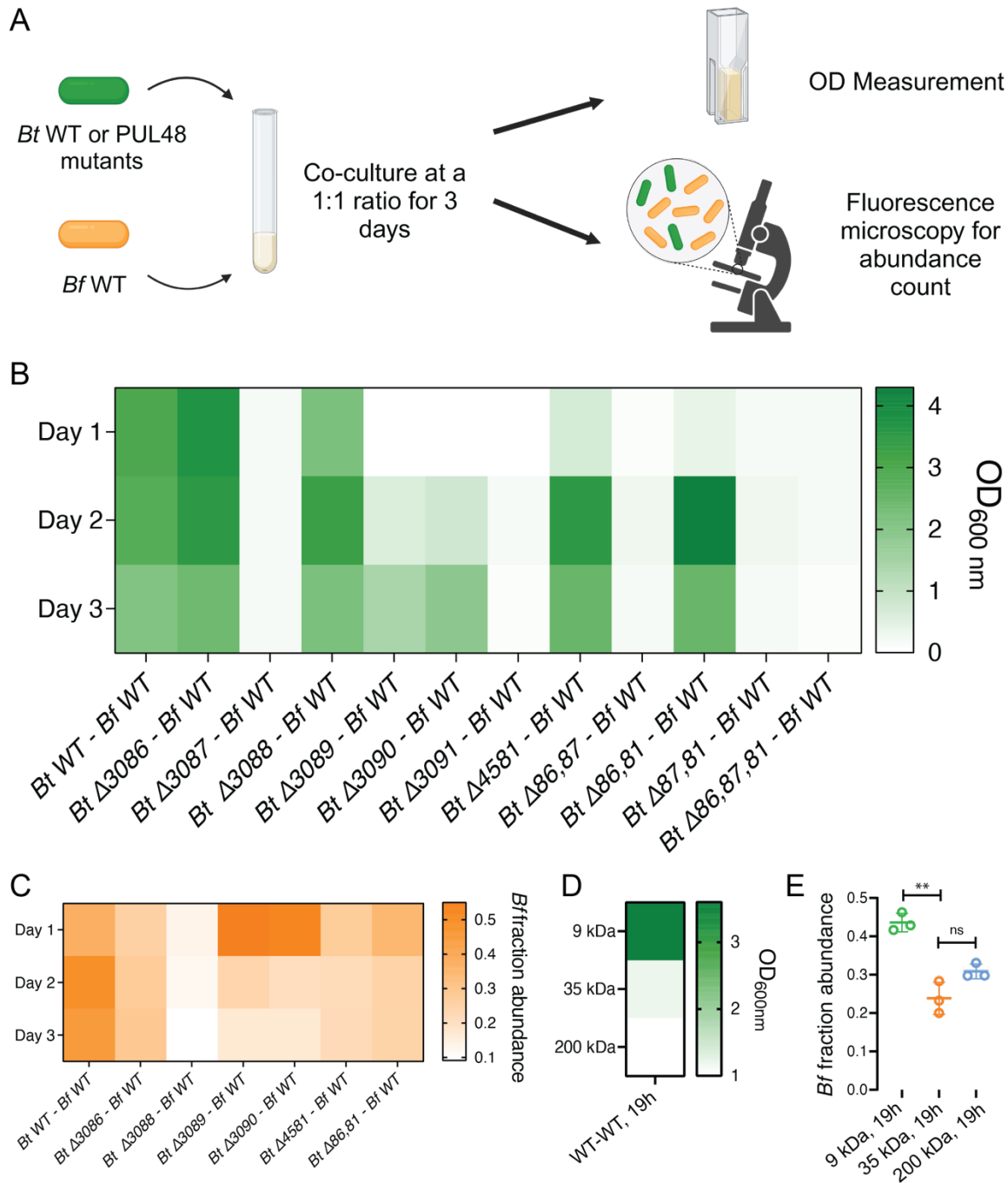


Figure 4.4: PUL48 proteins contributes to the extent of nutrient sharing from *Bt* to *Bf* in dextran. A) Schematic of experimental set-up. *Bt* WT or mutants expressing sfGFP are mixed with *Bf* WT at a 1:1 ratio. OD measurements and fluorescence microscopy were then performed on a daily basis to study coculture growth and *Bf* abundance. (B) Co-culture growths of *Bt* WT or PUL48 mutants with *Bf* in dextran. We

monitored the optical density (OD) daily over the course of 3 days. (C) *Bf* fraction abundance from competition experiments. *Bt* strains which failed to grow as monocultures has been omitted from co-culture analysis. Our results indicate that the loss of any one enzyme associated with PUL48 led to a decrease in nutrient sharing to *Bf* in comparison to WT levels. (D) Co-culture growths of *Bt* WT with *Bf* in 3 different sizes of dextran polymers. We monitored the OD of individual cultures upon 19 hours of growth. (E) *Bf* fraction abundance from *Bt* WT - *Bf* WT co-culture experiments in 3 different sizes of dextran upon 19 hours of growth.

4.4 Discussion

During cycles of dietary shifts, changes in glycan composition greatly contribute to defining microbiota composition¹³⁹. PULs functions are quite specific in processing glycans. However, within each polysaccharide family, these exists a variety of molecular structures introduce another layer of diversity, but how this impacts the functions of PULs has been largely overlooked. To comprehensively understand how diet modulates commensal species metabolism which ultimately shapes our gut microbiota, it is crucial to understand how this physical complexity impacts their metabolic pathways.

We identified a general trend of decreasing *Bt* growth rates as dextran MW increased. We attribute this decrease to the increased structural complexity of dextran polymers through branching, which reduces the processivity of PUL48¹⁵⁹. As structural complexity increases, the liberation of free oligosaccharides and glucose from dextran may become increasingly difficult for *Bt*. This leads to a reduced pool of oligosaccharides and glucose, leading to an overall decrease in growth rate in dextran polymers of higher MW. At the molecular level, we identified two enzymes whose contribution becomes crucial at high MW: the dextranase BT3087 and the SusE like protein BT3088. We found a cut-off at 9 kDa for BT3087. This differs from the Sus system SusC-SusD complex which selectively imports only short maltooligosaccharides with degree of polymerization of 5 – 16¹⁶⁰, much smaller in comparison to the dextran 9 kDa. This may be attributed to the overall structure of this particular dextran polymer as it is known that dextran 2 to 10 kDa exhibit properties of an expandable coil, with minimal branching¹¹³,

which potentially allow native dextran to pass through the importer BT3090 (SusC) without the aid of BT3087. Another protein which we found to contribute to dextran utilization in a size-dependent manner is BT3088 (SusE). The exact roles of SusE-like proteins polysaccharide utilization have remained unclear¹⁶⁰. However, we observed that the deletion of SusE led to a size dependent growth defect in *Bt* when cultured in dextran polymers greater than 35 kDa in size. Our results suggest that BT3088, a SusE like protein, likely plays an important role in *Bt*'s binding to complex dextran polymers or oligosaccharides generated by complex dextran metabolism, which subsequently facilitates the import of extra oligosaccharides into the cell.

Our results also show that dextran surface binding is a key function in its metabolism and depends on surface-exposed GHs. SusC-like and SusD-like proteins plays important roles in binding and uptake. Our fluorescein-dextran binding data for $\Delta BT3088$ further confirms that SusE plays an important role in *Bt* binding and accessing dextran greater than 70 kDa in size, suggesting the important role of SusE in the utilization of high molecular weight dextran by *Bt*. Our observations are reminiscent of adhesion of *Ruminococcus bromii*, a common member of the gut microbiota which also utilize starch, which expresses surface enzymes which facilitates adhesion to starch molecules¹⁶¹.

We then sort to understand the contribution of PUL enzymes and polysaccharide molecular weight on species interactions and abundance at the community level. It is known that in *B. ovatus* (*Bo*), the extent of nutrient sharing of metabolite by-products through xylan metabolism is dependent on the structural complexity of the polysaccharide and the availability of enzymes required for the degradation and utilization of the *Bo* released metabolic by-products¹⁶². Here, we observed that the deletion of any one protein within PUL48 led to a decrease in *Bf* abundance in a two-species community. Such decrease in *Bf* abundance is likely a result of the reduced availability of the public good glucose. The deletion of BT3086 or BT4581, 2 α -glucosidases which are localized in the periplasm, reduces the formation of glucose from oligosaccharides. As BT3087 also generate glucose as a product, extracellular

glucose may be preferentially imported by *Bt*, reducing the overall pool of public goods available for *Bf* to exploit. As the deletion of BT3088 also led to a significant decrease in *Bf* population, BT3088 also likely contribute to the uptake of oligosaccharides in *Bt*, hence also leading to the import of extracellular glucose and reducing nutrient availability to *Bf*.

Previous studies have demonstrated that different types of galactans with differing structural complexities have an impact on the species specific fermentation by gut microbes, which leads to changes in overall microbiota composition¹⁶³. More precisely, it had been previously demonstrated with blackberry polysaccharides that the MW of the polysaccharides impact the rate of fermentation and ultimately the composition of the overall microbial community¹⁶⁴. Our data also suggests a potential mechanism where polysaccharide size impacts nutrient sharing in microbial communities through defining the growth rate of the utilizer, restricting the amount of public goods generated and shared to the non-utilizer, which ultimately lead to an increasing delay in growth and colonization by the non-utilizer.

Overall, our work provides a novel mechanism of commensal selection based on the complexity of dietary polysaccharides. Our observations imply that at equal molecular composition and concentration, a seemingly identical dietary composition can lead to distinct community composition depending on the structure of polysaccharide molecules it contains. As many other dietary fibres also likely exist in large ranges of molecular weight, understanding how molecular weight impacts utilization by gut microbe may lead to the potential design of next generation precision prebiotics.

4.5 Methods

4.5.1 Strains and culture media

Bacteroides thetaiotaomicron VPI-5482 WT, *Bacteroides thetaiotaomicron* VPI-5482 sfGFP and *Bacteroides fragilis* NCTC-9343 mCherry, along with all *Bacteroides*

thetaiotaomicron VPI-5482 PUL48 knockout mutants (Table 1) were used for experiments in this work. TYG medium and *Bacteroides* minimal medium (BMM) supplemented with the indicated carbon source were used in all experiments.

For TYG medium, 10g tryptone, 5g yeast extract, 2.5g D-glucose and 0.5g L-Cysteine were dissolved in 465 mL of ddH₂O. The resulting solution was then immediately autoclaved and allowed to cool down to room temperature. In the meantime, Salt Solution A was prepared by mixing 0.26g of CaCl₂ and 0.48g of MgSO₄ in 300 mL of ddH₂O until fully dissolved where 500 mL of ddH₂O was then added. 1g KH₂PO₄, 1g K₂HPO₄ and 2g of NaCl were then added to the solution and stirred at room temperature until all salts are fully dissolved followed by the addition of 200 mL of ddH₂O to top up the volume. The salt solution was then stored at 4°C for future use. A 10% (w/v) NaHCO₃ solution was prepared by dissolve 50g of NaHCO₃ into 500 mL of ddH₂O followed by filter sterilization with a 0.22 µm filter. A 1.9 mM Hematin – 0.2M Histidine solution was prepared by dissolving 60.18 mg of hematin in 1 mL of 1M NaOH until fully solubilized, then neutralized with 1 mL of 1M HCl. In a separate beaker, 1.55 g of L-Histidine was dissolved in 48 mL of ddH₂O. The histidine solution was then combined with the hematin solution, filter sterilized with a 0.22 µm filter and stored at 4°C for future usage. 5 mL of hematin-histidine solution and 10 mL of 10% NaHCO₃ solution were added to the TYG base medium with a 0.22 µm filter. With a separate 0.22 µm filter, 20 mL of Salt Solution A was then added. The resulting complete TYG medium was then stored at 4°C for future usage.

The BMM medium was prepared as previously described^{77,78}. Briefly, a 10x medium stock containing 1 M KH₂PO₄, 150 mM NaCl and 85 mM (NH₄)₂SO₄ was first prepared and adjusted to a pH of 7.2. Solutions of 1 mg/mL vitamin K₃, 0.4 mg/mL FeSO₄, 0.1 M MgCl₂, 0.8% (w/v) CaCl₂, 0.01 mg/mL vitamin B₁₂ and 1.9 mM hematin–0.2 M histidine solutions were prepared separately. To prepare 100 mL of BMM, 10 mL of the 10x salts were mixed with 0.1 g of L-cysteine, 50 µL of vitamin B₁₂ solution, and 100 µL of each vitamin K₃, FeSO₄, MgCl₂, CaCl₂ and hematin-histidine solution. All carbon sources

were added to a final concentration of 5 mg/mL. The media were filter-sterilized using a 0.22 µm filter unit and degassed in the anaerobic chamber overnight.

All bacteria were cultured at 37 °C under anaerobic conditions in a vinyl anaerobic chamber (COY) inflated with a gas mix of approximately 5% carbon dioxide, 90% nitrogen and 5% hydrogen (CarbaGas). Bacteria were first streaked on brain heart infusion plates (SigmaAldrich) containing 10% sheep blood (TCS BioSciences). Single colonies were then inoculated in BMM and grown overnight.

4.5.2 Recombinant expression and purification of *Bt* GHs

The amino acid sequences of the GHs BT3086, BT3087 and BT4581 were collected from the *B. thetaiotaomicron* VPI-5482 genome. The amino acid sequences of each GHs were first analyzed by SignalP¹⁶⁵ in order to identify signal peptide and potential transmembrane domains of the GHs. Each of these genes were then amplified by PCR without the corresponding signal peptide regions, and cloned into the expression vector pET29b containing an N-terminal 10x His-tag. The vector was then transformed into *E. coli* XL10 gold for plasmid production and storage. The resulting plasmid was then transformed into *E. coli* BL-21, where then a 50 mL overnight culture is grown in LB-kanamycin (Kan). The overnight culture was then transferred into 2 L of LB-kan, and grown until the OD of 0.6 at 37 °C. The cells were then induced with 1M IPTG and cultured overnight at 19 °C. The culture was then pelleted, washed, lysed and centrifuged at 20000 rpm to remove membrane material. The resulting supernatant was then purified using an affinity Ni-NTA column, eluted in 1x PBS, and stored at -80 °C until usage. The resulting purified protein were then analyzed by SDS-PAGE to confirm expression and identity.

4.5.3 GH activity analysis by HPAEC-PAD

20 µL of 1 mg/mL purified GHs: BT3086, BT3087 or BT4581 were added to 1 mL of BMM-dextran M_w 9000-11000. The mixture was then incubated overnight anaerobically at 37°C. Cation and anion exchange chromatography with AmberChrom resins

(SigmaAldrich) were then used to remove protein and ions from the medium, followed by filtering through a 0.22 μm sterilization filter prior to analysis. The resulting flow-throughs were then analyzed by HPAEC-PAD. The sugars were separated on a Dionex CarboPac PA-20 column from Thermo Fisher Scientific with the following eluent: A) 100 mM NaOH; B) 150 mM NaOH and 500 mM sodium acetate at a flow rate of 0.4 mL/min. The gradient was 0 to 15 min, 100% A (monosaccharide elution); 15 to 26 min, gradient to 10% A and 90% B (malto-oligosaccharide elution); 26 to 36 min, 10% A, 90% B (column wash step); and 36 to 46 min step to 100% A (column re-equilibration). Peaks were identified by co-elution with known glucose, isomaltose standards using the Chromeleon software. The HPLC data was then exported and replotted with the graphing software GraphPad Prism 8, where area under the curve of peaks of corresponding samples were calculated.

4.5.4 In frame deletion knockouts in *B. theta*

Bt knockouts were generated as previously described¹⁶⁶. Briefly, 700 bp upstream and downstream of each gene of interest were amplified from *Bt* WT by PCR. The resulting PCR products were then analyzed on a 1% agarose gel and subsequently gel-extracted. The knockout plasmid pLGB13 was then restriction digested with PstI and BamHI, where the upstream fraction, downstream fraction and digested pLGB13 were assembled via Gibson Assembly. The assembled plasmid was then transformed into the donor strain *E. coli* S17. The donor strains carrying the knockout plasmids were then grown to an OD of 1-1.2 in LB-Amp 100. At the same time, *Bt* strains were grown anaerobically to an OD of roughly 0.1. The donor culture was then washed with PBS, pelleted, and mixed with the *Bt* culture. The culture is then puddled onto BHI plates supplemented with 10% sheep-blood and dried for conjugation aerobically overnight at 37 °C. The resulting carpet is then resuspended in TYG medium and restreaked onto BHI sheep blood plates with gentamycin (Gm) 200 $\mu\text{g/mL}$ and erythromycin (Er) 20 $\mu\text{g/uL}$ and grown anaerobically for 30 hours. Resulting colonies were picked and restreaked directly onto another BHI-sheep blood plate containing Gm/Er for another 30 hours anaerobically. Resulting single colonies were then picked and restreaked onto BHI-sheep blood plate containing 0.1 $\mu\text{g/mL}$ of anhydrotetracycline (aTc) for counter-

selection and grown anaerobically for 30 hours. Resulting single colonies were again picked, where colony PCR is then performed, and the resulting PCR product was sequenced to confirm whether the knockout was successful.

4.5.5 Insertion of sfGFP and mCherry into *B. theta* and *B. fragilis*

Fluorescent strains of *Bt* and *Bf* were generated as described previously.⁷⁶ Briefly, the plasmids pWW3452 (GFP) and pWW3515 (mCherry) were transformed into the donor strain *E. coli* S17. The donor was then grown to an OD of 1-1.2 in LB-Amp 100. At the same time, *Bt* or *Bf* strains were grown anaerobically to an OD of roughly 0.1 (for *Bf*, OD 0.01). The donor culture was then washed with PBS, pelleted and mixed with either the *Bt* or *Bf* culture. The culture is then puddled onto BHI plates supplemented with 10% sheep-blood and dried for conjugation aerobically overnight at 37 °C. The resulting carpet is then resuspended in TYG medium and restreaked onto BHI sheep blood plates with gentamycin (Gm) 200 ug/mL and erythromycin (Er) 20 ug/ uL and grown anaerobically for 30 hours. Resulting colonies were picked and restreaked directly onto another BHI-sheep blood plate containing Gm/Er for another 30 hours anaerobically. Resulting colonies were then resuspended and screened for fluorescent properties on the confocal fluorescence microscope.

4.5.6 Test tube mutant growths and competitions

For initial growth experiments, *Bt* and various mutants were cultured in BMM supplied with 5 mg/mL of D(+)- glucose (Carl Roth) overnight anaerobically. The resulting cultures were then pelleted by centrifugation and washed twice with PBS. The pellets were then resuspended in PBS, where the OD was measured. The various *Bt* strains were then diluted to a final OD of 0.1 or 0.01 in BMM dextran ($M_w = 35000$ Da). The cultures were then grown anaerobically for 3 days, where the OD of individual mutants were measured after day 1, 2 and 3. For *Bt* mutant competition experiments with *Bf*, *Bt* and *Bf* were cultured separately in 1 mL of BMM-glucose overnight. The resulting cultures were then pelleted by centrifugation and washed twice with PBS. The pellets

were then resuspended in PBS, where the OD was measured. *Bt* and *Bf* were then mixed at a 1:1 ratio to an initial OD of 0.1 in each of the carbon sources tested. The cultures were then grown anaerobically for 3 days. A microscopy approach was then used to quantify the relative abundances of *Bt* and *Bf* in these cultures. To achieve this, the cultures were mixed well and 10 μ L of each cell culture was sampled at day 1, 2 and 3. The cultures were then diluted in PBS and incubated at aerobic conditions. The samples were then spotted onto a glass coverslip and covered by a thin agarose pad prior to fluorescence imaging by widefield fluorescence microscopy. For each sample and replicate, 3 image frames across the agar pad were recorded. The relative abundance of sfGFP- and mCherry-expressing cells in each sample were then quantified using the 'analyze particle' function in Fiji and averaged across the 3 frames.

4.5.7 Growth dynamics of mutants by plate reader

Bt and various mutants were cultured in BMM supplied with 5 mg/mL of D(+)- glucose overnight anaerobically. The resulting cultures were then pelleted by centrifugation and washed twice with PBS. The pellets were then resuspended in PBS, where the OD was measured. The various *Bt* strains were then diluted to a final OD of 0.1 in BMM dextran ($M_w = 35000$ Da) in a clear COSTAR 96 wells plate with a final volume of medium at 200 μ L. The plate is then completely sealed with parafilm, moved into the Tecan Safire² plate reader, and grown anaerobically at 37 °C. settings: kinetic, 5 min cycles, 875 cycles, shake 10 seconds prior to each analysis cycle. The resulting data were then rearranged by a house-built python script, where all growth curves were then plotted by the graphing software GraphPad Prism 8. For further analysis for the lag time, max OD and maximum growth rate of each conditions, the file of rearranged data was analyzed using Pyphe growth curves¹⁶⁷.

4.5.8 *Bt* binding to fluorescent dextrans

Bt WT mCherry and various mutants containing mCherry were cultured in BMM supplied with 5 mg/mL of dextran $M_w = 35$ kDa overnight anaerobically. The resulting cultures were then pelleted by centrifugation and washed twice with PBS. The pellets

were then resuspended in PBS, where the OD was measured. We then diluted the cells to a final OD of 0.1 in PBS and added fluorescein-conjugated dextran of various sizes to the solution, incubated them aerobically for 1 hour and then imaged the solution by fluorescence confocal microscopy. For each sample and replicate, 3 image frames across the agar pad were recorded. The relative abundance of mCherry- expressing cells and sfGFP signal corresponding to dextran binding and import were recorded for each single cell within each samples using the 'analyze particle' function in Fiji. The ratio of sfGFP:mCherry were then quantified for every individual cells within an experiment and averaged per experiment.

4.5.9 Microscopy

All biofilm imaging were performed using a Nikon Eclipse Ti2-E inverted microscope coupled with a Yokogawa CSU W2 confocal spinning disk unit and equipped with a Prime 95B sCMOS camera (Photometrics). The two objectives used for imaging were the 20x APOChromat water immersion objective with a numerical aperture (N.A.) of 0.95 and the 60x water immersion objective with an N.A. of 1.20. Z-stacks were recorded at a 0.5 μm step-height. Fiji was then used for the display of all images. For the visualization of the full biofilm, frames were taken across the xy-plane and stitched together upon background subtraction as described in the image analysis section. All single cell counting experiments in liquid cultures were performed using the Nikon TiE epifluorescence microscope coupled with a Hamamatsu ORCA Flash 4 camera and a 40 x Plan APO NA 0.9 objective. Fiji was then used to display the images.

4.5.10 Sample preparation for *Bf* proteomics

Bf was cultured in BMM-glucose, BMM-dextran (M_w 9000-11000) supplemented with 20 μL of 1 mg/mL purified GHs BT3086, BT3087 and BT4581 or *Bt* spent medium overnight from an initial OD of 0.01. Cells were lysed and lysates containing 20 μg of protein content were collected for further analysis. Downstream peptide preparation and LC-MS analysis was performed as mentioned prior.

Protein identification and label free quantification were performed using MaxQuant 1.6.10.43¹³². The *B. fragilis* NCTC-9343 Uniprot reference proteome database was used for this search. Carbamidomethylation was set as fixed modification, whereas oxidation (M), phosphorylation (S, T, Y) and acetylation (Protein N-term) were considered as variable modifications. A maximum of two missed cleavages were allowed for this search. “Match between runs” was selected. A minimum of 2 peptides were allowed for protein identification and the false discovery rate (FDR) cut-off was set to 0.01 for both peptides and proteins. Label-free quantification and normalisation was performed by Maxquant using the MaxLFQ algorithm, with the standard settings¹³³.

In Perseus¹³⁴, reverse proteins, contaminants and proteins only identified by sites were filtered out. Biological replicates were grouped together and protein groups containing a minimum of two LFQ values in at least one group were conserved. Missing values were imputed with random numbers using a gaussian distribution (width = 0.3, down-shift = 1.8). Two-samples t-test was performed to identify the differentially expressed proteins, followed by a permutation-based correction (False Discovery Rate). Significance curves in the volcano plot corresponded to a S_0 value of 1.0 and FDR cut-off of 0.01.

4.6 Supplementary information appendix

4.6.1 Supplementary figures

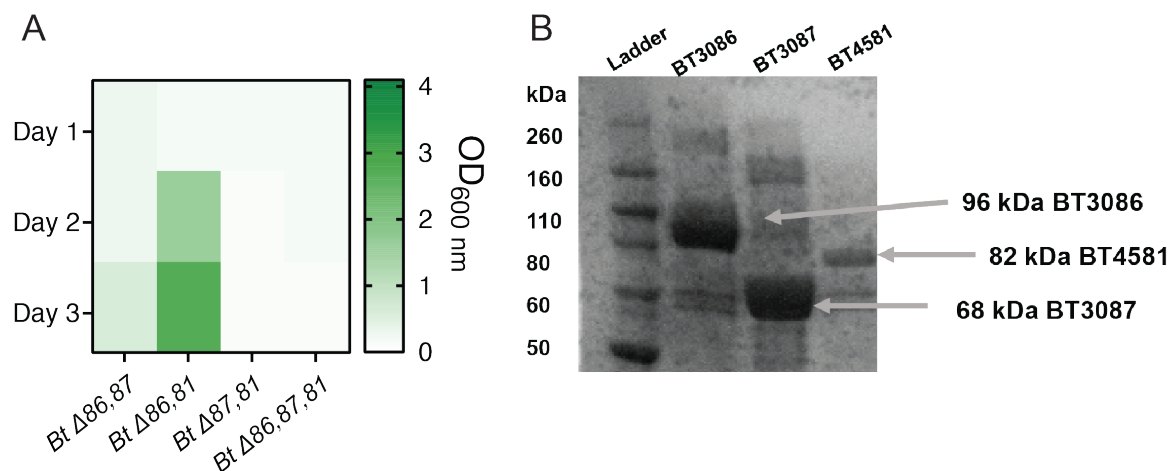


Figure S4.1: Involvement of GHs BT3086, BT3087 and BT4581 in *Bt* dextran metabolism. (A) Monoculture growths of *Bt* double and triple GH knockout mutants. We measured the optical density (OD) of individual cultures everyday over the course of 3 days (B) SDS-PAGE analysis of recombinantly expressed BT3086, BT3087 and BT4581 upon purification by Ni-NTA affinity chromatography.

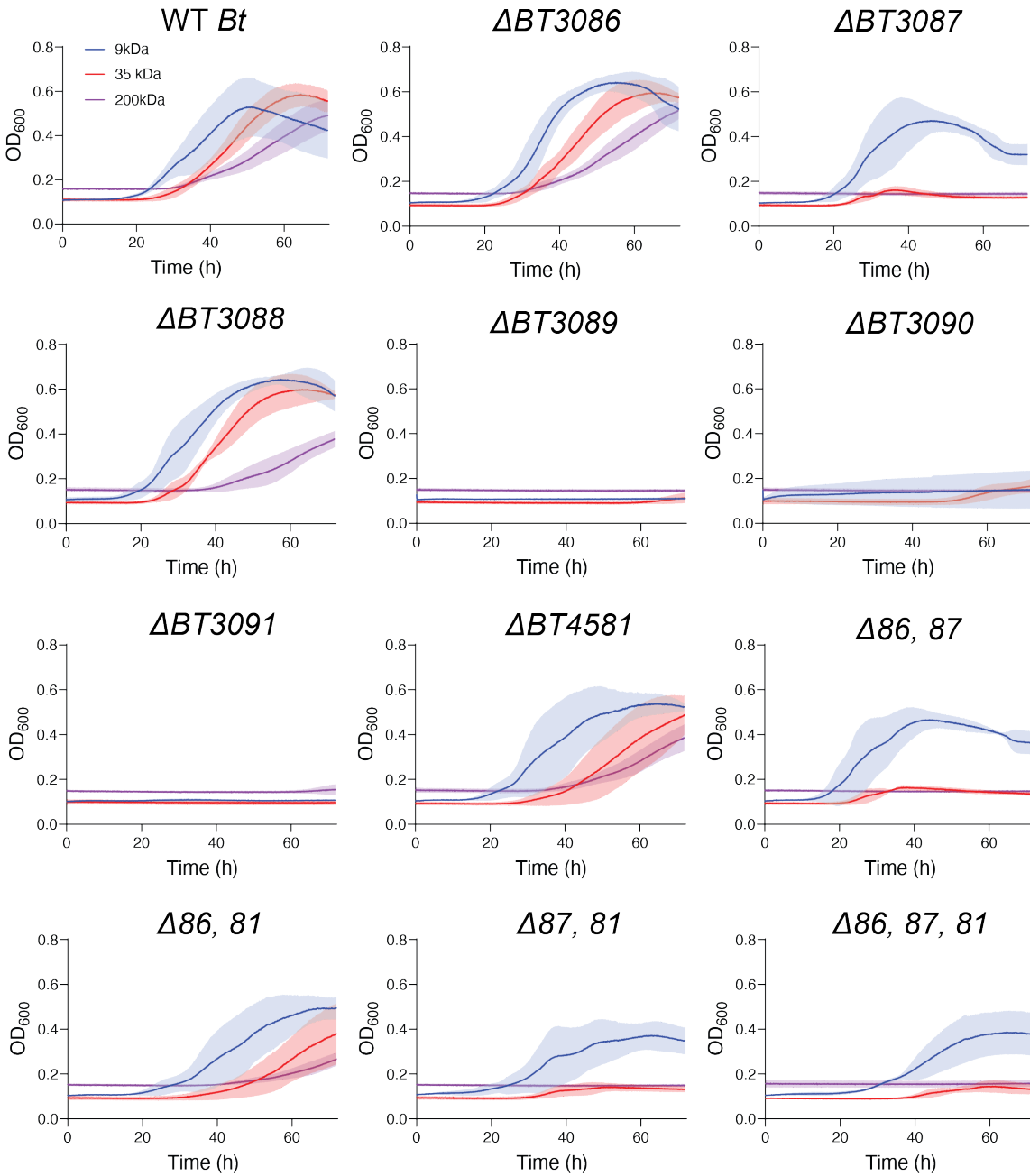


Figure S4.2: Growth curves of *Bt* WT and various PUL48 mutants in 3 different sizes of dextran over the course of 3 days. $N = 4$, shaded region: standard deviation.

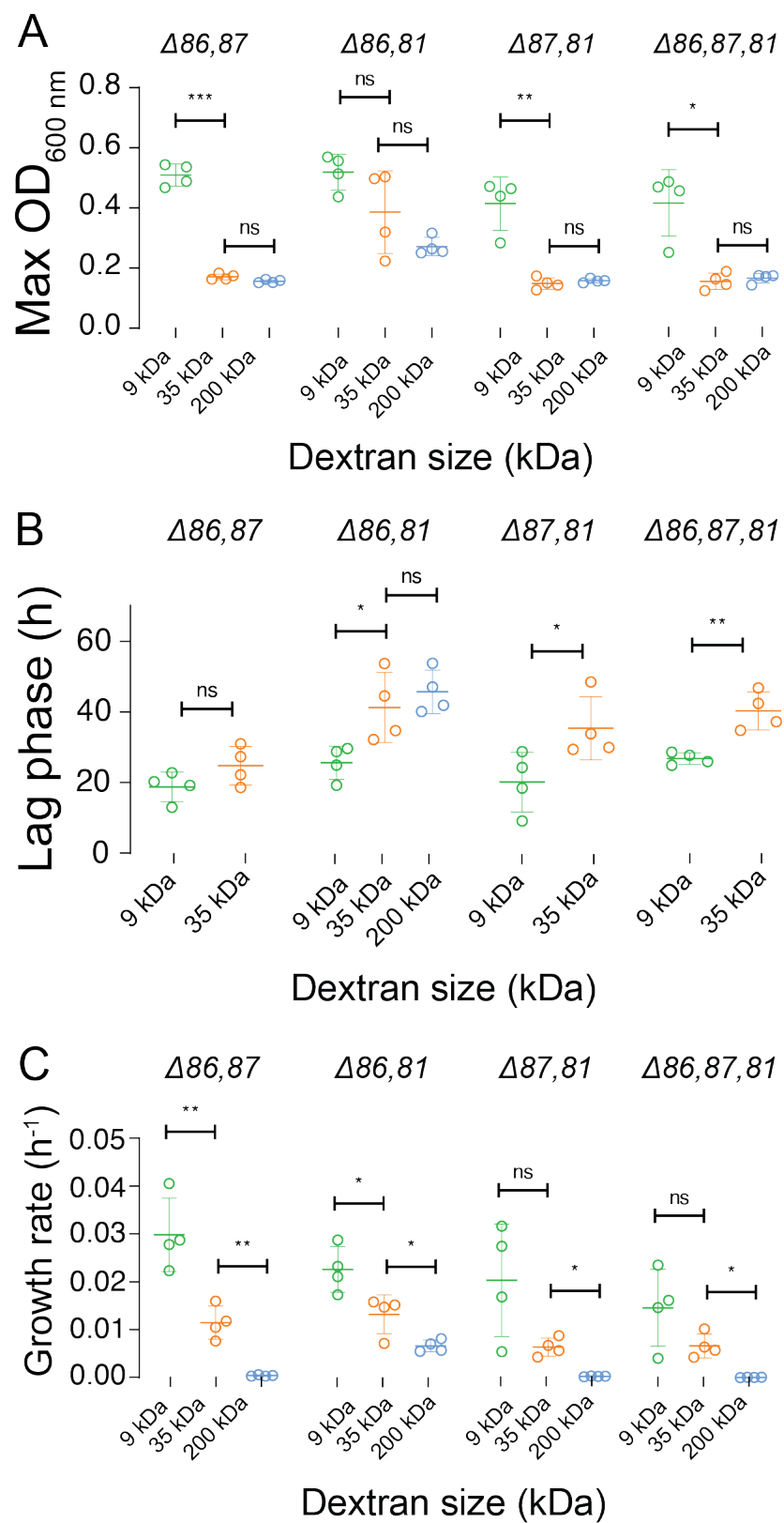
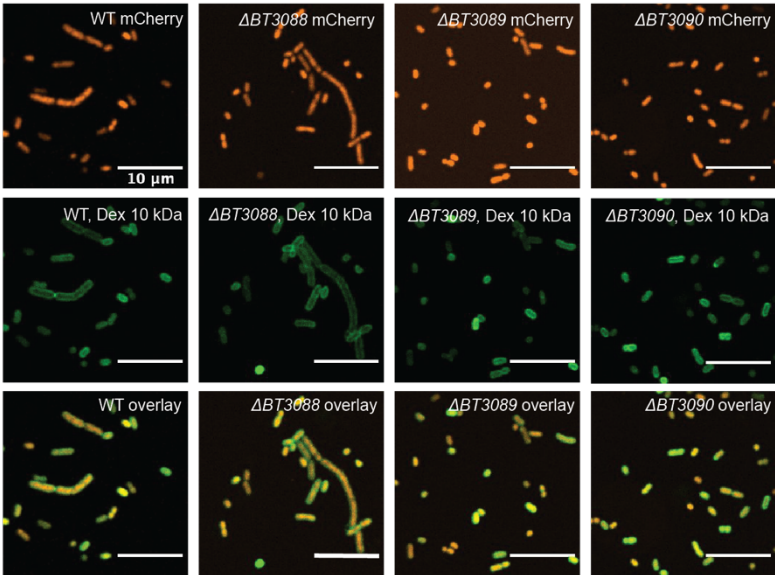
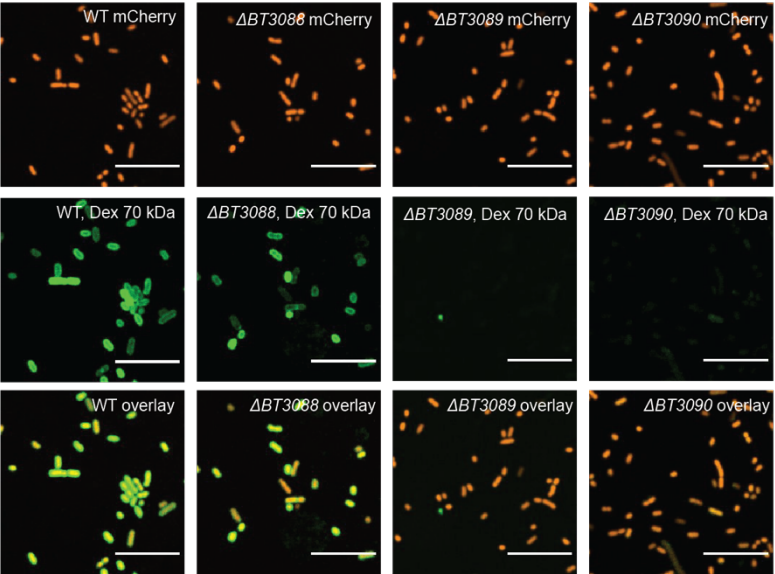


Figure S4.3: Growth of *Bt* double and triple GH mutants in 3 different sizes of dextran. (A) Quantified maximum OD of each mutant monocultures in dextrans (B) Quantified lag phase of double and triple GH mutants in 3 different sizes of dextrans. (C) Quantified growth rates of double and triple GH mutants in 3 different sizes of dextrans. All growth experiments: $N = 4$, error bars: standard deviation. Statistical test: t -tests were performed between pairs of dextran sizes. ns $p > 0.05$, * $p < 0.05$, ** $0.05 < p < 0.01$, *** $0.001 < p < 0.0001$.

A



B



C

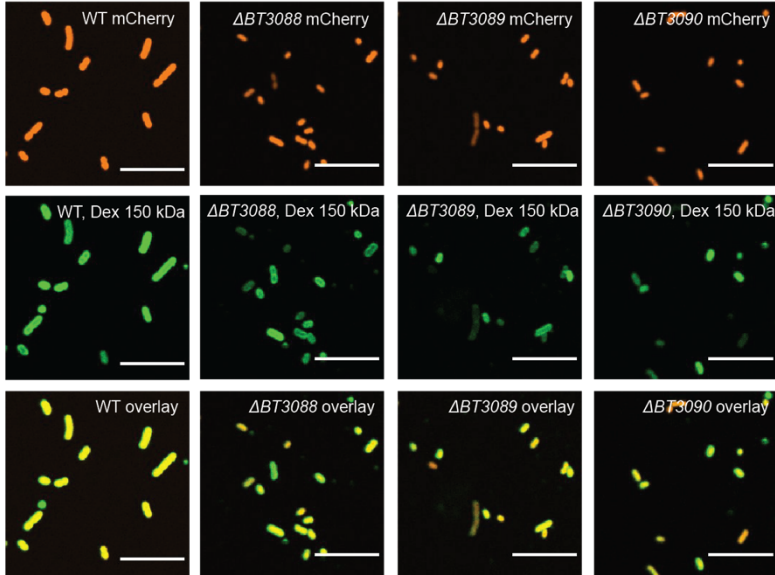


Figure S4.4: Visualization of dextran localization to *Bt* cells. Brightfield fluorescence microscopy images of *Bt* wildtype along with various mutants constitutively expressing mChery incubated in (A) dextran 10 kDa, (B) dextran 70 kDa, and (C) dextran 150 kDa. All dextrans conjugated to fluorescein.

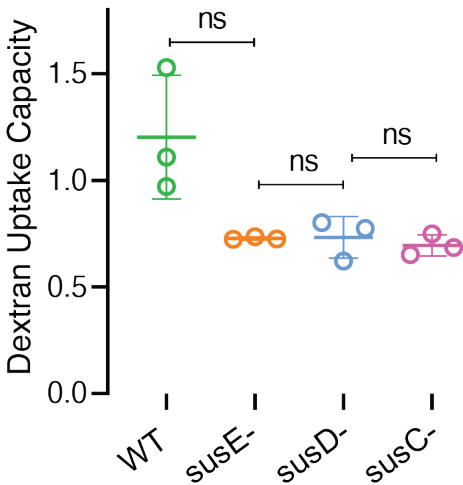


Figure S4.5: Dextran uptake capacity of 10 kDa dextran by *Bt* WT and 3 PUL48 mutants. No significant difference in the uptake capacity of dextran 10 kDa was observed across the 4 strains analyzed. *N* = 3, Statistical test: Statistical test: unpaired t-tests, ns *p* > 0.05.

4.6.2 Appendix

Reagent type	Background	Designation	Source	Description
Strain	<i>B. thetaiotaomicron</i> VPI-5482	<i>Bt</i> WT	⁷⁶	<i>Bt</i> wildtype
Strain	<i>B. thetaiotaomicron</i> VPI-5482	<i>Bt</i> WT - sfGFP	⁷⁶	<i>Bt</i> wildtype constitutively expressing sfGFP

Strain	<i>B. thetaiotaomicron</i> VPI-5482	<i>Bt</i> WT - mCherry	⁷⁶	<i>Bt</i> wildtype constitutively expressing mCherry
Strain	<i>B. thetaiotaomicron</i> VPI-5482	<i>Bt</i> Δ BT3086	This study	Deletion of α - glucosidase II BT3086
Strain	<i>B. thetaiotaomicron</i> VPI-5482	<i>Bt</i> Δ BT3087	This study	Deletion of dextranase BT3087
Strain	<i>B. thetaiotaomicron</i> VPI-5482	<i>Bt</i> Δ BT3088	This study	Deletion of SusE like BT3088
Strain	<i>B. thetaiotaomicron</i> VPI-5482	<i>Bt</i> Δ BT3089	This study	Deletion of SusD like BT3089
Strain	<i>B. thetaiotaomicron</i> VPI-5482	<i>Bt</i> Δ BT3090	This study	Deletion of SusC like BT3089
Strain	<i>B. thetaiotaomicron</i> VPI-5482	<i>Bt</i> Δ BT3091	This study	Deletion of SusR like BT3089
Strain	<i>B. thetaiotaomicron</i> VPI-5482	<i>Bt</i> Δ BT4581	This study	Deletion of α - glucosidase BT4581
Strain	<i>B. thetaiotaomicron</i> VPI-5482	<i>Bt</i> Δ BT3086 sfGFP	This study	<i>Bt</i> Δ BT3086 constitutively expressing sfGFP
Strain	<i>B. thetaiotaomicron</i> VPI-5482	<i>Bt</i> Δ BT3087 sfGFP	This study	<i>Bt</i> Δ BT3087 constitutively expressing sfGFP
Strain	<i>B. thetaiotaomicron</i> VPI-5482	<i>Bt</i> Δ BT3088 sfGFP	This study	<i>Bt</i> Δ BT3088 constitutively expressing sfGFP
Strain	<i>B. thetaiotaomicron</i> VPI-5482	<i>Bt</i> Δ BT3089 sfGFP	This study	<i>Bt</i> Δ BT3089 constitutively expressing sfGFP
Strain	<i>B. thetaiotaomicron</i> VPI-5482	<i>Bt</i> Δ BT3090 sfGFP	This study	<i>Bt</i> Δ BT3090 constitutively expressing sfGFP
Strain	<i>B. thetaiotaomicron</i> VPI-5482	<i>Bt</i> Δ BT3091 sfGFP	This study	<i>Bt</i> Δ BT3091 constitutively expressing sfGFP

Strain	<i>B. thetaiotaomicron</i> VPI-5482	<i>Bt</i> Δ BT4581 sfGFP	This study	<i>Bt</i> Δ BT4581 constitutively expressing sfGFP
Strain	<i>B. thetaiotaomicron</i> VPI-5482	<i>Bt</i> Δ BT3088 mCherry	This study	<i>Bt</i> Δ BT3088 constitutively expressing mCherry
Strain	<i>B. thetaiotaomicron</i> VPI-5482	<i>Bt</i> Δ BT3089 mCherry	This study	<i>Bt</i> Δ BT3089 constitutively expressing mCherry
Strain	<i>B. thetaiotaomicron</i> VPI-5482	<i>Bt</i> Δ BT3090 mCherry	This study	<i>Bt</i> Δ BT3090 constitutively expressing mCherry
Strain	<i>B. thetaiotaomicron</i> VPI-5482	<i>Bt</i> Δ 86,87	This study	Deletion of BT3086 and BT3087
Strain	<i>B. thetaiotaomicron</i> VPI-5482	<i>Bt</i> Δ 86,81	This study	Deletion of BT3086 and BT4581
Strain	<i>B. thetaiotaomicron</i> VPI-5482	<i>Bt</i> Δ 87,81	This study	Deletion of BT3087 and BT4581
Strain	<i>B. thetaiotaomicron</i> VPI-5482	<i>Bt</i> Δ 86,87,81	This study	Deletion of BT3086, BT3087 and BT4581
Strain	<i>B. thetaiotaomicron</i> VPI-5482	<i>Bt</i> Δ 86,87 sfGFP	This study	<i>Bt</i> Δ 86,87 constitutively expressing sfGFP
Strain	<i>B. thetaiotaomicron</i> VPI-5482	<i>Bt</i> Δ 86,81 sfGFP	This study	<i>Bt</i> Δ 86,81 constitutively expressing sfGFP
Strain	<i>B. thetaiotaomicron</i> VPI-5482	<i>Bt</i> Δ 87,81 sfGFP	This study	<i>Bt</i> Δ 87,81 constitutively expressing sfGFP
Strain	<i>B. thetaiotaomicron</i> VPI-5482	<i>Bt</i> Δ 86,87,81 sfGFP	This study	<i>Bt</i> Δ 86,87,81 constitutively expressing sfGFP
Strain	<i>B. fragilis</i> NCTC-9343	<i>Bf</i> mCherry	⁷⁶	<i>Bf</i> constitutively expressing mCherry
Plasmid	-	Δ pir pWW3452	⁷⁶	Plasmid for insertion of sfGFP into <i>Bt</i>
Plasmid	-	Δ pir pWW3515	⁷⁶	Plasmid for insertion of mCherry into <i>Bt</i>

Plasmid	pLGB13	pLGB13	¹⁶⁶	Plasmid backbone for <i>Bt</i> knockouts
Plasmid	pLGB13	pAB001	This study	Plasmid for the deletion of <i>BT3086</i>
Plasmid	pLGB13	pAB002	This study	Plasmid for the deletion of <i>BT3087</i>
Plasmid	pLGB13	pAB003	This study	Plasmid for the deletion of <i>BT3088</i>
Plasmid	pLGB13	pAB004	This study	Plasmid for the deletion of <i>BT3089</i>
Plasmid	pLGB13	pAB005	This study	Plasmid for the deletion of <i>BT3090</i>
Plasmid	pLGB13	pAB006	This study	Plasmid for the deletion of <i>BT3091</i>
Plasmid	pLGB13	pAB007	This study	Plasmid for the deletion of <i>BT4581</i>
Plasmid	pLGB13	pAB008	This study	Plasmid for the deletion of <i>BT3087</i> in $\Delta BT3086$
Plasmid	pET-29b	pAB010	This study	Plasmid for the recombinant expression of <i>BT3086</i>
Plasmid	pET-29b	pAB011	This study	Plasmid for the recombinant expression of <i>BT3087</i>
Plasmid	pET-29b	pAB012	This study	Plasmid for the recombinant expression of <i>BT4581</i>

Table S4.2. List of strains and plasmids generated for this study.

Primer number	Primer name	Description	Primer sequence (5' -> 3')
oAB001	3086 KO up FOR	Knockout BT3086 in WT	ATTAGCATTATGAGTCCCGAAGGAACATGGTAC
oAB002	3086 KO up REV	Knockout BT3086 in WT	CTTGAACTCAACGCCTACA
oAB003	3086 KO down FOR	Knockout BT3086 in WT	GGCGTTGAGTTCAAGACCTATCGTTTTTAGTTATTC CG
oAB004	3086 KO down REV	Knockout BT3086 in WT	CTTGATATCGAATTCAAAGCCGTCCTGTATGAAAA
oAB005	3087KO up FOR	Knockout BT3087 in WT	ATTAGCATTATGAGTATAATCACGGCTTTCCGTT
oAB006	3087 KO up REV	Knockout BT3087 in WT	GGCAGTTGCAACGGAATA
oAB007	3087 KO down FOR	Knockout BT3087 in WT	TCCGTTGCAACTGCCCTTGAATACTTGTTTATTGTT TTACAATTG
oAB008	3087 KO down REV	Knockout BT3087 in WT	CTTGATATCGAATTCGGCGATAATGGCTGGGG
oAB009	3088 KO up FOR	Knockout BT3088 in WT	ATTAGCATTATGAGTCTTCAATGCCCCGAAACA
oAB010	3088 KO up REV	Knockout BT3088 in WT	ACAAGTATTCAAGATGAAGAAGATAATATA
oAB011	3088 KO down FOR	Knockout BT3088 in WT	ATCTTGAATACTTGTCATATGATCTGTCTAAATGAAT GATTG

oAB012	3088 KO down REV	Knockout BT3088 in WT	CTTGATATCGAATTCCGGCAGTACGGAATACGA
oAB013	3089 KO up FOR	Knockout BT3089 in WT	ATTAGCATTATGAGTGCCGTAGTTCTTCTCCG
oAB014	3089 KO up REV	Knockout BT3089 in WT	TTGCTTTTACAATCATTCAATTAGAC
oAB015	3089 KO down FOR	Knockout BT3089 in WT	TGATTGTAAAAGCAATTTCTTCCTCCTGATTTAAAAG TT
oAB016	3089 KO down REV	Knockout BT3089 in WT	CTTGATATCGAATTCCAATTCATACGTGACCATGC
oAB017	3090 KO up FOR	Knockout BT3090 in WT	ATTAGCATTATGAGTGATTGGGCGCCAGCG
oAB018	3090 KO up REV	Knockout BT3090 in WT	ATCAGGAGGAAGAAAATGAAAAAGAAAC
oAB019	3090 KO down FOR	Knockout BT3090 in WT	TTTCTTCCTCCTGATGTACATCAATTTAAAGTTAATA TTAGGATTACT
oAB020	3090 KO down REV	Knockout BT3090 in WT	CTTGATATCGAATTGCGACTCCAATTCGCAACTGAA
oAB021	3091 KO up FOR	Knockout BT3091 in WT	ATTAGCATTATGAGTTTTAATGGTTACATTGTCCCC
oAB022	3091 KO up REV	Knockout BT3091 in WT	GAAATCCACTACTTTTTTTAGCAC
oAB023	3091 KO down FOR	Knockout BT3091 in WT	AAAGTAGTGGATTTTCAGCGCCATATGTATTATATCTG C

oAB024	3091 KO down REV	Knockout BT3091 in WT	CTTGATATCGAATTCTATAAAAAATTGATGGAGCAA TGGC
oAB025	4581 KO up FOR	Knockout BT4581 in WT	ATTAGCATTATGAGTAGAAATATATCAGCATTAACT TCTCC
oAB026	4581 KO up REV	Knockout BT4581 in WT	GATATAAATGAATTAGTTAATAATCATATGGC
oAB027	4581 KO down FOR	Knockout BT4581 in WT	TAATTCATTTATATCGACGCGACTAAAACGATTGTTC
oAB028	4581 KO down REV	Knockout BT4581 in WT	CTTGATATCGAATTCACCGGAGTACGTCCCCAT
oAB046	pET29_BT30 86 FOR	Expression of BT3086	ATCGAATTCGGGATCCGAAAACGCAAAAAGTATATG TACC
oAB047	pET29_BT30 86 REV	Expression of BT3086	GTGGTGGTGGTGCTCGAGTCATAAACGCAGGGAA ATCC
oAB050	pET29_BT30 87 FOR	Expression of BT3087	GATCGAATTCGGGATCCTGCAGCGACGATCATGA
oAB051	pET29_BT30 87 REV	Expression of BT3087	GTGGTGGTGGTGCTCGAGTTATTCAGCTACAATCA TTGTCCA
oAB052	pET29_BT45 81 FOR	Expression of BT4581	GGATCGAATTCGGGATCCGAAAGTATCACTTCTCC TGACG
oAB053	pET29_BT45 81 REV	Expression of BT4581	TGGTGGTGGTGGTGCTCGAGTCATTTCCATTCTT AATTGATTCC
oAB095	3086 3087 KO up FOR	Knockout BT3087 in BT3086 background	GATTAGCATTATGAGTAGAAATATGAAGGCAACCGT
oAB096	3086 3087 KO up REV	Knockout BT3087 in BT3086 background	AAACAAGTATTCAAGGGCAGTTGCAACGGAAT

oAB097	3086 3087 KO down FOR	Knockout BT3087 in BT3086 background	CTTGAATACTTGTTTATTGTTTACAATTG
oAB098	3086 3087 KO down REV	Knockout BT3087 in BT3086 background	CTTGATATCGAATTCGGCGATAATGGCTGGG

Table S4.3. List of primers used for this study.

Chapter 5. Conclusions

Throughout my PhD, I have studied the nutrient sharing and biofilm formation by *Bacteroides* under the influence of physical force generated by fluid flow. In this chapter, I will briefly summarize key results and present ideas for future directions.

5.1 Achieved results and discussion

5.1.1 Biofilm formation by the gut commensals *Bacteroides*

As described in chapter 2, I first studied the biofilm formation capabilities of gut commensals under anaerobic environments. To achieve this goal, I developed an anaerobic microfluidics-based technique which allowed for the growth of biofilms under anaerobic environments. Using this anaerobic biofilm growth system, I studied the *in-vitro* biofilm formation by 4 *Bacteroides* species: *Bt*, *Bf*, *Bo* and *Bv* under constant flow of the nutrient rich TYG medium. With fluorescence confocal microscopy, I was able to, for the first time, observe the surface attachment and subsequent biofilm formation by 4 *Bacteroides* species in flow. Each species formed biofilms of interesting, and highly varying morphologies, from meteorite like colonies to thick filaments. To further understand the underlying mechanisms of biofilm formation which are responsible for such differing morphologies, I analyzed both the proteome and transcriptome of these species grown as a biofilm versus as a liquid culture. I identified potential genes coding for various surface associated cellular filaments such as pili and fimbriae which may play crucial roles in the biofilm formation by these commensal bacteria. As the goal of the project was to study biofilm communities, I then co-cultured *Bacteroides* species in combinations of two in the nutrient rich TYG medium. I observed that in general, under nutrient rich environments where competition dominates, these species all grow independently of each other within the co-culture and the abundance of individual species are likely determined by growth rates and access to surface space. To understand further the role of carbon source on biofilm formation by gut microbes, I grew *Bt*, *Bf* and *Bo* biofilms in BMM, a minimal medium where I can control the carbon

source. In general, I observed that changes in carbon sources leads to changes in biofilm morphologies, suggesting the important role of carbon source in regulating gut biofilm structure, which may confer the abundance of species within the community and host health.

5.1.2 Nutrient sharing biofilms in fluid flow

Since the *Bacteroides* attached to surfaces and formed biofilms *in-vitro* under anaerobic conditions, I then proceeded to study the possibilities of nutrient sharing within the gut microbiota community. To achieve this goal, I constructed a model gut microbiota consisting of two species: *Bt* and *Bf*. I identified dextran as a polysaccharide metabolite which is readily metabolized by *Bt* but not *Bf*. *Bt* metabolizes dextran into glucose and small oligosaccharides of glucose which are then released into the surrounding environment as common goods. Non-utilizers of dextran such as *Bf* may then feed onto the released glucose and grow in the presence of *Bt*. I then studied how nutrient sharing can impact the organization of biofilm communities by co-culturing *Bf* and *Bt* in dextran. I observed that *Bf* grows into biofilms in the presence of *Bt* in an evenly distributed manner in the absence of flow. However, in the presence of low flow, the general population of *Bf* is shifted downstream of *Bt* populations, and this populational shift of *Bf* is dependent on the flow rate of the system. Under conditions of sufficiently high flow, *Bf* population is completely abolished from the ecosystem. These results highlight the role of fluid flow in defining the chemical landscape of secreted public goods in the environment, which leads to changes in biofilm organization and individual species abundance in the gut microbiota, as described in Chapter 3.

5.1.3 Mechanisms of dextran utilization and nutrient sharing

In chapter 4 of my thesis, I sought to further understand the molecular mechanisms of dextran utilization and nutrient sharing by *Bt*. To achieve this, I analyzed the proteome of *Bt* grown in dextran versus in glucose and identified a cluster of proteins belonging to the polysaccharide utilization locus 48 (PUL48) which were significantly upregulated in

dextran growth. I generated a mutant library of *Bt*, consisting of genetic knockouts of single genes within PUL48 along with multi glycosoylhydrolase (GHs) knockouts. I assessed the growth of individual mutants in various dextran sizes to study the importance of individual PUL48 proteins in the growth of *Bt* in various dextran sizes. My results suggested that the proteins BT3089 (SusD), BT3090 (SusC) and BT3091 (SusR) are crucial for *Bt* growth in dextran of any size. The proteins BT3087 (dextranase) and BT3088 (SusE) becomes more important to *Bt* growth as dextran size increases. The GH BT3087 (dextranase) was the most crucial GH for growth in dextran, however, its activity is not required for the metabolism of dextran smaller than 9000 Da, suggesting the importer protein SusC can import dextrans of high degree of polymerization directly without prior processing. In terms of the role of polysaccharide size in *Bt* dextran metabolism, I observed a general trend in *Bt* growth where growth in increasing molecular weights of dextran lead to increased lag time and decreased growth rate, suggesting an important link between microbial growth and polysaccharide size. Through culturing *Bt* and various mutants in fluorescently labelled dextran, I also observed that the proteins BT3089 and BT3090 are crucial for the localization of dextran to *Bt*'s cell membrane, BT3088 is important for the binding of high molecular weight dextran and that the low molecular weight dextran binds to *Bt* in a non-specific manner. Finally, I then co-cultured individual *Bt* mutants with *Bf* to study the impact of individual PUL48 proteins and dextran size on nutrient sharing by *Bt* to *Bf*. In general, I observed a decrease in nutrient sharing to *Bf* in all *Bt* mutants in comparison to *Bt* WT and also as the size of dextran increased. These results suggest that PULs and intrinsic properties like polymer sizes of polysaccharides may impact the overall composition of a gut microbial community.

5.2 Future directions

5.2.1 Roles of fimbriae and pili in *Bacteroides* biofilm formation

Through the proteome and transcriptome analysis of *Bt* and *Bf* biofilms, I identified various genes upregulated under conditions of biofilm growth which corresponds to

fimbriae or pili family proteins. To further investigate the importance of extracellular filaments such as pili and fimbriae on the surface attachment, biofilm formation and structural maintenance, I propose to produce single and multiple knockout mutants of the gene targets which were upregulated in biofilm growth. Fluorescent proteins such as mCherry or sfGFP may then be inserted into mutants lacking the specific pili or fimbriae components and used for experiments including surface adhesion test in flow, biofilm growth and biofilm structural analysis.

5.2.2 Fluid flow and nutrient source in *Bf* filamentation

When grown as a biofilm in the nutrient rich TYG medium, *Bf* cells attach to one another and assemble into thick filaments which extends far from the surface. However, interestingly, this growth morphology was not observed in the absence of flow, or when the growth medium was switched to a minimal medium with a fixed carbon source. Therefore, to further understand the mechanism behind cellular filamentation by *Bf*, I propose to individually study the contribution by fluid flow and nutrient source. It would be interesting to grow *Bf* biofilms in TYG medium under various flow rates and analyze the growth morphologies as a function of growth rates as shear forces and nutrient availabilities are different across differing flow conditions. It would also be interesting to analyze the nutrient conditions contributing to *Bf* filamentation because perhaps such morphology is only favoured only under nutrient rich conditions in order to maximize nutrient uptake and minimize competition for space with other species. Overall, these experiments together may provide further insights regarding the ecological advantages of forming filamentous biofilms.

5.2.3 Dynamics of gut microbiota biofilms

During my PhD, I have developed a method for the growth of anaerobic biofilms under conditions of medium flow. However, most of the work I have done so far involve solely a single carbon source. In the real world, our diets are constantly changing from meal to meal. Therefore, it would be interesting to understand how microbial abundance and biofilm structure changes because of altering carbon and nutrient sources. To mimic the

change in diet, I propose the growth of an initial multi-species biofilm in my microfluidic devices under simple, glucose conditions until the community stabilizes. The stabilized community will then be exposed to various carbon sources through the changing of medium. We can then monitor the abundance of individual species over the course of various carbon source changes, and whether a “perturbed” community may return to its stabilized state as nutrient source stabilizes.

5.2.4 Biofilm growth of other anaerobes such as *C. difficile*

Using my anaerobic microfluidic devices, I was able to grow *in-vitro* biofilms of various anaerobic *Bacteroides* species. However, this setup may be extended to the growth of other anaerobic species such as the notorious pathogen *C. difficile* (Fig. 5.1). With my microfluidic devices, we can study the attachment properties of *C. difficile* to surfaces, along with their biofilm forming capabilities along with morphology. The ability to grow biofilms in flow also reduces the amount of non-biofilm cells present in the system, which allows for accurate proteome and transcriptome analysis of surface attached biofilm cells. Studies of the proteome and transcriptome of surface attached *C. difficile* cells may provide important insights to the mechanisms of surface attachment and biofilm formation by the pathogen, which may become future therapeutic targets for the prevention of *C. difficile* infections.

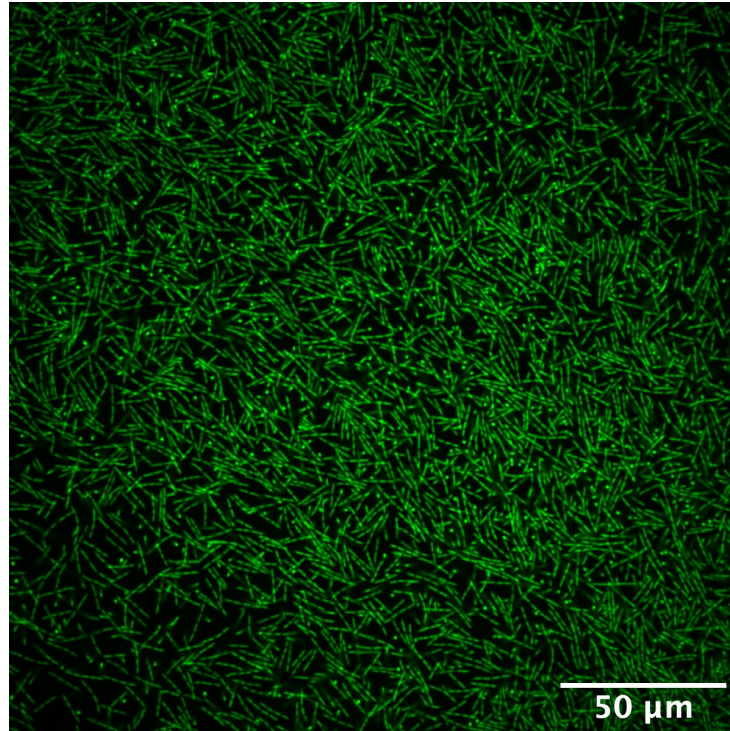


Fig. 5.1: Biofilm formation by *C. difficile*. The pathogen was cultured in the nutrient rich TYG medium for 3 days anaerobically, under a flow rate of 1 $\mu\text{L}/\text{min}$. Surface attached cells were then stained with the SYTO green dye and imaged by fluorescence confocal microscopy.

5.2.5 A carbohydrate screen for the metabolic steering of microbiota communities

Throughout my PhD, I have performed small carbohydrate screens with various commercially available dietary glycans such as inulin, arabinan, dextran and xylans, which led to the discovery of nutrient sharing from *Bt* to *Bf* in dextran. However, the gut microbiota is highly complex and contains 100s of species. Therefore, to get a realistic understanding of the overall metabolic interactions shaping the overall stability of the microbiota, a more complex model microbiota must be employed. I propose to start with sourced microbiota consortia from the Broad Institute-OpenBiome Microbiome library. We can then expose this consortium to various “dietary nutrients” including high fibre diets versus high fat diets. We can simply measure the changes in abundances of individual species within the consortia by performing 16S-RNA sequencing and

measuring the short chain fatty acid metabolic output of both consortia exposed to healthy versus unhealthy diets.

With the hope of identifying new carbohydrate-based prebiotics which may steer a altered microbiome into its normal state, I propose to then expose the altered gut microbiota as a result of unhealthy diet to a high-throughput polysaccharide screen containing various polysaccharide sources from human milk oligosaccharides (HMOs) to various mammalian N-linked glycans (high mannose, complex and hybrid), O-glycans (mucin, O-fucosyl and O-mannosyl), glycosaminoglycans (hyaluronic acid, chondroitin sulfates, heparin), and plant and bacterial oligosaccharides (glucans, chitins, mannan, arabinan, xylan and fructans). We will then perform 16S-RNA sequencing and short chain fatty acid profiling on individual communities incubated in different polysaccharide sources to assess the impact of individual polysaccharide sources on influencing community abundance and metabolic output of the initially altered community (Fig. 5.2). This may then provide interesting polysaccharide candidates which may serve as prebiotic molecules for the treatment of dysbiosis.

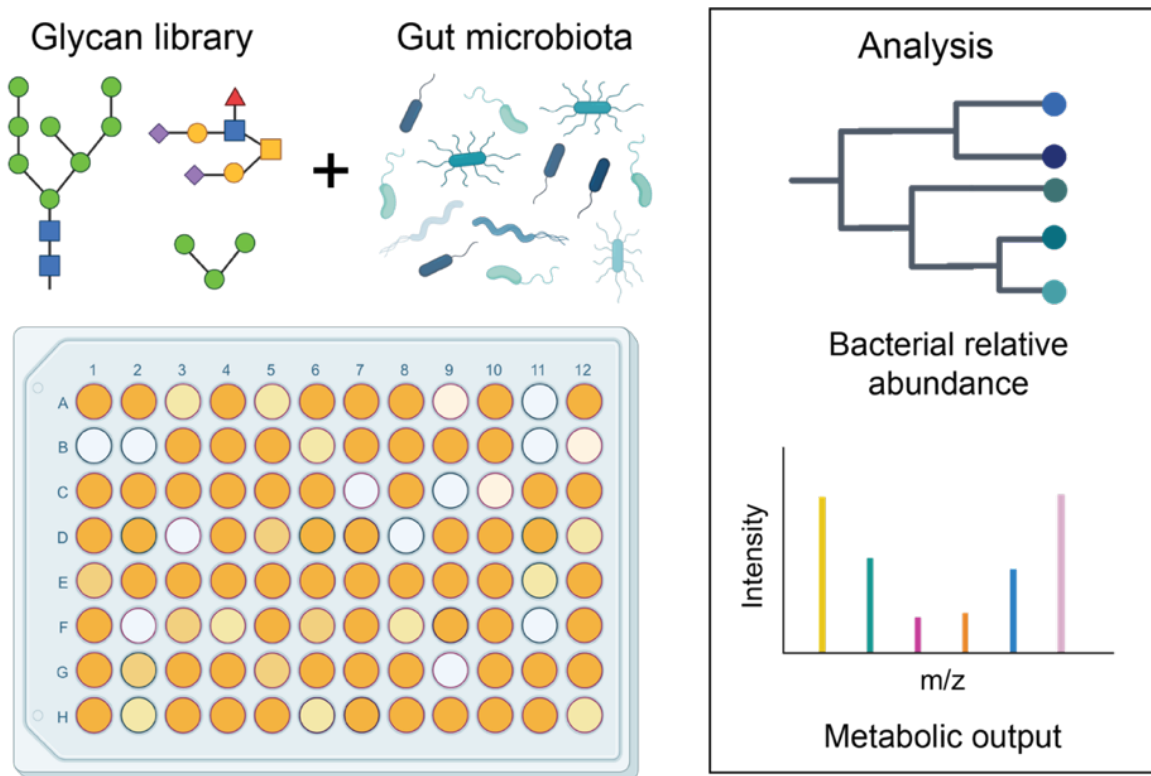


Fig. 5.2: Experimental set-up for identifying polysaccharide targets which steers the metabolism of infant microbiota communities. In a 96-well plate, we will generate an array containing different carbohydrate sources. We will then culture an altered gut microbiota in each condition, quantify the relative abundance of each species by 16S-RNA sequencing and analyze the SCFA metabolic output to perform relative quantification of butyrate, acetate, and propionate by GC-MS.

5.2.6 Microbiota-host interactions in the colon

The gut microbiota plays important roles in host health: providing butyrate as an energy source³¹ to the host, aid in complex fibre digestion³² and also training host immunity³³. However, studies involving microbiota and host health are often performed in mice, which does not allow for real-time, dynamic measurements of the gut microbiome. Recent advances in technology have led to the development of *in-vitro* mammalian cell models termed organoids, which resembles *in-vivo* cell physiology. Using organoid

models provides several advantages to studying bacteria-host interactions, including the use of human cells, which resembles more the actual host physiology and the possibility for dynamic studies and imaging. Therefore, as a future direction of this project, I propose to bring mammalian cells into the picture, and study how gut microbes colonize and interact with the host cells in the human colon using human colon organoids.

First, we will produce organoids from human colonic stem cell as starting biological material to better replicate the relevant intestinal section. We will ensure that the colon organoids produce a mucosal surface, which is crucial for bacterial colonization and subsequent mutualistic interactions with the host. Once a mucosal surface is produced, we may then inoculate single bacteria strains commonly found in the gut microbiota, expressing fluorescent proteins such as *Bt*. Fluorescence microscopy may then be performed to study the real-time colonization and growth of the bacteria within the organoid, which resembles the host environment. With this set-up, we can also then easily isolate bacteria and colon cells, where we can then perform transcriptomics to study how bacteria host interactions interact the metabolic output of both the bacteria and the host. Overall, the future direction of this project would be to further increase the complexity of the gut microbe consortia as much as possible, ultimately leading to an *in-vitro*, highly physiologically relevant platform which may be used for future studies concerning the gut microbiota.

5.2.7 Nutrient sharing and T6SS

In this thesis, I demonstrated that *Bt* can nutrient share metabolic by-products to *Bf* through its metabolism of the polysaccharide dextran, supporting the growth of the non-dextran utilizing *Bf*. Interestingly, when I analyzed the proteome of *Bf* in the presence of nutrient sharing, I observed that *Bf* strongly downregulates its Type VI secretion system (T6SS), a system used for the antagonization of other members of the *Bacteroides* genus when grown in *Bt* spent medium or a synthetic dextran medium treated with GHs BT3086 (Fig. 5.3B, C) and BT4581 (Fig. 5.3B, C).

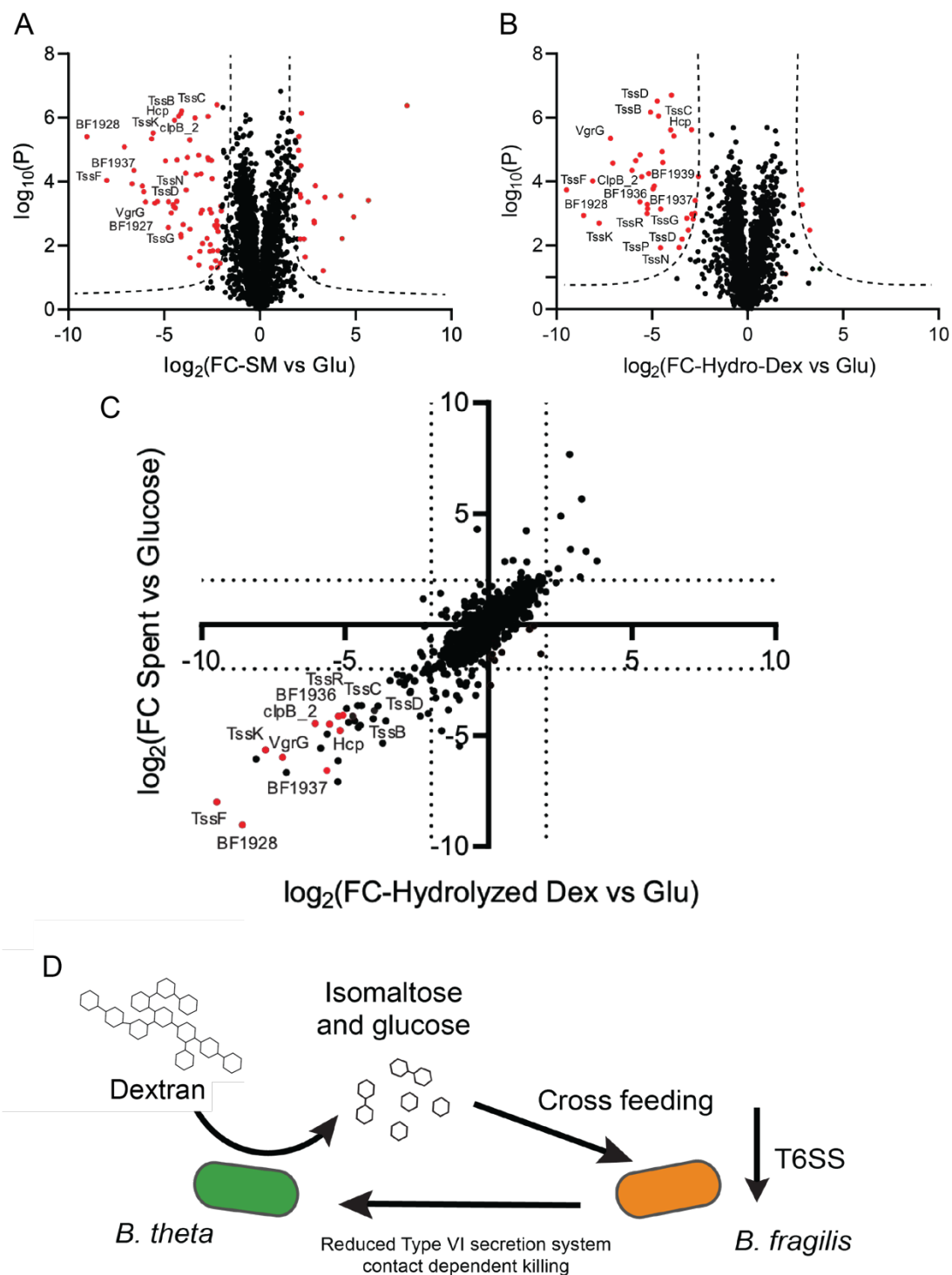


Fig. 5.3 *Bf* downregulates T6SS in the presence of *Bt* nutrient sharing. (A) Proteomic analysis of *Bf* growing in *Bt* spent medium. We generated the volcano plot based on fold-change in dextran relative to culture in glucose ($N = 3$). Red dots

correspond to T6SS proteins with statistically significant different fold changes (S_0 value of 1.0 and FDR cut-off of 0.01). (B) Proteomic analysis of *Bf* growing in dextran medium along with GHs BT3086, BT3087 and BT4581. We generated the volcano plot based on fold-change in dextran relative to culture in glucose ($N = 3$). Red dots correspond to T6SS proteins with statistically significant different fold changes (S_0 value of 1.0 and FDR cut-off of 0.01). (C) Correlation analysis between proteins upregulated in SM versus Hydro-Dex medium. Red dots correspond to downregulated T6SS proteins observed in both conditions. In general, the expression of most proteins across the two conditions correlate linearly. (D) Proposed mechanism of *Bf* “giving back” to *Bt* in dextran, where *Bf* downregulates its T6SS in order to reduce the killing of *Bt*, which provides itself with the nutrient critical for survival in an environment with polysaccharide sources which it cannot utilize itself.

Hence, I hypothesize that polysaccharide utilization and nutrient sharing potentially regulates the overall social behaviour of the *Bacteroides*, including the regulation of T6SSs (Fig. 5.3D). To demonstrate this, I would like to first study the regulation of Type VI secretion systems under various systems of nutrient sharing and polysaccharide sources by RNA-seq and RT-qPCR experiments. To further confirm the validity of the *Bf* proteome data suggesting downregulation of T6SS, microbiology assays will be performed, such as the contact dependent killing assay (Fig. 5.3), to confirm the changes in bacterial social behaviour.

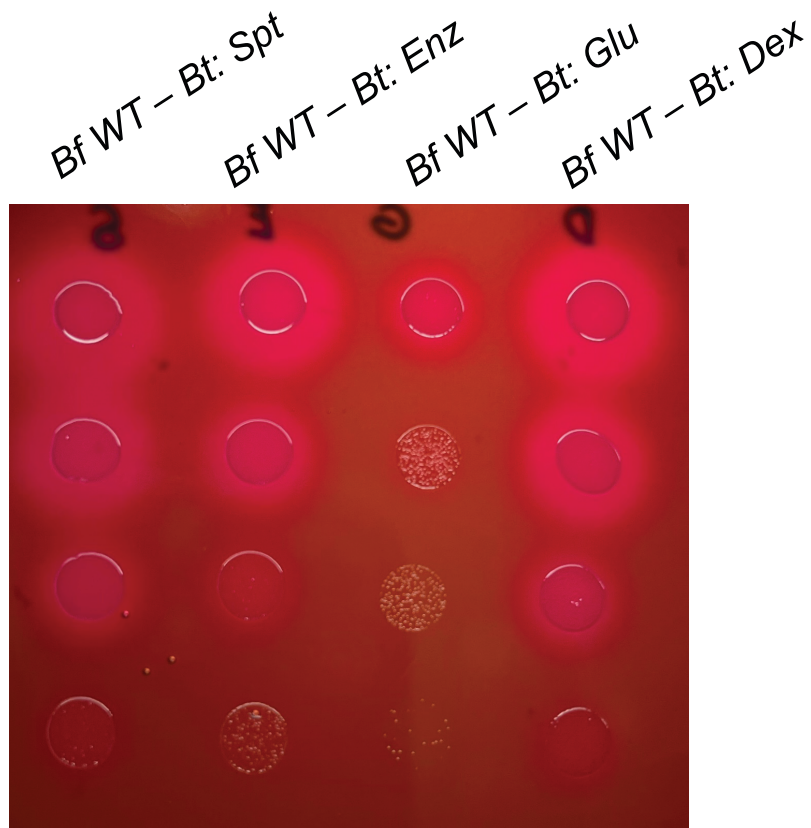


Fig. 5.4: Contact dependent killing by *Bf* on *Bt*. *Bf* wildtype and *Bt* with erythromycin (Er) resistance were mixed at a 10:1 ratio and spotted onto BMM plates containing other *Bt* spent medium, dextran treated with GHs BT3086, BT3087 and BT4581 (Enz), glucose or dextran. The colonies were grown on BMM plates for 3 days anaerobically, followed by resuspension in PBS. Cultures were then serial diluted and plated onto a BHIB plate in the presence of Er. The spotted cultures were allowed to grow for 2 days anaerobically, where cfu counts were then performed.

References

1. Flemming, H.-C. *et al.* Biofilms: an emergent form of bacterial life. *Nat. Rev. Microbiol.* **14**, 563–575 (2016).
2. Battin, T. J., Kaplan, L. A., Denis Newbold, J. & Hansen, C. M. E. Contributions of microbial biofilms to ecosystem processes in stream mesocosms. *Nature* **426**, 439–442 (2003).
3. Arnosti, C. Microbial extracellular enzymes and the marine carbon cycle. *Annu. Rev. Mar. Sci.* **3**, 401–425 (2011).
4. Macfarlane, S., Bahrami, B. & Macfarlane, G. T. Mucosal biofilm communities in the human intestinal tract. *Adv. Appl. Microbiol.* **75**, 111–143 (2011).
5. Høiby, N., Bjarnsholt, T., Givskov, M., Molin, S. & Ciofu, O. Antibiotic resistance of bacterial biofilms. *Int. J. Antimicrob. Agents* **35**, 322–332 (2010).
6. Harding, J. L. & Reynolds, M. M. Combating medical device fouling. *Trends Biotechnol.* **32**, 140–146 (2014).
7. Drescher, K., Shen, Y., Bassler, B. L. & Stone, H. A. Biofilm streamers cause catastrophic disruption of flow with consequences for environmental and medical systems. *Proc. Natl. Acad. Sci.* **110**, 4345–4350 (2013).
8. Deep, A., Chaudhary, U. & Gupta, V. Quorum sensing and Bacterial Pathogenicity: From Molecules to Disease. *J. Lab. Physicians* **3**, 4–11 (2011).
9. Baker, P. *et al.* Exopolysaccharide biosynthetic glycoside hydrolases can be utilized to disrupt and prevent *Pseudomonas aeruginosa* biofilms. *Sci. Adv.* **2**, e1501632 (2016).

10. Sauer, K. *et al.* The biofilm life cycle: expanding the conceptual model of biofilm formation. *Nat. Rev. Microbiol.* **20**, 608–620 (2022).
11. Stewart, P. S. & Franklin, M. J. Physiological heterogeneity in biofilms. *Nat. Rev. Microbiol.* **6**, 199–210 (2008).
12. Nadell, C. D., Xavier, J. B. & Foster, K. R. The sociobiology of biofilms. *FEMS Microbiol. Rev.* **33**, 206–224 (2009).
13. Rendueles, O. & Ghigo, J.-M. Mechanisms of Competition in Biofilm Communities. *Microbiol. Spectr.* **3**, (2015).
14. Hibbing, M. E., Fuqua, C., Parsek, M. R. & Peterson, S. B. Bacterial competition: surviving and thriving in the microbial jungle. *Nat. Rev. Microbiol.* **8**, 15–25 (2010).
15. Basler, M., Ho, B. T. & Mekalanos, J. J. Tit-for-Tat: Type VI Secretion System Counterattack during Bacterial Cell-Cell Interactions. *Cell* **152**, 884–894 (2013).
16. Chatzidaki-Livanis, M., Geva-Zatorsky, N. & Comstock, L. E. *Bacteroides fragilis* type VI secretion systems use novel effector and immunity proteins to antagonize human gut Bacteroidales species. *Proc. Natl. Acad. Sci. U. S. A.* **113**, 3627–3632 (2016).
17. Russell, A. B. *et al.* A type VI secretion-related pathway in Bacteroidetes mediates interbacterial antagonism. *Cell Host Microbe* **16**, 227–236 (2014).
18. Kim, H. J., Boedicker, J. Q., Choi, J. W. & Ismagilov, R. F. Defined spatial structure stabilizes a synthetic multispecies bacterial community. *Proc. Natl. Acad. Sci.* **105**, 18188–18193 (2008).
19. Griffin, A. S., West, S. A. & Buckling, A. Cooperation and competition in pathogenic bacteria. *Nature* **430**, 1024–1027 (2004).

20. Allison, S. D. Cheaters, diffusion and nutrients constrain decomposition by microbial enzymes in spatially structured environments. *Ecol. Lett.* **8**, 626–635 (2005).
21. West, S. A., Diggle, S. P., Buckling, A., Gardner, A. & Griffin, A. S. The Social Lives of Microbes. *Annu. Rev. Ecol. Evol. Syst.* **38**, 53–77 (2007).
22. Mee, M. T., Collins, J. J., Church, G. M. & Wang, H. H. Syntrophic exchange in synthetic microbial communities. *Proc. Natl. Acad. Sci. U. S. A.* **111**, E2149–2156 (2014).
23. Nadell, C. D., Drescher, K. & Foster, K. R. Spatial structure, cooperation and competition in biofilms. *Nat. Rev. Microbiol.* **14**, 589–600 (2016).
24. Kerr, B., Riley, M. A., Feldman, M. W. & Bohannan, B. J. M. Local dispersal promotes biodiversity in a real-life game of rock-paper-scissors. *Nature* **418**, 171–174 (2002).
25. Dal Co, A., van Vliet, S., Kiviet, D. J., Schlegel, S. & Ackermann, M. Short-range interactions govern the dynamics and functions of microbial communities. *Nat. Ecol. Evol.* **4**, 366–375 (2020).
26. Drescher, K., Nadell, C. D., Stone, H. A., Wingreen, N. S. & Bassler, B. L. Solutions to the public goods dilemma in bacterial biofilms. *Curr. Biol. CB* **24**, 50–55 (2014).
27. Ursell, L. K., Metcalf, J. L., Parfrey, L. W. & Knight, R. Defining the Human Microbiome. *Nutr. Rev.* **70**, S38–S44 (2012).
28. Lynch, S. V. & Pedersen, O. The Human Intestinal Microbiome in Health and Disease. *N. Engl. J. Med.* **375**, 2369–2379 (2016).
29. Fan, Y. & Pedersen, O. Gut microbiota in human metabolic health and disease. *Nat. Rev. Microbiol.* **19**, 55–71 (2021).

30. Pluznick, J. L. *et al.* Olfactory receptor responding to gut microbiota-derived signals plays a role in renin secretion and blood pressure regulation. *Proc. Natl. Acad. Sci. U. S. A.* **110**, 4410–4415 (2013).
31. Silva, Y. P., Bernardi, A. & Frozza, R. L. The Role of Short-Chain Fatty Acids From Gut Microbiota in Gut-Brain Communication. *Front. Endocrinol.* **11**, (2020).
32. Koropatkin, N. M., Cameron, E. A. & Martens, E. C. How glycan metabolism shapes the human gut microbiota. *Nat. Rev. Microbiol.* **10**, 323–335 (2012).
33. Belkaid, Y. & Hand, T. Role of the Microbiota in Immunity and inflammation. *Cell* **157**, 121–141 (2014).
34. Townsend, E. M. *et al.* The Human Gut Phageome: Origins and Roles in the Human Gut Microbiome. *Front. Cell. Infect. Microbiol.* **11**, (2021).
35. Rinninella, E. *et al.* What is the Healthy Gut Microbiota Composition? A Changing Ecosystem across Age, Environment, Diet, and Diseases. *Microorganisms* **7**, 14 (2019).
36. Piquer-Esteban, S., Ruiz-Ruiz, S., Arnau, V., Diaz, W. & Moya, A. Exploring the universal healthy human gut microbiota around the World. *Comput. Struct. Biotechnol. J.* **20**, 421–433 (2021).
37. Yatsunenko, T. *et al.* Human gut microbiome viewed across age and geography. *Nature* **486**, 222–227 (2012).
38. Leeming, E. R., Johnson, A. J., Spector, T. D. & Le Roy, C. I. Effect of Diet on the Gut Microbiota: Rethinking Intervention Duration. *Nutrients* **11**, 2862 (2019).

39. Nakajima, A. *et al.* A Soluble Fiber Diet Increases *Bacteroides fragilis* Group Abundance and Immunoglobulin A Production in the Gut. *Appl. Environ. Microbiol.* **86**, e00405-20 (2020).
40. Murphy, E. A., Velazquez, K. T. & Herbert, K. M. Influence of High-Fat-Diet on Gut Microbiota: A Driving Force for Chronic Disease Risk. *Curr. Opin. Clin. Nutr. Metab. Care* **18**, 515–520 (2015).
41. Nadell, C. D. *et al.* Cutting through the complexity of cell collectives. *Proc. R. Soc. B Biol. Sci.* **280**, 20122770 (2013).
42. Sharma, D., Misba, L. & Khan, A. U. Antibiotics versus biofilm: an emerging battleground in microbial communities. *Antimicrob. Resist. Infect. Control* **8**, 76 (2019).
43. Costerton, J. W., Stewart, P. S. & Greenberg, E. P. Bacterial biofilms: a common cause of persistent infections. *Science* **284**, 1318–1322 (1999).
44. Davies, J. C. *Pseudomonas aeruginosa* in cystic fibrosis: pathogenesis and persistence. *Paediatr. Respir. Rev.* **3**, 128–134 (2002).
45. Talà, L., Fineberg, A., Kukura, P. & Persat, A. *Pseudomonas aeruginosa* orchestrates twitching motility by sequential control of type IV pili movements. *Nat. Microbiol.* **4**, 774–780 (2019).
46. Persat, A., Inclan, Y. F., Engel, J. N., Stone, H. A. & Gitai, Z. Type IV pili mechanochemically regulate virulence factors in *Pseudomonas aeruginosa*. *Proc. Natl. Acad. Sci.* **112**, 7563–7568 (2015).

47. Ghafoor, A., Hay, I. D. & Rehm, B. H. A. Role of Exopolysaccharides in *Pseudomonas aeruginosa* Biofilm Formation and Architecture. *Appl. Environ. Microbiol.* **77**, 5238–5246 (2011).
48. Periasamy, S. *et al.* *Pseudomonas aeruginosa* PAO1 exopolysaccharides are important for mixed species biofilm community development and stress tolerance. *Front. Microbiol.* **6**, (2015).
49. Garnett, J. A. *et al.* Structural insights into the biogenesis and biofilm formation by the *Escherichia coli* common pilus. *Proc. Natl. Acad. Sci.* **109**, 3950–3955 (2012).
50. Klemm, P. Fimbrial adhesions of *Escherichia coli*. *Rev. Infect. Dis.* **7**, 321–340 (1985).
51. Maldarelli, G. A. *et al.* Type IV pili promote early biofilm formation by *Clostridium difficile*. *Pathog. Dis.* **74**, ftw061 (2016).
52. Yan, J., Sharo, A. G., Stone, H. A., Wingreen, N. S. & Bassler, B. L. *Vibrio cholerae* biofilm growth program and architecture revealed by single-cell live imaging. *Proc. Natl. Acad. Sci.* **113**, E5337–E5343 (2016).
53. Cont, A., Vermeil, J. & Persat, A. Material Substrate Physical Properties Control *Pseudomonas aeruginosa* Biofilm Architecture. *mBio* **14**, e03518-22 (2023).
54. Lozupone, C. A., Stombaugh, J. I., Gordon, J. I., Jansson, J. K. & Knight, R. Diversity, stability and resilience of the human gut microbiota. *Nature* **489**, 220–230 (2012).
55. Bäckhed, F., Ley, R. E., Sonnenburg, J. L., Peterson, D. A. & Gordon, J. I. Host-bacterial mutualism in the human intestine. *Science* **307**, 1915–1920 (2005).

56. Singh, R. K. *et al.* Influence of diet on the gut microbiome and implications for human health. *J. Transl. Med.* **15**, 73 (2017).
57. Wexler, H. M. Bacteroides: the Good, the Bad, and the Nitty-Gritty. *Clin. Microbiol. Rev.* **20**, 593–621 (2007).
58. Xu, Q. *et al.* A Distinct Type of Pilus from the Human Microbiome. *Cell* **165**, 690–703 (2016).
59. Mihajlovic, J. *et al.* A Putative Type V Pilus Contributes to Bacteroides thetaiotaomicron Biofilm Formation Capacity. *J. Bacteriol.* **201**, e00650-18 (2019).
60. Porter, N. T., Canales, P., Peterson, D. A. & Martens, E. C. A Subset of Polysaccharide Capsules in the Human Symbiont Bacteroides thetaiotaomicron Promote Increased Competitive Fitness in the Mouse Gut. *Cell Host Microbe* **22**, 494-506.e8 (2017).
61. Béchon, N. *et al.* Capsular Polysaccharide Cross-Regulation Modulates Bacteroides thetaiotaomicron Biofilm Formation. *mBio* **11**, e00729-20 (2020).
62. Béchon, N. & Ghigo, J.-M. Gut biofilms: Bacteroides as model symbionts to study biofilm formation by intestinal anaerobes. *FEMS Microbiol. Rev.* **46**, fuab054 (2022).
63. Schwalm, N. D., Townsend, G. E. & Groisman, E. A. Multiple Signals Govern Utilization of a Polysaccharide in the Gut Bacterium Bacteroides thetaiotaomicron. *mBio* **7**, 10.1128/mbio.01342-16 (2016).
64. Shi, H. *et al.* Highly multiplexed spatial mapping of microbial communities. *Nature* **588**, 676–681 (2020).
65. Huttenhower, C. *et al.* Structure, function and diversity of the healthy human microbiome. *Nature* **486**, 207–214 (2012).

66. Salyers, A. A., Vercellotti, J. R., West, S. E. & Wilkins, T. D. Fermentation of mucin and plant polysaccharides by strains of *Bacteroides* from the human colon. *Appl. Environ. Microbiol.* **33**, 319–322 (1977).
67. Wexler, A. G. & Goodman, A. L. An insider's perspective: *Bacteroides* as a window into the microbiome. *Nat. Microbiol.* **2**, 1–11 (2017).
68. Abee, T., Kovács, Á. T., Kuipers, O. P. & van der Veen, S. Biofilm formation and dispersal in Gram-positive bacteria. *Curr. Opin. Biotechnol.* **22**, 172–179 (2011).
69. Wucher, B. R. *et al.* *Vibrio cholerae* filamentation promotes chitin surface attachment at the expense of competition in biofilms. *Proc. Natl. Acad. Sci.* **116**, 14216–14221 (2019).
70. Tuncil, Y. E. *et al.* Reciprocal Prioritization to Dietary Glycans by Gut Bacteria in a Competitive Environment Promotes Stable Coexistence. *mBio* **8**, 10.1128/mbio.01068-17 (2017).
71. Mechanisms of Competition in Biofilm Communities | Microbiology Spectrum. <https://journals.asm.org/doi/10.1128/microbiolspec.mb-0009-2014>.
72. Barken, K. B. *et al.* Roles of type IV pili, flagellum-mediated motility and extracellular DNA in the formation of mature multicellular structures in *Pseudomonas aeruginosa* biofilms. *Environ. Microbiol.* **10**, 2331–2343 (2008).
73. Jones, C. H. *et al.* FimC is a periplasmic PapD-like chaperone that directs assembly of type 1 pili in bacteria. *Proc. Natl. Acad. Sci. U. S. A.* **90**, 8397–8401 (1993).
74. Sarkar, M. K., Paul, K. & Blair, D. Chemotaxis signaling protein CheY binds to the rotor protein FliN to control the direction of flagellar rotation in *Escherichia coli*. *Proc. Natl. Acad. Sci.* **107**, 9370–9375 (2010).

75. Huang, B., Whitchurch, C. B. & Mattick, J. S. FimX, a multidomain protein connecting environmental signals to twitching motility in *Pseudomonas aeruginosa*. *J. Bacteriol.* **185**, 7068–7076 (2003).
76. Whitaker, W. R., Shepherd, E. S. & Sonnenburg, J. L. Tunable Expression Tools Enable Single-Cell Strain Distinction in the Gut Microbiome. *Cell* **169**, 538-546.e12 (2017).
77. Martens, E. C., Chiang, H. C. & Gordon, J. I. Mucosal Glycan Foraging Enhances Fitness and Transmission of a Saccharolytic Human Gut Bacterial Symbiont. *Cell Host Microbe* **4**, 447–457 (2008).
78. Wong, J. P. H., Fischer-Stettler, M., Zeeman, S. C., Battin, T. J. & Persat, A. Fluid flow structures gut microbiota biofilm communities by distributing public goods. 2022.11.11.516095 Preprint at <https://doi.org/10.1101/2022.11.11.516095> (2022).
79. Cont, A., Rossy, T., Al-Mayyah, Z. & Persat, A. Biofilms deform soft surfaces and disrupt epithelia. *eLife* **9**, e56533 (2020).
80. Leventhal, G. E., Ackermann, M. & Schiessl, K. T. Why microbes secrete molecules to modify their environment: the case of iron-chelating siderophores. *J. R. Soc. Interface* **16**, 20180674 (2019).
81. Allison, S. D. Cheaters, diffusion and nutrients constrain decomposition by microbial enzymes in spatially structured environments. *Ecol. Lett.* **8**, 626–635 (2005).
82. West, S. A., Diggle, S. P., Buckling, A., Gardner, A. & Griffin, A. S. The Social Lives of Microbes. *Annu. Rev. Ecol. Evol. Syst.* **38**, 53–77 (2007).
83. Nadell, C. D., Drescher, K. & Foster, K. R. Spatial structure, cooperation and competition in biofilms. *Nat. Rev. Microbiol.* **14**, 589–600 (2016).

84. Rumbaugh, K. P. *et al.* Quorum sensing and the social evolution of bacterial virulence. *Curr. Biol. CB* **19**, 341–345 (2009).
85. D'Souza, G. *et al.* Ecology and evolution of metabolic cross-feeding interactions in bacteria. *Nat. Prod. Rep.* **35**, 455–488 (2018).
86. Tropini, C., Earle, K. A., Huang, K. C. & Sonnenburg, J. L. The Gut Microbiome: Connecting Spatial Organization to Function. *Cell Host Microbe* **21**, 433–442 (2017).
87. Persat, A. *et al.* The Mechanical World of Bacteria. *Cell* **161**, 988–997 (2015).
88. Labavić, D., Loverdo, C. & Bitbol, A.-F. Hydrodynamic flow and concentration gradients in the gut enhance neutral bacterial diversity. *Proc. Natl. Acad. Sci.* **119**, e2108671119 (2022).
89. Kim, M. K., Ingremeau, F., Zhao, A., Bassler, B. L. & Stone, H. A. Local and global consequences of flow on bacterial quorum sensing. *Nat. Microbiol.* **1**, 1–5 (2016).
90. Drescher, K., Nadell, C. D., Stone, H. A., Wingreen, N. S. & Bassler, B. L. Solutions to the public goods dilemma in bacterial biofilms. *Curr. Biol. CB* **24**, 50–55 (2014).
91. Cremer, J. *et al.* Effect of flow and peristaltic mixing on bacterial growth in a gut-like channel. *Proc. Natl. Acad. Sci.* **113**, 11414–11419 (2016).
92. Arumugam, M. *et al.* Enterotypes of the human gut microbiome. *Nature* **473**, 174–180 (2011).
93. Porter, N. T., Luis, A. S. & Martens, E. C. *Bacteroides thetaiotaomicron*. *Trends Microbiol.* **26**, 966–967 (2018).
94. Xu, J. *et al.* A genomic view of the human-*Bacteroides thetaiotaomicron* symbiosis. *Science* **299**, 2074–2076 (2003).

95. Sonnenburg, E. D. *et al.* Specificity of polysaccharide use in intestinal bacteroides species determines diet-induced microbiota alterations. *Cell* **141**, 1241–1252 (2010).
96. Cuskin, F. *et al.* Human gut Bacteroidetes can utilize yeast mannan through a selfish mechanism. *Nature* **517**, 165–169 (2015).
97. Sonnenburg, J. L. *et al.* Glycan foraging in vivo by an intestine-adapted bacterial symbiont. *Science* **307**, 1955–1959 (2005).
98. Anderson, K. L. & Salyers, A. A. Genetic evidence that outer membrane binding of starch is required for starch utilization by *Bacteroides thetaiotaomicron*. *J. Bacteriol.* **171**, 3199–3204 (1989).
99. Martens, E. C., Koropatkin, N. M., Smith, T. J. & Gordon, J. I. Complex glycan catabolism by the human gut microbiota: the Bacteroidetes Sus-like paradigm. *J. Biol. Chem.* **284**, 24673–24677 (2009).
100. Briliūtė, J. *et al.* Complex N-glycan breakdown by gut *Bacteroides* involves an extensive enzymatic apparatus encoded by multiple co-regulated genetic loci. *Nat. Microbiol.* **4**, 1571–1581 (2019).
101. Grondin, J. M., Tamura, K., Déjean, G., Abbott, D. W. & Brumer, H. Polysaccharide Utilization Loci: Fueling Microbial Communities. *J. Bacteriol.* **199**, e00860-16 (2017).
102. Rogowski, A. *et al.* Glycan complexity dictates microbial resource allocation in the large intestine. *Nat. Commun.* **6**, 7481 (2015).
103. Rakoff-Nahoum, S., Foster, K. R. & Comstock, L. E. The evolution of cooperation within the gut microbiota. *Nature* **533**, 255–259 (2016).

104. Tuncil, Y. E. *et al.* Reciprocal Prioritization to Dietary Glycans by Gut Bacteria in a Competitive Environment Promotes Stable Coexistence. *mBio* **8**, e01068-17 (2017).
105. Naessens, M., Cerdobbel, A., Soetaert, W. & Vandamme, E. J. Leuconostoc dextransucrase and dextran: production, properties and applications. *J. Chem. Technol. Biotechnol.* **80**, 845–860 (2005).
106. De Vos & M, W. Microbial biofilms and the human intestinal microbiome. *Npj Biofilms Microbiomes* **1**, 1–3 (2015).
107. Mihajlovic, J. *et al.* A Putative Type V Pilus Contributes to Bacteroides thetaiotaomicron Biofilm Formation Capacity. *J. Bacteriol.* **201**, e00650-18 (2019).
108. Bjursell, M. K., Martens, E. C. & Gordon, J. I. Functional Genomic and Metabolic Studies of the Adaptations of a Prominent Adult Human Gut Symbiont, Bacteroides thetaiotaomicron, to the Suckling Period. *J. Biol. Chem.* **281**, 36269–36279 (2006).
109. Terrapon, N. *et al.* PULDB: the expanded database of Polysaccharide Utilization Loci. *Nucleic Acids Res.* **46**, D677–D683 (2018).
110. Pudlo, N. A. *et al.* Symbiotic Human Gut Bacteria with Variable Metabolic Priorities for Host Mucosal Glycans. *mBio* **6**, e01282-15 (2015).
111. Kamada, N. *et al.* Regulated Virulence Controls the Ability of a Pathogen to Compete with the Gut Microbiota. *Science* **336**, 1325–1329 (2012).
112. Schwalm, N. D., Townsend, G. E. & Groisman, E. A. Multiple Signals Govern Utilization of a Polysaccharide in the Gut Bacterium Bacteroides thetaiotaomicron. *mBio* **7**, e01342-16 (2016).
113. Granath, K. A. Solution properties of branched dextrans. *J. Colloid Sci.* **13**, 308–328 (1958).

114. Liu, H. *et al.* Functional genetics of human gut commensal *Bacteroides* thetaiotaomicron reveals metabolic requirements for growth across environments. *Cell Rep.* **34**, 108789 (2021).
115. Pittrof, S. L., Kaufhold, L., Fischer, A. & Wefers, D. Products Released from Structurally Different Dextrans by Bacterial and Fungal Dextranases. *Foods* **10**, 244 (2021).
116. Yang, C.-Y. *et al.* Inhibitory effects of pu-erh tea on alpha glucosidase and alpha amylase: a systemic review. *Nutr. Diabetes* **9**, 1–6 (2019).
117. Nadell, C. D. *et al.* Cutting through the complexity of cell collectives. *Proc. Biol. Sci.* **280**, 20122770 (2013).
118. Hoces, D., Arnoldini, M., Diard, M., Loverdo, C. & Slack, E. Growing, evolving and sticking in a flowing environment: understanding IgA interactions with bacteria in the gut. *Immunology* **159**, 52–62 (2020).
119. Cremer, J., Arnoldini, M. & Hwa, T. Effect of water flow and chemical environment on microbiota growth and composition in the human colon. *Proc. Natl. Acad. Sci.* **114**, 6438–6443 (2017).
120. Rivière, A., Gagnon, M., Weckx, S., Roy, D. & De Vuyst, L. Mutual Cross-Feeding Interactions between *Bifidobacterium longum* subsp. *longum* NCC2705 and *Eubacterium rectale* ATCC 33656 Explain the Bifidogenic and Butyrogenic Effects of Arabinoxylan Oligosaccharides. *Appl. Environ. Microbiol.* **81**, 7767–7781 (2015).
121. Wheeler, J. D., Secchi, E., Rusconi, R. & Stocker, R. Not Just Going with the Flow: The Effects of Fluid Flow on Bacteria and Plankton. *Annu. Rev. Cell Dev. Biol.* **35**, 213–237 (2019).

122. Ghosh, O. M. & Good, B. H. Emergent evolutionary forces in spatial models of luminal growth and their application to the human gut microbiota. *Proc. Natl. Acad. Sci.* **119**, e2114931119 (2022).
123. Donaldson, G. P., Lee, S. M. & Mazmanian, S. K. Gut biogeography of the bacterial microbiota. *Nat. Rev. Microbiol.* **14**, 20–32 (2016).
124. Martinez-Guryn, K., Leone, V. & Chang, E. B. Regional Diversity of the Gastrointestinal Microbiome. *Cell Host Microbe* **26**, 314–324 (2019).
125. Lee, S. M. *et al.* Bacterial colonization factors control specificity and stability of the gut microbiota. *Nature* **501**, 426–429 (2013).
126. Nikolaev, M. *et al.* Homeostatic mini-intestines through scaffold-guided organoid morphogenesis. *Nature* **585**, 574–578 (2020).
127. Huang, X. *et al.* *Vibrio cholerae* biofilms use modular adhesins with glycan-targeting and nonspecific surface binding domains for colonization. *Nat. Commun.* **14**, 2104 (2023).
128. Puschhof, J. *et al.* Intestinal organoid cocultures with microbes. *Nat. Protoc.* **16**, 4633–4649 (2021).
129. Bashkatov, A. N. *et al.* Glucose and Mannitol Diffusion in Human Dura Mater. *Biophys. J.* **85**, 3310–3318 (2003).
130. Wiśniewski, J. R., Zougman, A., Nagaraj, N. & Mann, M. Universal sample preparation method for proteome analysis. *Nat. Methods* **6**, 359–362 (2009).
131. Kulak, N. A., Pichler, G., Paron, I., Nagaraj, N. & Mann, M. Minimal, encapsulated proteomic-sample processing applied to copy-number estimation in eukaryotic cells. *Nat. Methods* **11**, 319–324 (2014).

132. Cox, J. & Mann, M. MaxQuant enables high peptide identification rates, individualized p.p.b.-range mass accuracies and proteome-wide protein quantification. *Nat. Biotechnol.* **26**, 1367–1372 (2008).
133. Cox, J. *et al.* Accurate Proteome-wide Label-free Quantification by Delayed Normalization and Maximal Peptide Ratio Extraction, Termed MaxLFQ. *Mol. Cell. Proteomics MCP* **13**, 2513–2526 (2014).
134. Tyanova, S. *et al.* The Perseus computational platform for comprehensive analysis of (prote)omics data. *Nat. Methods* **13**, 731–740 (2016).
135. Mizrahy, S. & Peer, D. Polysaccharides as building blocks for nanotherapeutics. *Chem. Soc. Rev.* **41**, 2623–2640 (2012).
136. Mohammed, A. S. A., Naveed, M. & Jost, N. Polysaccharides; Classification, Chemical Properties, and Future Perspective Applications in Fields of Pharmacology and Biological Medicine (A Review of Current Applications and Upcoming Potentialities). *J. Polym. Environ.* **29**, 2359–2371 (2021).
137. Lovegrove, A. *et al.* Role of polysaccharides in food, digestion, and health. *Crit. Rev. Food Sci. Nutr.* **57**, 237–253 (2017).
138. Guo, M. Q. *et al.* Polysaccharides: Structure and Solubility. in *Solubility of Polysaccharides* (IntechOpen, 2017). doi:10.5772/intechopen.71570.
139. Koropatkin, N. M., Cameron, E. A. & Martens, E. C. How glycan metabolism shapes the human gut microbiota. *Nat. Rev. Microbiol.* **10**, 323–335 (2012).
140. Glowacki, R. W. P. & Martens, E. C. If You Eat It or Secrete It, They Will Grow: the Expanding List of Nutrients Utilized by Human Gut Bacteria. *J. Bacteriol.* **203**, 10.1128/jb.00481-20 (2021).

141. Schwalm, N. D. & Groisman, E. A. Navigating the Gut Buffet: Control of Polysaccharide Utilization in *Bacteroides* spp. *Trends Microbiol.* **25**, 1005–1015 (2017).
142. Reeves, A. R., Wang, G. R. & Salyers, A. A. Characterization of four outer membrane proteins that play a role in utilization of starch by *Bacteroides thetaiotaomicron*. *J. Bacteriol.* **179**, 643–649 (1997).
143. Sonnenburg, E. D. *et al.* Specificity of polysaccharide use in intestinal bacteroides species determines diet-induced microbiota alterations. *Cell* **141**, 1241–1252 (2010).
144. Bolam, D. N. & Sonnenburg, J. L. Mechanistic insight into polysaccharide use within the intestinal microbiota. *Gut Microbes* **2**, 86–90 (2011).
145. Ndeh, D. *et al.* Complex pectin metabolism by gut bacteria reveals novel catalytic functions. *Nature* **544**, 65–70 (2017).
146. Marcobal, A. *et al.* *Bacteroides* in the Infant Gut Consume Milk Oligosaccharides via Mucus-Utilization Pathways. *Cell Host Microbe* **10**, 507–514 (2011).
147. Foley, M. H., Cockburn, D. W. & Koropatkin, N. M. The Sus operon: a model system for starch uptake by the human gut Bacteroidetes. *Cell. Mol. Life Sci. CMLS* **73**, 2603–2617 (2016).
148. Shipman, J. A., Cho, K. H., Siegel, H. A. & Salyers, A. A. Physiological characterization of SusG, an outer membrane protein essential for starch utilization by *Bacteroides thetaiotaomicron*. *J. Bacteriol.* **181**, 7206–7211 (1999).

149. Reeves, A. R., D'Elia, J. N., Frias, J. & Salyers, A. A. A *Bacteroides* thetaiotaomicron outer membrane protein that is essential for utilization of maltooligosaccharides and starch. *J. Bacteriol.* **178**, 823–830 (1996).
150. D'Elia, J. N. & Salyers, A. A. Contribution of a neopullulanase, a pullulanase, and an alpha-glucosidase to growth of *Bacteroides thetaiotaomicron* on starch. *J. Bacteriol.* **178**, 7173–7179 (1996).
151. Smith, K. A. & Salyers, A. A. Characterization of a neopullulanase and an alpha-glucosidase from *Bacteroides thetaiotaomicron* 95-1. *J. Bacteriol.* **173**, 2962–2968 (1991).
152. D'Elia, J. N. & Salyers, A. A. Effect of regulatory protein levels on utilization of starch by *Bacteroides thetaiotaomicron*. *J. Bacteriol.* **178**, 7180–7186 (1996).
153. Martens, E. C., Koropatkin, N. M., Smith, T. J. & Gordon, J. I. Complex glycan catabolism by the human gut microbiota: the Bacteroidetes Sus-like paradigm. *J. Biol. Chem.* **284**, 24673–24677 (2009).
154. Bertoft, E. Understanding Starch Structure: Recent Progress. *Agronomy* **7**, 56 (2017).
155. Wong, J. P. H., Fischer-Stettler, M., Zeeman, S. C., Battin, T. J. & Persat, A. Fluid flow structures gut microbiota biofilm communities by distributing public goods. *Proc. Natl. Acad. Sci.* **120**, e2217577120 (2023).
156. Díaz-Montes, E. Dextran: Sources, Structures, and Properties. *Polysaccharides* **2**, 554–565 (2021).

157. Liu, H. *et al.* Functional genetics of human gut commensal *Bacteroides thetaiotaomicron* reveals metabolic requirements for growth across environments. *Cell Rep.* **34**, 108789 (2021).
158. Kim, D., Robyt, J. F., Lee, S.-Y., Lee, J.-H. & Kim, Y.-M. Dextran molecular size and degree of branching as a function of sucrose concentration, pH, and temperature of reaction of *Leuconostoc mesenteroides* B-512FMCM dextransucrase. *Carbohydr. Res.* **338**, 1183–1189 (2003).
159. Lindberg, B., Svensson, S., Sjövall, J. & Zaidi, N. A. Structural Studies on Dextran from *Leuconostoc mesenteroides* NRRL B-512. *Acta Chem. Scand.* **22**, 1907–1912 (1968).
160. Foley, M. H., Martens, E. C. & Koropatkin, N. M. SusE facilitates starch uptake independent of starch binding in *B. thetaiotaomicron*. *Mol. Microbiol.* **108**, 551–566 (2018).
161. Cerqueira, F. M. *et al.* Sas20 is a highly flexible starch-binding protein in the *Ruminococcus bromii* cell-surface amylosome. *J. Biol. Chem.* **298**, 101896 (2022).
162. Rogowski, A. *et al.* Glycan complexity dictates microbial resource allocation in the large intestine. *Nat. Commun.* **6**, 7481 (2015).
163. Li, S., Hu, J., Yao, H., Geng, F. & Nie, S. Interaction between four galactans with different structural characteristics and gut microbiota. *Crit. Rev. Food Sci. Nutr.* **63**, 3653–3663 (2023).
164. Li, Q.-Y. *et al.* Study on the Effect of Molecular Weight on the Gut Microbiota Fermentation Properties of Blackberry Polysaccharides In Vitro. *J. Agric. Food Chem.* **70**, 11245–11257 (2022).

165. Teufel, F. *et al.* SignalP 6.0 predicts all five types of signal peptides using protein language models. *Nat. Biotechnol.* **40**, 1023–1025 (2022).
166. García-Bayona, L. & Comstock, L. E. Streamlined Genetic Manipulation of Diverse *Bacteroides* and *Parabacteroides* Isolates from the Human Gut Microbiota. *mBio* **10**, 10.1128/mbio.01762-19 (2019).
167. Kamrad, S. *et al.* Pyphe, a python toolbox for assessing microbial growth and cell viability in high-throughput colony screens. *eLife* **9**, e55160 (2020).



JEREMY WONG

PhD Student

@ jeremy.wong@epfl.ch

076 435 58 42

Sion, Switzerland

Work Permit B

Citizenship: Canadian

Date of birth: July 27, 1996

STRENGTHS

Teamwork Dedicated

Independent Flexible

Organized Innovative

Team work Mentoring

Project management

Public speaking

SKILLS

Chromatography

Microbiology

Biochemistry

Glycan analysis

Food and nutrition

Gut microbiota

Mass spectrometry

Synthetic biology

Chemical synthesis

Protein production

Proteomics

Metabolomics

LC-MS

Python

Microscopy

Transcriptomics

Microfluidics

Nanoparticles

LANGUAGES

English, Cantonese: **Native**

Mandarin: **Intermediate**

French, German, Japanese: **Beginner**

ABOUT ME

I am a scientist with previous training spanning the fields of chemistry, biochemistry, microbiology and ecology. I am passionate about biotechnologies, in particular, the development of tools for disease diagnosis. Some of my hobbies include hiking, playing the violin and sculpting.

EXPERIENCE

PhD Student in Microbiology and Biogengineering | EPFL

Dec 2018 - Oct 2023

Lausanne and Sion, Switzerland

- Project: Gut Microbiota: Metabolic Interactions and Spatial Organization
- Supervisors: Prof. Alexandre Persat and Prof. Tom Battin
- Tasks: Culturing of anaerobic bacteria and spores, lecturer for proteomics and metabolomics, mentoring of MSc students, analysis of carbohydrates and proteins by LC-MS and HPLC, microfluidics, quantitative confocal fluorescence microscopy, synthetic biology, bio-orthogonal chemistry, and biochemical assays

McCaul McBain Foundation Research Student in Bioengineering | EPFL

Jul 2018 - Sep 2018

Lausanne, Switzerland

- Project: Influence of Fluid Flow on Biofilm Formation by *Caulobacter crescentus*
- Supervisors: Prof. Alexandre Persat
- Tasks: Growth of microbes in microfluidics, cell imaging by fluorescence microscopy, image analysis by python and genetic manipulation in microbes.

CIHR Funded Research Student | University of Toronto, Department of Chemistry

Apr 2018 - Jun 2018

Toronto, Canada

- Project: The Roles of Two Lysine Residues in the Nickel and DNA binding by the Master Regulator HpNikR in *Helicobacter pylori*
- Supervisor: Prof. Deborah Zamble
- Tasks: Bacterial culture, protein expression and purification, HPLC, chromatography, biochemical assays, radioactive labelling, DNA- protein interactions, mass spectrometry, LC-MS, top-down proteomics, protein NMR.

BSc. Thesis Student | University of Toronto, Department of Chemistry

Sep 2017 - Apr 2018

Toronto, Canada

- Project: Investigation of Protein Aggregation Dynamics and Non-Covalent Binding Using High Resolution Mass Spectrometry
- Supervisor: Prof. Rebecca Jockusch
- Tasks: Protein sample preparation, analysis of protein by ICR-MS, protein chromatography, fluorescence spectroscopy, mass spectrometry data analysis, and proteomics.

DAAD and MITAC Exchange Research Scholar | [Leibniz-Institut für Polymerforschung Dresden](#)

📅 May 2017 - Sep 2017

📍 Dresden, Germany

- Project: Design of Drug Delivery Systems Based on Polyelectrolyte Complex Nanoparticles
- Supervisor: Prof. Dr. Martin Müller
- Tasks: Synthesis of polyelectrolyte nanoparticles, dynamic light scattering (DLS), ATR-FTIR and UV-Vis Spectroscopy, and conjugation of the drug bortezomib to polymers.

Research Student | [University of Toronto, Department of Biochemistry](#)

📅 May 2016 - May 2017

📍 Toronto, Canada

- Project: Unveiling the Mechanisms of Nickel Induced DNA Binding by the Master Regulator HpNikR Using ¹⁹F NMR
- Supervisor: Prof. Dr. Deborah Zamble
- Tasks: Site directed mutagenesis, protein expression, development of purification protocols, HPLC, LC-MS, mass spectrometry, DNA- protein interactions, metal-protein interactions, radioactive labelling, circular dichroism, thermal denaturation and protein NMR

EDUCATION

PhD in Bioengineering and Biotechnology | [EPFL](#)

📅 Dec 2018 - Present

📍 Lausanne and Sion, Switzerland

- Interdisciplinary PhD student shared between the School of Life Sciences (SV) and the School of Environmental Sciences and Engineering (ENAC)

HBSc. in Chemistry | [Victoria University at the University of Toronto](#)

📅 Sep 2014 - Jun 2018

📍 Toronto, Canada

- GPA: 3.7/4

PUBLICATIONS

1. **Wong, J. P. H.**, Chillier, N., Fischer-Stettler, M., Zeeman, S. C., Battin, T. J. and Persat, A. Size dependent dextran metabolism by the gut commensal *B. thetaiotaomicron*. *bioRxiv*. 2023 Sep 21; <http://doi.org/10.1101/2023.09.21.558885>.
2. **Wong, J. P. H.**, Fischer-Stettler, M., Zeeman, S. C., Battin, T. J. and Persat, A. Fluid flow structures gut microbiota biofilm communities by distributing public goods. *PNAS*. 2023 Jun 12; 120(25): e2217577120.
3. Pierrat, X., Pham, A., **Wong, J. P. H.**, Al-Mayyah, Z., and Persat, A. Engineering *Agrobacterium tumefaciens* Adhesion to Target Cells. *ACS Synthetic Biology*. 2022 Jul 26;11(8), pp. 2662–2671.
4. Pierrat, X., **Wong, J. P. H.**, Al-Mayyah, Z., and Persat, A. The Mammalian Membrane Microenvironment Regulates the Sequential Attachment of Bacteria to Host Cells. *mBio*. 2021 Aug 31;12(4):e0139221.
5. Vehlow, D., **Wong, J. P. H.**, Urban, B., Weißpflog, J., Gebert, A., Schumacher, M., Gelinsky, M., Stamm, M., and Müller, M. Catechol Containing Polyelectrolyte Complex Nanoparticles as Local Drug Delivery System for Bortezomib at Bone Substitute Materials. *Pharmaceutics*. 2020 Aug 24;12(9):799

REFERENCES

1. Prof. Alex Persat - alexandre.persat@epfl.ch
2. Prof. Tom Battin - tom.battin@epfl.ch
3. Prof. Giovanni D'Angelo (teaching) - giovanni.dangelo@epfl.ch
4. Prof. Loic Dayon (proteomics teaching) - loic.dayon@epfl.ch
5. Prof. Rebecca Jockusch - rebecca.jockusch@utoronto.ca
6. Prof. Martin Müller - mamuller@ipfdd.de